INFORMATION TO USERS

This manuscript has been reproduced from the microfilm master. UMI films the text directly from the original or copy submitted. Thus, some thesis and dissertation copies are in typewriter face, while others may be from any type of computer printer.

The quality of this reproduction is dependent upon the quality of the copy submitted. Broken or indistinct print, colored or poor quality illustrations and photographs, print bleedthrough, substandard margins, and improper alignment can adversely affect reproduction.

In the unlikely event that the author did not send UMI a complete manuscript and there are missing pages, these will be noted. Also, if unauthorized copyright material had to be removed, a note will indicate the deletion.

Oversize materials (e.g., maps, drawings, charts) are reproduced by sectioning the original, beginning at the upper left-hand corner and continuing from left to right in equal sections with small overlaps.

ProQuest Information and Learning
300 North Zeeb Road, Ann Arbor, MI 48106-1346 USA
800-521-0600

DISSERTATION

DESIGN METHODOLOGY USING EMPIRICAL AND VIRTUAL ANALYSIS WITH APPLICATION TO COMPLIANT SYSTEMS

Submitted by

John Joseph Wood

Department of Mechanical Engineering

In partial fulfillment of the requirements

for the Degree of Doctor of Philosophy

Colorado State University

Fort Collins, Colorado

Summer 2002

COLORADO STATE UNIVERSITY

May 31, 2002

WE HEREBY RECOMMEND THAT THE DISSERTATION PREPARED UNDER OUR SUPERVISION BY JOHN JOSEPH WOOD, ENTITLED, "DESIGN METHODOLOGY USING EMPIRICAL AND VIRTUAL ANALYSIS WITH APPLICATION TO COMPLIANT SYSTEMS," BE ACCEPTED AS FULLFILLING IN PART REQUIREMENTS FOR THE DEGREE OF DOCTOR OF PHILOSOPHY.

Committee on Graduate Work

Advisor – Dr. Hiroshi Sakurai

Advisor – Dr. Daniel Jensen

Advisor – Dr. Louis Bjostad

Advisor – Dr. Wade Troxell

Department Head – Dr. Allan Kirkpatrick

ABSTRACT OF DISSERTATION

DESIGN METHODOLOGY USING EMPIRICAL AND VIRTUAL ANALYSIS WITH APPLICATION TO COMPLIANT SYSTEMS

Successful engineering design results from the application of suitable product design methods to an identified customer need. The generation and evaluation of conceptual designs satisfying engineering and customer requirements is a primary purpose of existing methods. Numerical and experimental techniques often can determine the feasibility of meeting the specified performance requirements.

The concept generation design phase is expanded through a formalized process geared toward the design evolution of products characterized specifically by reduced part count through the incorporation of compliant materials and structures. Compliance offers a new dimension to evolutionary product design by introducing flexible components for direct component combination or replacement. Effort flow analysis is a technique that provides a framework for identifying component combination opportunities. This graphical method maps the flow of effort across component interfaces and systematically provides insights based upon the type of relative motion required between them.

A formalized method for identifying and classifying these component groups is developed. An empirical study of existing products is conducted with the outcome being a deduced set of product evolution specific directive guidelines. The derived guidelines support the directed product evolution effort flow analysis methodology.

Evaluation of conceptual designs is critical in the determination of functional performance. Similarity methods offer performance predictions of products based upon functional testing of scale models to correlate measured model behavior with predicted product behavior. Traditional methods can be improved in both accuracy and domain of applicability by the infusion of empirical data, derived from simplified tests, into the equations that characterize the system parameters of interest. Similarity methods have been developed that overcome the constraints associated with the traditional methods and provide increased analysis capability and improved insight into the phenomenon governing the problem.

The product evolutionary design methodology incorporates an analytical feasibility determination to provide a conceptual design and evaluation approach for design focusing on component combination and incorporation of compliant solutions. The method has demonstrated successful evolutionary design of compliant systems and accurate similarity-based predictions of product performance. Future endeavors include expansion of effort flow analysis and advanced similarity methods to include the design of systems outside the mechanical domain.

John Joseph Wood
Department of Mechanical Engineering
Colorado State University
Fort Collins, CO 80523
Summer 2002

ACKOWLEDGEMENTS

So many people have been influential in the decisions that led me down this path and so many more have impacted the course and content of this final dissertation. Where does one begin to acknowledge all those who have contributed in one form or another to the completion of such a monumental task as this?

Of the many I owe a sincere debt of gratitude to there is one who has been with me since the very beginning and supported me every step of the way. He walked along side me through the easy times, carried me through the difficult times, shared joy in my successes and encouraged me in my failures. Jesus Christ has been, and continues to be, a source of unbending strength, courage, and peace and whose light provides both direction and enlightenment as I travel down life's path.

It could be said that this research project required three generations for its successful completion. Endless thanks go out to my parents who have always been a source of tremendous inspiration and who first fueled my intellectual curiosity for discovering why things work the way they do. Thanks mom and dad for the abundance of love and encouragement and for not discouraging me when I couldn't put the car, the lawnmower, the stereo, or all of those other things back together without the usual handful of spare parts. Without your guidance this certainly would not have been possible. Dad, growing up I always wanted to follow in your footsteps, to be just like you. I knew that if I could be half the father, husband, and friend that you are I would be extremely successful.

Now that I have teenagers of my own, I still strive to be the man you are. Thanks for setting such high standards and showing me how to be both gentle and strong.

The second generation includes friends, family, and colleagues, who have all been influential in helping to complete this work. Thanks DJ for the many brainstorming sessions and the collaborative work, which offered a fun, and challenging change from the normal grind. Your unique perspective on what is really important was a welcome relief more often than you know. Paul Townsend, although you contributed absolutely nothing to the technical content of this research I can say with confidence and humbleness that I wouldn't have made it without you. Thanks Paul. Jeff, your inquisitiveness and ability to ask the simplest but thought provoking questions about where I was going with all of this and why kept the journey focused and my eyes on the road. Thanks for all your support over the past few years. Monty, your hard work in helping develop the effort flow analysis methodology is greatly appreciated as is your ability to keep the fun in the research.

A special thanks to Dr. Kris Wood for years of friendship, encouraging me to follow my heart down this path, and in providing invaluable guidance during the course of this work which allowed me to maintain focus, again and again. Thanks for the dedication of my committee; Dr. Wade Troxell, advisor and friend, Dr. Dan Jensen (DJ), Dr. Hiroshi Sakuri, and Dr. Lou Bjostad. Each contributed in their unique way and share in this success. I have truly been blessed to have such very special people I can call my friends.

The third generation consists of five kids who are collectively responsible for keeping me sufficiently sidetracked to not loose sight of the wonderful rewards of being a dad. Thanks Dan, Josh, Kevin, Lisa, and Ethan. Each of you has always been a source of such

incredible joy with your youthful spirits and individual personalities I only hope you learn as much from me as I have from you. Of all the sacrifices that come with an endeavor of this magnitude yours is possibly the greatest. You have endured my absences, both mental and physical, and I can't begin to thank you enough for your patience, love, and support these past few years. Your creative innocence has been both inspiring and, at times, confusing (Dad, are sharks teeth sharper than the sun is hot?) but I wouldn't have it any other way. With this dissertation I have also achieved a secondary life goal; to not be a college student and the same time my kids are. That one was close!

And finally, I wish I could find the words to express my deepest appreciation to my very best friend, my wife Resia. Without your encouragement and support I would not have even entered this race. Now, as we stand at the finish line looking both back at where we have been and forward to what lies ahead, I begin to appreciate the effort you have put forth made to help make my dreams come true. Thank you Resia, for your undying love, your friendship, and your sacrifices to keep the family running on all 7 cylinders. You are a precious gift from God and the most important part of my life and only together have we succeeded in this endeavor.

JOHN J. WOOD

Colorado State University

May 2002

TABLE OF CONTENTS

LIST OF TABLES

LIST OF FIGURES

NOMENCLATURE

C	C-Link Interface
cir($\bar{X}_m$)	Circulent Matrix of $\bar{X}_m$
DFA	Design For Assembly
$\hat{e}$	Unit Vector
E	Modulus of Elasticity
EFA	Effort Flow Analysis
EFD	Effort Flow Diagram
FFD	Force Flow Diagram
ESM	Empirical Similarity Method
F	Force
[F]	Form Transformation Matrix
[G]	Geometry Transformation Matrix
I	Identity Matrix
I	I-Link Interface
L	Length
[M]	Material Transformation Matrix
N	N-Link Interface
P	Load
R	R-Link Interface
[S]	Scale Transformation Matrix
[S_0]	Scaled Identity Matrix Component
T	Transformation Matrix
TSM	Traditional Similarity Method
$\bar{X}_m$	Model State Vector
$\bar{X}_{ms}$	Model Specimen State Vector

$\bar{X}_p$	Product State Vector
$\bar{X}_{ps}$	Product Specimen State Vector
[δS]	Perturbed Matrix Component
λ	Scale Factor
π_i	i^{th} π term
ρ	Density

Chapter 1

Motivation for Research

It has long been recognized that the variables affecting a problem

"cannot be decided by the philosopher in his armchair,"

but rather the choice must be made based upon considerable physical experience.

P.W. Bridgman,
Founder of Modern Dimensional Analysis
(Bridgman, 1922)

1.1 Overture

Design methods studies have generated a wealth of processes for the design, development, optimization, and redesign of products. A common thread in the vast majority of design methods is the requirement to both develop and evaluate design concepts, a phase commonly referred to as conceptual design. In the design of conventional rigid body mechanisms, the elastic deformation of members is often considered undesirable and significant effort is expended to reduce or eliminate any deformation deemed detrimental to the function of the product. Structural compliance of members offers a new dimension to evolutionary design by providing elasticity that can be integrated into the design for use as a source of desired relative motion. The conceptual design and feasibility evaluation of compliant inclusive design solutions could

greatly benefit from both a logical and complete process for development and an efficient method for evaluation of the functional performance of the design.

Mapping the flow of forces and torques through the individual components of a system and dissection of the interfaces between components offers a high degree of insight into the components interaction during their intended operation. These interfaces can be studied for modification to take advantage of the relative motion opportunities offered through the creative use of compliant materials and structures. The potential benefit of integrated compliance includes, at a minimum, reduced part count, reduced complexity, and improved assemblability.

Traditional dimensional analysis techniques for predicting the performance of system components can be greatly improved in both accuracy and domain of applicability by the infusion of empirical data into the equations that characterize the system parameters of interest. Application of modern dimensional analysis techniques provides an integral feasibility verification element to the conceptual design process by providing a crucial analytical tool for the evolutionary re-design of products.

1.2 Research Goal

The primary goal is to further the development of an enhanced effort flow analysis methodology designed to systematically evolve a product, characterized by relative motion based functionality, through component combination and the utilization of material and structural compliance.

An effort flow analysis method is developed to identify and take advantage of product characteristics and architectures that suggest potential product evolution paths. To

ground this development in sound engineering design, an extensive study of existing products and their evolved compliant counterparts is be conducted, with the result a set of compliant evolution design guidelines. This study forms the initial basis of the effort flow analysis methodology and allows application of the method to the re-design of existing products for potential product evolution.

Integral to this research is an advancement of the current state of similarity techniques to the point where they can be used as a viable analytical design tool providing both improved accuracy and range of applicability over traditional methods of dimensional analysis. The results of this study become an integral element of the effort flow analysis methodology. In order to achieve this goal, the theoretical foundation for traditional dimensional analysis as well as the current state of similarity based research methods must first be fully understood including constraints and limits of applicability. The method is then pushed forward to develop a useable design tool for the analytical prediction of component and/or system performance.

The advanced development of similarity methods provides a crucial analytical tool to the effort flow analysis method affording both conceptual and detailed design selection capabilities while allowing the functional design requirements to maintain their influence throughout the re-design process.

1.3 Research Objectives

The specific objectives required for the successful completion are as follows:

- Further the development of effort flow analysis as a design methodology
- Develop a representative set of effort flow analysis design guidelines

- Conduct and document results of an empirical study of existing products and their evolved compliant counterparts
- Develop an advanced similarity method for use as a design feasibility verification technique
- Evolve a set of existing products using the effort flow analysis design guidelines and similarity feasibility analysis

1.4 Research Methodology

The proposed research resulted in the development of a methodology for use in the design evolution of relative motion based products as depicted in Fig. 1.1. The method provides the capability to both determine and impact the realization potential of the design as it evolves through the effort flow analysis evolution process. The analysis component is founded upon the theories and background of dimensional analysis combined with the infusion of empirical data to effect an improvement in overall predictive capability. The feasibility method is integrated into a design methodology centered on the process defined as effort flow analysis (Lefever, 1995). As part of this process the flow of effort is mapped as it traverses through the system components. The individual processes described above are integrated into an overall design evolution methodology for use on relative motion based functional products.

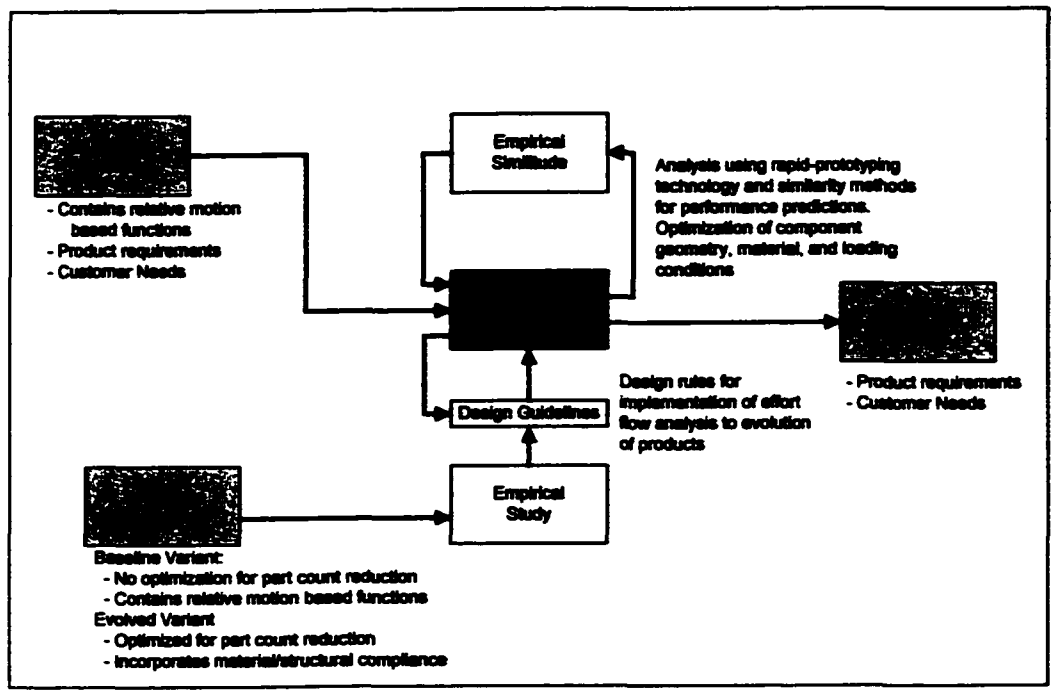

Fig. 1.1. Research Methodology

1.5 Commencement

The exploration begins with a study of previous work accomplished in the realm of kinematic analysis and the use of graph theory to understand the interactions of system component parts. This theory offers a graphical method of visualization and manipulation of components to enhance the possibility of successful conceptual design and maximizes the potential for integration of compliant systems. This study leads to the development of effort flow analysis as a systematic tool that guides to piece count reduction through part combination. A required compliment to the generation of design concepts is the engineering analysis of functional performance or, more simply, evaluation of the concept.

The Traditional Similarity Method (TSM) is well understood as a methodology that uses the concept of dimensional analysis, based upon the Buckingham Π theorem, to correlate the respective states of a representative model and a product. The primary goal of TSM is to allow the prediction of the performance of a product based upon the measured state(s) of a representative model. This process has been used to save considerable time and expense in contrast to testing complex and expensive full-scale products.

Dimensional analysis, theory of dimensions, theory of models, similitude, theory of similarity; all of these terms have been used interchangeably over the past century to describe the process of using the exponents of variables as a starting point for a more detailed dimension-based analysis (Becker, 1976). Dimensional analysis has long been recognized as a valuable design and analysis tool but has suffered from severe constraints and limits of applicability.

Advanced similarity analysis methods, in tandem with recent advances in rapid prototyping technology, have afforded the development of functional testing for geometrically complex physical models (Cho et al., 1998) free of many of the constraints that limit the application of traditional methods. Until recently, functional tests on rapid prototyped products was rare with the key factor the severe material properties limitations (Wall, 1991). The methods represent an opportunity to overcome these limitations and those imposed by traditional methods by using scale testing on rapid-prototyped models or other traditionally non-functional models in concert with advanced similarity prediction techniques. Advanced similarity methods represent a powerful class of analysis tools in development, derived from the basic principles of dimensional analysis.

The theoretical foundation of traditional dimensional analysis is reviewed to gain a full understanding of the method including constraints and limits of applicability. This review is followed by an introduction to an advanced method called the Empirical Similarity Method (ESM) to include the derivation of the method and evaluation using both a numerical example and an empirical example to demonstrate the potential of the new methods for empirical engineering analysis. This review is followed by the development of a new empirically based approach which demonstrates both increased accuracy and improved insight into the prediction characteristics over previous methods.

Chapter 2

Foundations of Research

2.1 Design of Mechanisms – Opportunities for Compliant Design

Douglas Commercial Aircraft Company conducted a comprehensive manufacturing and assembly review to determine the primary influences in the cost of their commercial airframe construction. They discovered that the costs of assembly, fabrication, quality assurance, overhead-inventory levels, tracking, and purchasing are all dependent, to a significant degree, on the number of components that make up the system (Ashley, 1995). Reducing the number of components in a system through part combination redesign is a recognized goal of Design For Assembly (DFA). Current DFA methods and research in this area (Defazio and Whitney, 1987; Ishii et al., 1995; Lee and Ui, 1994; Pine et al., 1993; Poli et al., 1986) focus primarily on quantitatively measuring the assemblability of a product. However, very minimal insights into methods to systematically create designs that are more easily assembled have been provided.

Current research into the area of improved assemblability through part count reduction does offer insight into design characteristics or processes that negatively affect how easily a product can be assembled, but lacks a detailed and robust solution for addressing these issues. Answering the "why" question is the straightforward part:

reduced number of assembly operations, reduced procurement costs, cycle time reduction, supply chain reduction, higher potential profits, etc. However, answering the "how" question continues to be a formidable challenge.

Within the framework of DFA, the specific area of part count reduction through part combination has gained significant momentum of late. Part combination involves the combination of separate components into a single part. Boothroyd *et al.* (Boothroyd et al., 1994) performed an extensive study of mechanical-domain products with the goal of defining design-based limitations to the application potential of component combination. Their study concluded with the following guidelines:

Components of the original product should be considered for combination with other components unless:

- The part moves relative to all other parts already assembled during the normal operating mode of the final product
- The part must be of a different material than, or must be isolated from, all other parts assembled
- The part must be separate from all other assembled parts, otherwise assembly, or parts meeting one of the above criteria would be prevented

According to these guidelines, components exhibiting relative motion with respect to other components are not candidates for combination. Based upon this and supporting research, systems of components with these characteristics were traditionally considered to be either un-combinable, or to require significant redesign if part count reduction was to be successful. In the wake of new material, processing, and design developments, these limitations are now being challenged.

As proof of this design revolution, product examples successfully designed using compliant materials and structures have brought a new focus to compliant design and have relaxed the limitations that once constrained the design of mechanical-domain products. Possibly the most straightforward example of such a design is achieved through combination of parts having relative motion using monolithic materials in the redesign of jointless compliant devices (Ananthasuresh and Kota, 1995). An example of such a device is the commercially available device as known as the "ComPlier™" (see Fig. 2.1). These pliers are designed and constructed using multiple compliant joints in place of mechanical pin joints (Salamon and Midha, 1998).

Fig. 2.1. "Complier™" Compliant Pliers

This compliant product, a redesign once considered to be beyond the limitations of part combination, is manufactured from a single piece of polymeric material and replaces an assembly of at least four rigid components. For the successful compliant redesign of this product, the original spatial component layout, or topology, of the multi-part device was allowed to change as part of the redesign. This was necessary to achieve the desired degree of deflection at the jaws within reasonable actuation constraints on the handles.

The ideal scenario, from a redesign simplicity standpoint, is to simply maintain the original topology and geometric features by directly replacing connected components

with single compliant components. In this case, only minor shape modifications and material property issues must be considered to successfully accomplish the part combination redesign.

But engineering design is very rarely ideal and methods must be researched and developed which will afford the opportunity to redesign mechanical-domain products not restricted by the topology, geometric features, or materials of the original design. Part combination within this framework has the goal of decreasing the number of parts that comprise a product while maintaining its essential functionality. This reduction in many cases is the predominant parameter in improving the overall assemblability of a product and results in the time and cost advantages discussed previously.

2.2 Effort Flow Analysis as a Design Tool

The recognized impracticalities or even impossibilities of successfully redesigning the majority of mechanical-domain products with fewer parts by simply replacing systems of rigid-body components with compliant components are accepted. The search for a method that will help capture the design characteristics of products that matches the design attributes provided by compliant components leads to Effort Flow Analysis (EFA). Effort Flow Analysis is a design methodology in its infancy as a process with its origins in research conducted at the University of Texas at Austin and by Jensen et al (Jensen et al., 2000) at the United States Air Force Academy.

The method is used to identify opportunities to improve the manufacturability and/or the assemblability of an existing product through modeling and analysis of the individual components and their interactions with adjacent components (Lefever, 1995). The

method is defined as a model representation of the transfer, or flow, of effort through a relative motion based product's components via the interfaces connecting the individual components. The effort flow begins with the input of force or torque into the product space and is tracked through the system to its final destination, typically an operation on an object outside the product space. An example of an effort flow diagram (EFD) for the commercially available original-design and compliant evolution redesign wire strippers of Fig. 2.2. is shown in Fig. 2.3. In this example, the input force is the human or hand force applied to Grips A and B and the final destination is the force exerted on the insulated wire. As shown in the figures the original product contains seven separate components while the evolved product contains only a polymeric frame and a single blade.

Fig. 2.2. Baseline and Fully Evolved Wire Strippers

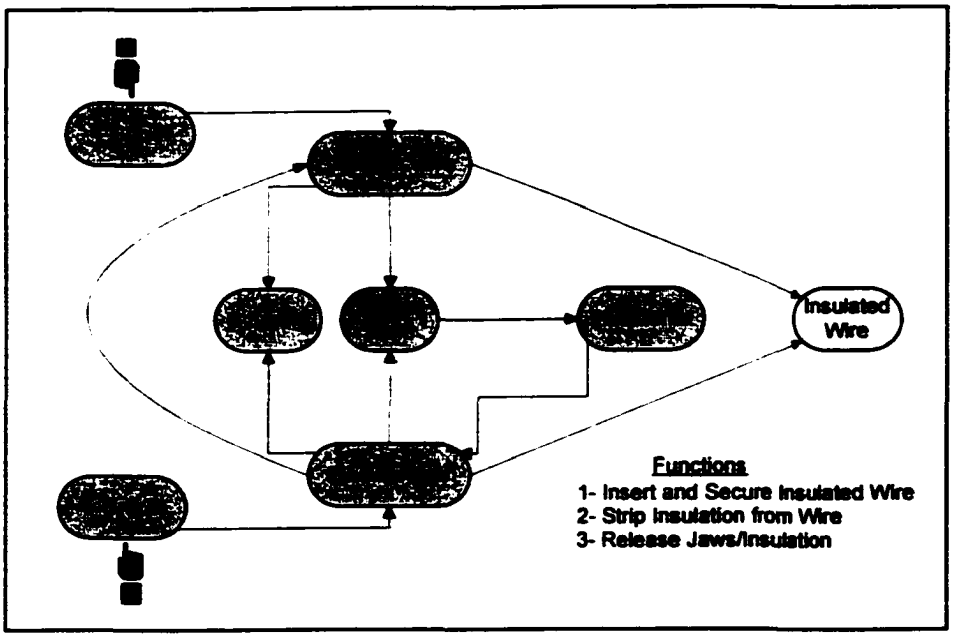

Fig. 2.3. Baseline Design Effort Flow Diagram

Effort Flow Analysis involves modeling the product as a set of nodes representing each of the product's components. The nodes are connected by links that represent the interface between adjacent or connected components for a particular function. The nodes and connecting links are arranged such that the product's topology is mapped spatially by the layout of the diagram whenever possible. The links between components are provided with a designation (not shown) based upon the presence or absence of relative motion in the link and with respect to the connecting components. The realized value of the effort flow analysis method is in the understanding and manipulation afforded by the assignment of link designations between the components as will be demonstrated.

2.3 Traditional Similarity Method

The redesign of products with the incorporation of compliant components in an effort to reduce the number of components must not only be physically possible but must also be feasible from an engineering material strength standpoint. A method is sought that will allow the detailed design and verification of the structural integrity of the redesign and the ability to perform design iterations while evaluating the anticipated performance of the redesigned product. The desire is to use scaled models, as a cost and time savings measure over full-scale prototypes, to optimize the design iteration and analysis process.

The Traditional Similarity Method (TSM) in the context of this research is defined as a methodology that uses the concept of dimensional analysis, based upon the Buckingham Π theorem, to correlate the respective state(s) of a product and a representative model. The primary goal of the technique is to allow the estimation or prediction of the performance of a product from the measured state or states of a model. The attractiveness of the method stems in part from the freedom to develop and test relatively inexpensive models without the often-excessive time and expense associated with fabrication of full-scale tests models.

Dimensional analysis, theory of dimensions, theory of models, similitude, theory of similarity; all of these terms have been used interchangeably over the past century to describe the process of using the exponents of variables as a starting point for a more detailed analysis (Becker, 1976). Dimensional analysis has long been recognized as a valuable design and analysis tool and has demonstrated its usefulness in all major fields of science and engineering.

The generality of dimensional analysis is both its strength and its weakness. With minimal effort and insight, a partial solution to nearly any problem can be obtained. However, a complete solution and a thorough understanding of the phenomena at work in the problem is more difficult to acquire. Dimensional analysis has become an important mathematical tool of experimenters, as its greatest asset is in the reduction of the number of variables that must be tested in order to formulate or describe a useable function. It has the advantage of not requiring complicated math background, but the disadvantage of requiring additional postulates (e.g. objective functions) to provide boundaries to the problem at hand. A primary disadvantage to dimensional analysis is that it provides no basis for deciding *a priori* which derived variables are crucial for consideration in a particular problem. It has long been recognized, and perhaps best stated by Bridgman (Bridgman, 1922), that the variables affecting the problem "cannot be decided by the philosopher in his armchair." The choice must be made often based upon considerable physical experience or extensive investigation into the parameters affecting the problem.

Dimensional analysis has the ability to predict results without an understanding or even knowledge of the governing differential equations and often provides acceptable results without expensive or complex computational or physical models.

2.3.1 History – Dimensional Analysis

The origins of dimensional analysis can be traced back to the ancient Greeks and their use of the basic principles of geometric similarity, ratios, and proportionality. Early in the 17th century Galileo used these fundamental principles, and the resulting dimensionless terms, in his attempts to characterize the strength and predict the failure of

beams (Birkhoff, 1960). Although earlier scientists had undoubtedly recognized the inherent value of units, Baron Jean-Baptiste Fourier was certainly one of the first scientists to apply and document the concept of "dimensions" or "fundamental units" to actual quantities and, as a result, is often referred to as the founder of dimensional analysis (Fourier, 1822; Palacios y Martínez, 1964). Experimental scientists applied the ideas first formalized by Fourier with great success at the end of the 19th century. During the 1900-1920 timeframe, physicists attempted to determine the limitations of the newly introduced methods by clarifying the assumptions required for the successful application of dimensional analysis.

In 1914, E. W. Buckingham gave the first generally accepted proof of the Π Theorem which stated that if an equation is dimensionally homogeneous, it can be reduced to a relationship among a complete set of dimensionless products (Birkhoff, 1960; Buckingham, 1914). His publishing's came at a time when physicists were just becoming aware of the power of the methods and as such, Buckingham is often recognized as the founder of the newly labeled Buckingham Π Theorem. Lord Rayleigh was another major contributor to the advancement of the methods of dimensional analysis (Palacios y Martínez, 1964).

In 1915 Rayleigh published his "Method of Indices," (Rayleigh, 1915) which attempted to take the next step in considering similitude as a method for comparison between the states of two similar systems. This work, along with Buckingham's Π Theorem, were combined by Bridgman in 1922 and formalized into what is now known as dimensional analysis (Becker, 1976).

2.3.2 Development of the Traditional Similarity Method

Dimensional analysis provides a qualitative relationship, by way of specific groups of problem parameters. However, when combined with experimental results or procedures, it provides quantitative results in the form of both prediction equations and similarity constraints within recognized limitations (Murphy, 1950). The principal advantage to dimensional analysis lies in formulating dimensionless groups of problem variables known as π terms which allows a reduction in the number of variables that must be investigated to obtain useful analysis results. The number of π terms required to express a relationship among the variables in any problem is equal to the number of quantities involved, minus the rank of the dimensional matrix (Bridgman, 1931), a mathematical representation of the number of independent fundamental dimensions. In equation form (Murphy, 1950):

$$N = n - b \tag{2.1}$$

where: N – number of π terms

n – total number of quantities involved

b – number of basic dimensions involved

The only restriction on the π terms is that they be dimensionless and independent.

The fundamental premise of the TSM and the limitations in its application can best be understood by considering the mathematical foundations of the method. Investigation begins by considering the model and product systems, both comprised of relevant physical parameters (q_i), which characterize parameters of interest for the respective

systems. The two systems are described by the following complete and homogeneous equations:

$$f(q_{m,1}, q_{m,2}, \ldots, q_{m,n}) = 0$$

$$g(q_{p,1}, q_{p,2}, \ldots, q_{p,n}) = 0$$

Here the subscripts m and p denote the scaled model and product parameters respectively.

The Buckingham Π theorem states that a complete equation written in terms of dimensional system parameters q_j, j = 1, ..., n, can be reformulated in terms of dimensionless parameters π_i, i = 1, ..., N, where $N < n$ as described in eqn. (2.1). By applying the Π theorem, the above system of equations can be equivalently represented in terms of the π terms as:

$$F(\pi_{m,1}, \pi_{m,2}, \ldots, \pi_{m,N}) = 0$$

$$G(\pi_{p,1}, \pi_{p,2}, \ldots, \pi_{p,N}) = 0$$

Note that the number of parameters characterizing the system has been reduced from "n" to "N". One can refer to (Barr, 1984) for a comprehensive and systematic derivation of the dimensionless parameters.

Any physical phenomena can be described by a complete homogeneous equation (e.g. drag on a ship, stress in a shaft, etc.) (Langhaar, 1980) as demonstrated in the following example where the fundamental dimensions of force (F) and length (L) are chosen. A tapered, cantilevered beam subject to a concentrated, or point, load at the free end is as

shown in Fig. 2.4. The variables and their respective dimensions involved in characterizing the deflection of, and normal stresses in, the beam are shown in Table 2.1.

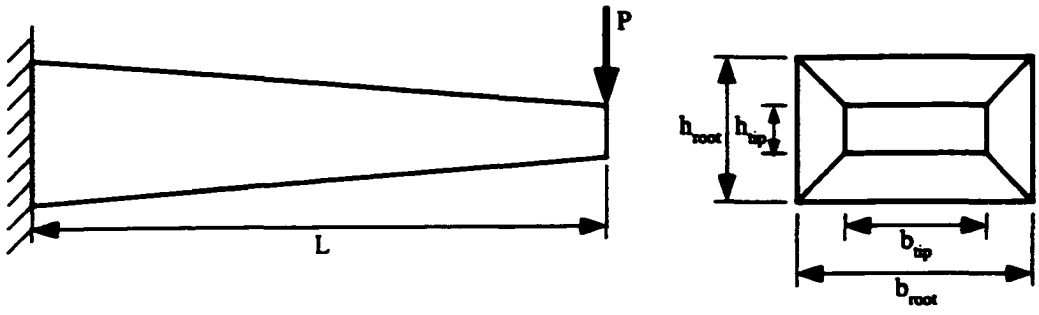

Fig. 2.4. Cantilevered Tapered Beam

Table 2.1. Variables Involved in Analysis of a Tapered Cantilevered Beam

Variable	Symbol	Dimensions
Applied Load	P	F
Beam Length	L	L
Modulus	E	FL^{-2}
Density	ρ	FL^{-3}
Normal Stress	σ	FL^{-2}
Root Height	h_r	L
Root Width	b_r	L
Tip Height	h_t	L
Tip Width	b_t	L

A product, π, of these variables will have the following form (Langhaar, 1980):

$$\pi = f(P, L, E, \rho, \sigma, h_r, b_r, h_t, b_t)$$

or;

$$\pi = P^{k1} L^{k2} E^{k3} \rho^{k4} \sigma^{k5} h_r^{k6} b_r^{k7} h_t^{k8} b_t^{k9}$$

where ki, $i = 1, \ldots, n$, denotes the exponent of the variable

The dimensions of π (denoted by brackets around the variable) must then be:

$$[\pi] = [F]^{k1}[L]^{k2}[FL^{-2}]^{k3}[FL^{-3}]^{k4}[FL^{-2}]^{k5}[L]^{k6}[L]^{k7}[L]^{k8}[L]^{k9}$$

$$[\pi] = [F]^{k1+k3+k4+k5}[L]^{k2-2k3-3k4-2k5+k6+k7+k8+k9}$$

Since π is required to be dimensionless; the exponents of each of the fundamental variables (F and L in this example) must be zero. Therefore, any solution to the following set of linear equations is a set of exponents in a viable dimensionless product π.

$$k1 + k3 + k4 + k5 = 0$$
$$k2 - 2k3 - 3k4 - 2k5 + k6 + k7 + k8 + k9 = 0$$

A century of research has provided us with several efficient methods to solve the above equations to obtain a combination of exponents that will provide useful sets of variables we can use to compare the equality of two systems. A completely similar system results when all π terms ($\pi_1, \pi_2, \ldots, \pi_N$) are the same for both the model and the product since a complete set of dimensionless products determines all dimensionless products of the given variables (Langhaar, 1980). Here we will use the echelon matrix

formulation (Barr, 1984; Murphy, 1950) to obtain a set of π terms for analysis of the stated tapered beam problem. The original dimensional matrix is shown in Table 2.2.

Table 2.2. Cantilevered Tapered Beam Dimensional Matrix

Fundamental Dimensions	P	L	E	ρ	σ	h_r	b_r	h_t	b_t
F	1	0	1	1	1	0	0	0	0
L	0	1	-2	-3	-2	1	1	1	1

Due to the choice of fundamental dimensions of F and L, the above matrix is already in Echelon form and we can therefore proceed with derivation of the π terms. From the matrix in Table 2.2. the following π terms are obtained:

$$\pi_1 = EL^2 / P \qquad \pi_5 = b_r / L$$
$$\pi_2 = \rho L^3 / P \qquad \pi_6 = h_t / L$$
$$\pi_3 = \sigma L^2 / P \qquad \pi_7 = b_t / L$$
$$\pi_4 = h_r / L$$

The dimensionless parameters, or π terms, containing the state of interest of the two systems can now be described explicitly in terms of the other dimensionless parameters as:

$$\pi_{m,x} = f\left(\pi_{m,1}, \pi_{m,2}, \ldots, \pi_{m,N-1}\right) = 0$$

$$\pi_{p,x} = g\left(\pi_{p,1}, \pi_{p,2}, \ldots, \pi_{p,N-1}\right) = 0$$

From this set of equations it can be said that $\pi_{m,x}$ and $\pi_{p,x}$ are identical, if $\pi_{m,i} = \pi_{p,i}$ for i = 1, 2, ..., *N-1*. As a result, the states of the model and the product can be correlated based upon the following derived equation:

$$\pi_{m,x}(Q_m) = \pi_{p,x}(Q_p)$$

or,

$$\pi_{i,m} = \pi_{i,p} \tag{2.2}$$

Equation (2.2) represents the prediction equation correlating a π term for the model with the same π term for the product. This correlation is only valid if the following equation is also true:

$$\pi_{m,i}(Q_m) = \pi_{p,i}(Q_p); \quad \forall i \tag{2.3}$$

This equation represents the similarity constraints that must be satisfied for the prediction equation to be valid. The prediction equation (eqn. (2.2)), coupled with the similarity constraints (eqn. (2.3)) form the fundamental basis of the TSM. In order to predict the state of a product using the above prediction equation, the model should be designed such that all of the similarity constraints are satisfied. If all the similarity constraints for a model-product pair are satisfied, the system is defined as non-distorted or well-scaled. If, however, any of the similarity constraints are not satisfied, the system is defined as distorted and the TSM may provide inaccurate predictions as a result.

Distortion of the model-product pair is defined simply as:

$$\pi_{i,m} \neq \pi_{i,p}$$

Often it is not possible or feasible to impose complete similarity in the model test of a product (Huntley, 1951). When one or more of the dimensionless products (i.e. π terms) is not equal for the model and product, distortion of the problem occurs. Distortion of the model can be caused by a number of phenomena including (Murphy, 1950):

- Unavailability of proper modeling materials
- Required model details may impose excessive fabrication costs or time
- Available testing equipment may not meet test requirements for similarity between model and product (e.g. wind tunnel speeds, temperatures, etc.)
- Failure to include critical problem variables in the analysis

As mentioned previously, the generality of dimensional analysis makes it an easy method to apply but also severely limits its application. The method is extremely susceptible to geometric, material, and boundary condition distortions between the model and the product. Such challenges make predictions using the TSM difficult and have caused the utility and reliability of scale testing results to be frequently challenged (Barr, 1984). Traditional dimensional analysis techniques for predicting the performance characteristics of a product can be greatly improved in both accuracy and domain of applicability by the infusion of empirical data, derived from specimen tests, into the equations that characterize the system parameters of interest. Advanced similarity methods are investigated in subsequent chapters, which overcome many of the constraints associated with the traditional methods, and provide increased analysis capability and improved insight into the phenomenon governing the problem.

Chapter 3

Theoretical Background

3.1 Introduction

Development of a systematic approach for the conceptual design of relative motion based products is the overall task at hand. A methodology is developed to accomplish this beginning with a thorough review of the current state of research in the supporting areas. This methodology is designed to systematically evolve a product, characterized by relative motion based functionality in the mechanical domain, through component combination and the utilization of material and structural compliance. The emphasis on compliance is required in order to maintain the functionality, which is dependent on the relative motion, required between product components.

Integral to this research is the advancement of the current state of similarity techniques to the point where they can be used as a viable analytical design tool providing both improved accuracy and range of applicability over traditional methods of dimensional analysis. The developed results will become an integral element of the effort flow analysis methodology.

The theoretical foundation for Traditional Similarity Methods (TSM) analysis was introduced in the previous chapter. Here the discussion continues with a detailed look at

the severe limitations imposed on the method and introduce the current state of advanced similarity based research methods. By attempting to fully understand the theoretical basis for the development of preceding methods we will be better equipped to overcome their constraints and limits of applicability.

3.2 Effort Flow Analysis

Effort Flow Analysis (EFA) as a design methodology has evolved from successful research into the graphical representation of the flow of forces through a system's components on the one hand and the infusion of design decision theory on the other hand (Jensen et al., 2000; Paul and Beitz, 1996). The result is the capability to iteratively extract useful but limited design information from the process based upon the guidelines, which define the framework of the problem at hand. The flow of forces through the components of a system was originally modeled using a technique know as a Force Flow Diagram (FFD).

Force Flow Diagrams are used to represent the transfer of force from the location(s) of force application, or input, to the product, through all components making up the product. The forces are mapped up to and including the location(s) where the force exits the product, typically into the object the product is operating on. The FFD uses nodes to represent each of the components of the product. The nodes are then connected by links, which represent the physical interfaces between the individual components. An attempt is made to arrange the diagram nodes such that the topology of the product is symbolically represented by the topology of the diagram, a technique that provides a visual mapping between the product components and the graphical representation of the same components.

The concept of using diagrams to model the flow of forces has been used in the past to enhance understanding through visualization of parameter gradients. Chow (Chow, 1978) used the force flow concept to visualize lines of force that converge in areas where geometric discontinuities exist, hence highlighting stress concentrations in structures. Juvenal and Marshek (Juvenal and Marshek, 2000) use the force flow concept to assist in visualizing the transfer of forces through machine elements. Sketches of the individual elements are complimented with lines representing the flow of the forces through the components. Steiner (Steiner, 1999) used flows to aid in quantification of the connectivity of component assemblies. He used interaction graphs to analyze the number of component interfaces and the mechanical strength of those interfaces to determine the degree of integration of an assembly.

The commonality between interaction graphs and FFDs rests in the representation of interfaces between components of an assembly. Force Flow Diagrams are concerned with the degree of freedom constraints of the interfaces between components, while interaction graphs are concerned with the number and strength of those interfaces.

The force flow concept applied in the framework of this research adapts the visualization insights afforded by the graphical depiction of force flows developed in the pursuit of other goals. Effort Flow Analysis is concerned primarily with representing the overall product and the flow of effort (forces and torques) between components at their interfaces. The basis for this adaptation of force flow analysis was first presented by Lefever (Lefever, 1995), and subsequently advanced by Jensen, *et al.* (Jensen et al., 2000).

The motivation behind constructing a FFD for a product is to develop a graphical depiction of the flow of forces through the products components for further analysis. The diagram offers insightful analysis into the products potential opportunities for component combination. The first step in developing a FFD is to separate the individual components and represent each as a node in the diagram. Next an "R" is placed on the links between components that have relative motion between the components. Two interfacing components will be considered to have relative motion between them if, during the operation of the device, all points on one component experience some degree of relative velocity with respect to any point on the other component. Once this step is completed, the diagram can be decomposed into groups of parts separated by "R's." These groups of components then become candidates for component combination.

Components within these created groups do not move with respect to each other for the specific operation modeled in the FFD. As a result, they are considered candidates for component combination unless combination is prohibited by functions that require separate materials or special assembly/disassembly operations. These two exceptions on component combination are directly related to the criteria set forth by Boothroyd and Dewhurst (Boothroyd et al., 1994) regarding the feasibility of combining components.

3.2.1 Example Application

As a demonstration of the insight provided by FFDs into the component combination potential of a product consider the stapler shown in Fig. 3.1. and analyzed by Lefever (Lefever, 1995). Original designs of this type consist of up to 24 components as shown in the component view of Fig. 3.2.

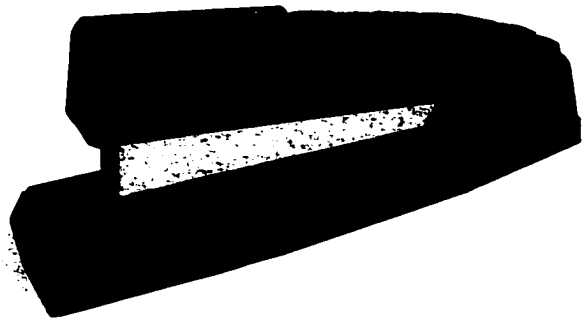

Fig. 3.1. Rendering of a Swingline™ Stapler Product.

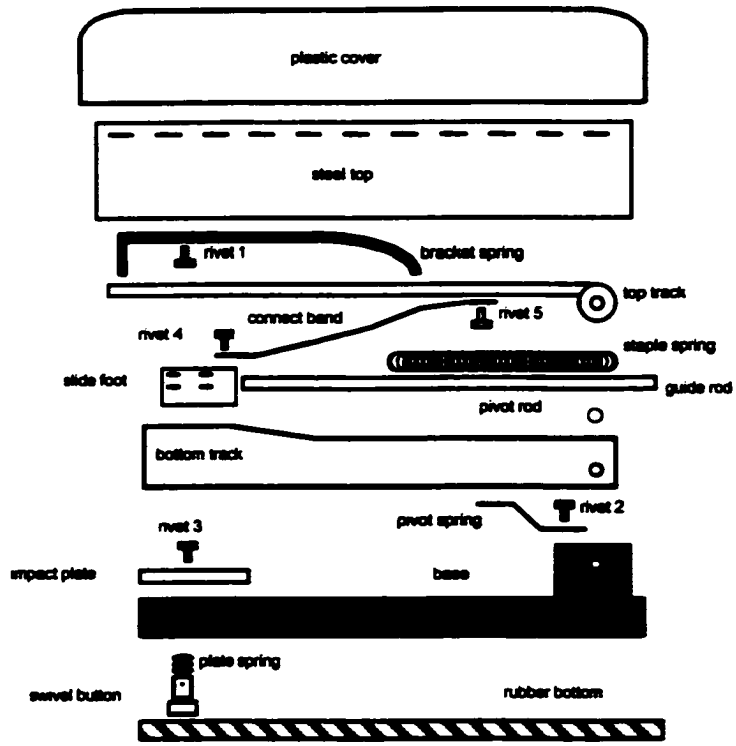

Fig. 3.2. Side View of Stapler Components.

A typical stapling operation involves the traceable transfer of forces through the products components (Lefever, 1995). Force is input to the system by a hand that pushes down on the plastic cover. This force is transferred to the steel top, rivet #1 and the

bracket-spring, to the top track, then to the bottom track. The force flow from the bottom track is now divided into two paths. One path goes through the pivot rod and pivot spring and finally into rivet #2 and the base, and out to an external supporting surface. The second path arises when the pivot spring is deflected enough to allow contact between the bottom track and the impact plate, then the force flows to the base and finally to the external supporting surface. When the upward reaction force between the impact plate and the bottom track overcomes the opposing bracket-spring force, relative motion between the bracket-spring and the top and bottom tracks arises. This motion allows the bracket-spring to push a staple out and onto the impact plate. In the meantime, the staple spring transfers force through the slide foot to the staples keeping the front staple in place and moving the next staple into place after the front staple has been displaced.

Force flow for this operation occurs through all components except the connection band and rivets 4 and 5, which are required for other stapler operations (e.g. reloading staples). The fact that these 3 components are not involved in this operation should be evident from the exclusion of the components from the completed FFD shown in Fig. 3.3.

The FFD shown in Fig. 3.3. is complete for the staple operation only. Similar diagrams are required for each of the product's operations to ensure the functionality of all component interactions are accurately captured. As the diagram shows, this operation leads to the isolation of 5 groups of components separated by "R" links. Each of these groups represents the potential for component combinations. For example, consider the components captured into group 1. It is conceivable that the plastic cover, the steel top, and the rivet could all be combined into a single component. This component could be a plastic top with snap fasteners for connection to the bracket-spring.

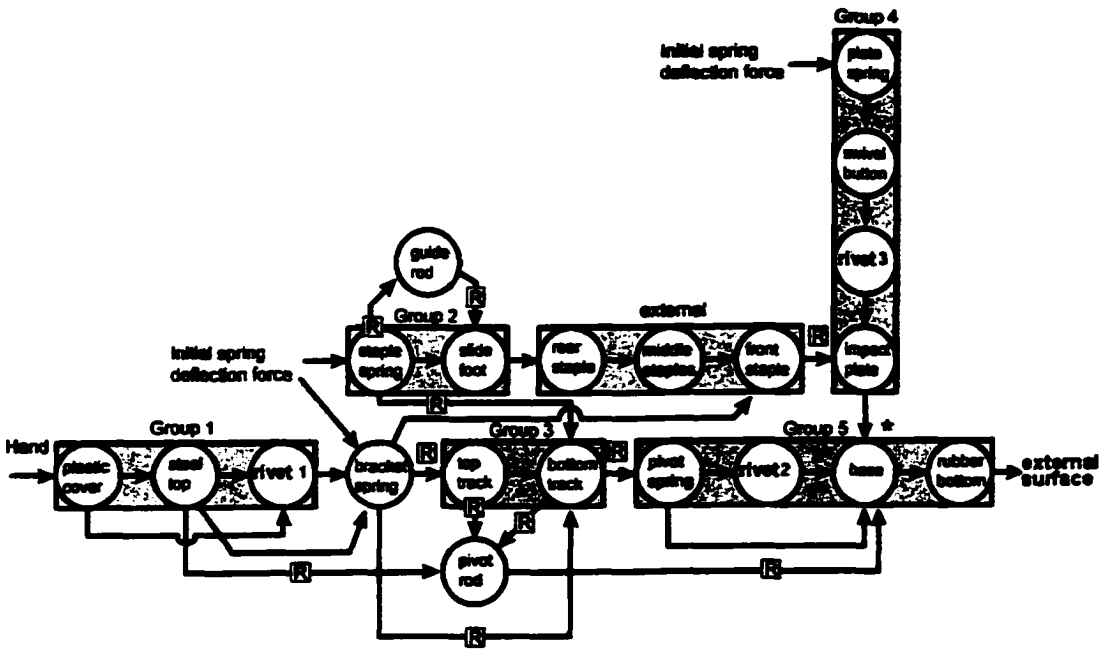

Fig. 3.3. Swingline™ Stapler Evaluated Force Flow Diagram

This combination of Group 1 components is a redesign that could be performed without affecting the functionality of the other components in the product. The next logical step is to consider the combination of individual components characterized by "R" interface links. Combination of these components means combining components that exhibit relative motion with respect to each other. Such combinations require a higher level of redesign, which is a main focus of this research.

3.3 Advanced Similarity Methods

Traditional dimensional analysis techniques for predicting the performance of system components can be greatly improved in both accuracy and domain of applicability by the infusion of empirical data, derived from material specimen tests, into the equations that characterize the system parameters of interest.

3.3.1 Foundations for the New Method

It has been observed from the review and application of the TSM that it can be very difficult to characterize the performance of a designed product by performing tests on a prototype model. This is often due to the severe constraints imposed by the required similarity conditions that are often impractical or impossible to satisfy. The recognized deficiencies of the TSM lead to the investigation of alternative methods to provide improved prediction accuracy and also to increase the range of applicability and/or decrease the constraints required for an accurate prediction. This section serves to establish a theoretical basis by reviewing the current states of both the TSM and new empirical similarity methods (ESMs) with the intent to identify specific areas where the methods are both successful and deficient. This will pave the way for the next advancement in the method, which will be covered in later chapters.

The primary parameters that influence the static performance of mechanical-domain products can be grouped into three distinct and yet broad categories:

- Material properties (e.g. density, elastic modulus, thermal conductivity)
- Geometrical characteristics (e.g. length, diameter)
- Boundary conditions (e.g. temperature, applied loads, constraints)

With an understanding of the underlying principles of the TSM it is reasonable to expect that through the correct combination of parameters in these three areas, which the TSM is often not able to do, the performance of a product can be accurately represented through the performance of a prototype model. It has been shown that through application of the TSM we can derive the correct expressions, in the form of π terms, to represent the model characteristics in terms of material properties, geometry, and boundary conditions required for a similar model-product system. A similar system is required by the TSM in order to be confident of accurately predicting the performance of a product from the measured state or states of a model. This process of transforming the state of a model, through the influential parameters described above, to the state of a product is shown graphically in Fig. 3.4.

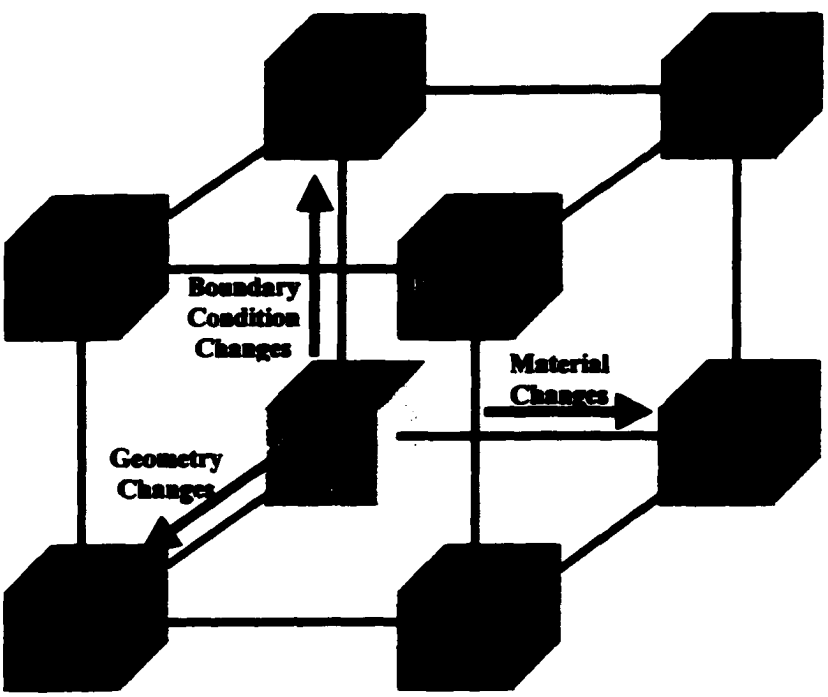

Fig. 3.4. Transformation from Model to Product

The analysis task, as in TSM, is to determine the transformation required to get from the model state to successful prediction of the product state. While the TSM uses a single multiplication factor or scale factor for this transformation, derived from the appropriate π term(s), the ESM takes a different approach.

The graphic representation of the relationship between the model and product shown in Fig. 3.4. depicts a relationship characterized by the material properties, geometry, and boundary conditions. In equation form this transformation is represented as follows:

$$Product = Model \times T(material properties, geometry, boundary conditions)$$

Where: T = Transformation between the model and product

However, It can be shown that the three factors included in the transformation "T" are not independent in the framework defined by the limitations of similarity set forth under the TSM. By way of an illustrative example, recall the π terms derived for the cantilevered tapered beam introduced in the previous chapter (see Fig. 3.5.):

$$\pi_1 = \frac{EL^2}{P} \qquad \pi_5 = \frac{b_r}{L}$$

$$\pi_2 = \frac{\rho L^3}{P} \qquad \pi_6 = \frac{h_t}{L}$$

$$\pi_3 = \frac{\sigma L^2}{P} \qquad \pi_7 = \frac{b_t}{L}$$

$$\pi_4 = \frac{h_r}{L}$$

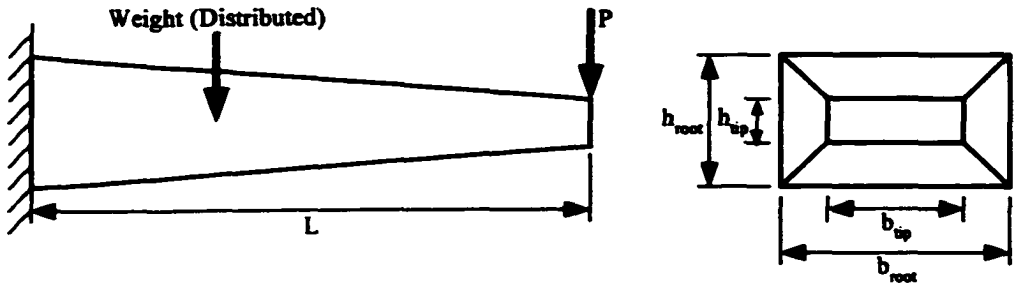

Fig. 3.5. Tapered Cantilevered Beam

Values of elastic modulus (*E*) and density (ρ) for the representative model are selected to correspond with the selected model material. An arbitrary model length is also selected. As a result, the terms π_1 and π_2 both specify the boundary condition in the form of the applied transverse load *P* acting on the end of the beam. In addition, by selecting the length of the model beam, the other dimensions of the beam are uniquely determined by the terms π_4 - π_7. As this example demonstrates, only two of the three-parameter groups need to be specified for a complete description of the system to be modeled.

Based upon this hypothesis of dependence of one of the above groups on the remaining two, the graphical representation of the functional relationship between the model and the product is modified as depicted in Fig. 3.6. The representation is simplified further by considering the overall goal of predicting the state of a product ($\bar{X}_p$) from the measured state of a model ($\bar{X}_m$) as shown in Fig. 3.7.

In Fig. 3.7., and in the ESM, the states are represented by vectors containing the measured or analytically determined and predicted (model and product, respectively) values of interest. These states are specific to the problem at hand and can be stress,

strain, deflection, temperature, etc. The vector quantities often include values at multiple points on or in the object of interest. In the following expression, the vector $\bar{X}_m$ represents the temperature at various points on the model as shown in Fig. 3.7.

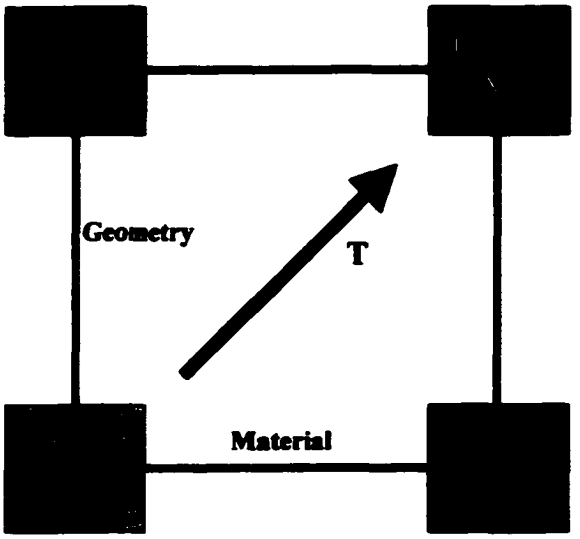

Fig. 3.6. Product a Function of Model Material and Geometry

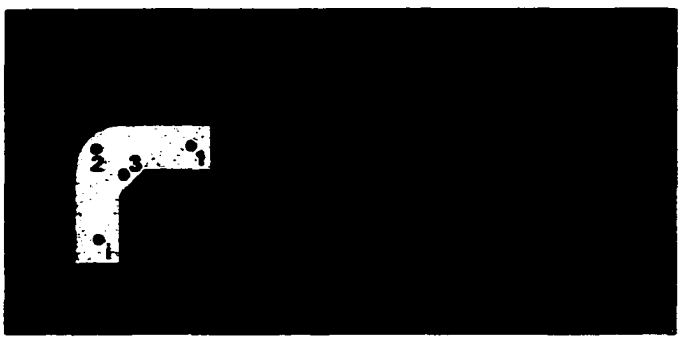

Fig. 3.7. Transformation from Model to Product

$$\bar{X}_m = \begin{bmatrix} T_1 \\ T_2 \\ T_3 \\ T_i \end{bmatrix}$$

The ESM (Cho et al., 1998) is viewed as a two-phase process that uses state vector transformations in two distinct parameter spaces, material ([*M*]) and geometry ([*G*]), to transform the state of a predictive model ($\bar{X}_m$) to that of a product ($\bar{X}_p$). In the derivation of the two transformations, they are assumed to be orthogonal and can therefore be considered independently. The orthogonal assumption allows the consideration of the material transformation independent of any complexities associated with the geometry. With this in mind the material transformation [*M*] can be determined by simplifying the geometry of the model and product through the introduction of representative specimens used specifically to derive the material transformation as shown in Fig. 3.8. The model and product specimens are constructed using the same materials, and the same processes where appropriate, as the model and product respectively.

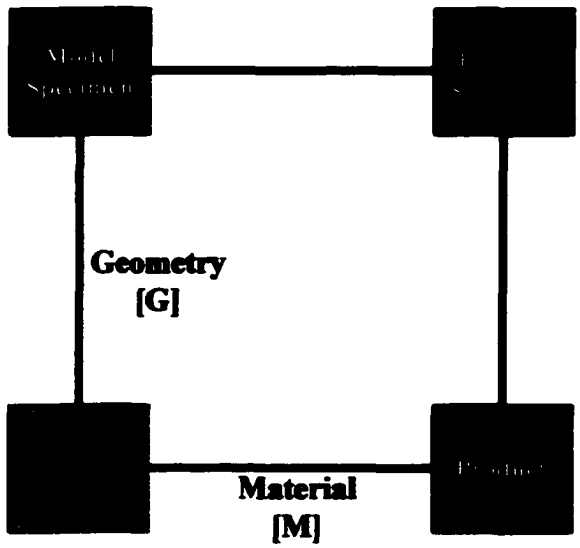

Fig. 3.8. Graphic Relationship Depiction between Specimens, Model and Product

Although research to envelope the degree of geometric similarity required between the specimen family and model-product family is ongoing, for the purpose of this research the geometric deviations are limited to product specimens that retain the same basic relative dimensions but do not require complex machining to manufacture. Thus the specimens, through their simplified geometry, afford a reduced effort alternative to fabrication of detailed prototypes. The specimens, model, and product are generally characterized as shown in Table 3.1.

Table 3.1. Specimen, Model, and Product Characteristics

	Geometry	Material/Process
Model Specimen	Simple	Expedient (e.g. RP)
Product Specimen	Simple	Product Material/Process
Model	Product Replica	Expedient (e.g. RP)
Product	Product Geometry	Product Material/Process

The ESM process is graphically depicted in Fig. 3.9. with its now four distinct vector states of parameter values ($\bar{X}_{ms}, \bar{X}_{ps}, \bar{X}_{m}, \bar{X}_{p}$) as shown below.

$$\bar{X}_{ms} = \begin{bmatrix} X_{ms,1} \\ X_{ms,2} \\ \vdots \\ X_{ms,J} \end{bmatrix} \qquad \bar{X}_{ps} = \begin{bmatrix} X_{ps,1} \\ X_{ps,2} \\ \vdots \\ X_{ps,J} \end{bmatrix}$$

$$\bar{X}_{m} = \begin{bmatrix} X_{m,1} \\ X_{m,2} \\ \vdots \\ X_{m,J} \end{bmatrix} \qquad \bar{X}_{p} = \begin{bmatrix} X_{p,1} \\ X_{p,2} \\ \vdots \\ X_{p,J} \end{bmatrix}$$

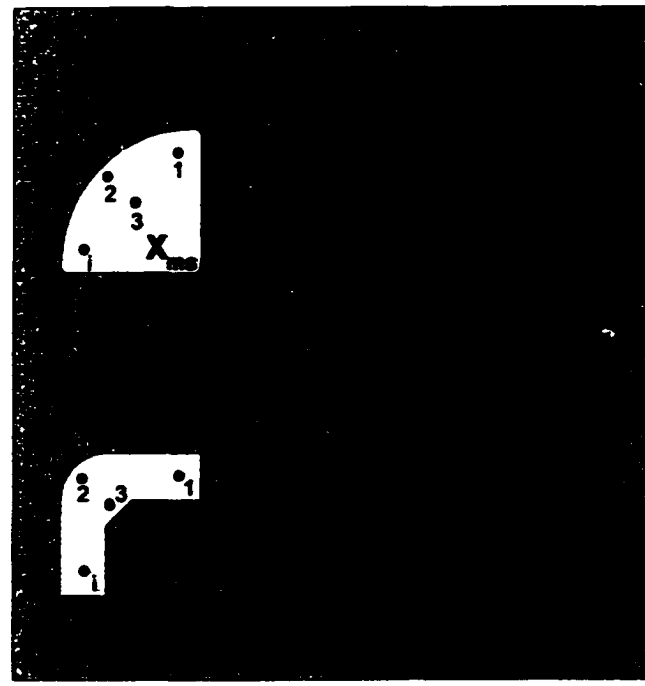

Fig. 3.9. Data Points and Transformation Matrices

The goal of the ESM is to be able to accurately predict the state of a product ($\vec{X}_p$) from the measured states of the model specimen, product specimen and model ($\vec{X}_{ms}$, $\vec{X}_{ps}$, $\vec{X}_m$) according to the following generic formulation:

$$\vec{X}_p = f\left(\vec{X}_{ms}, \vec{X}_{ps}, \vec{X}_m\right)$$

3.3.1.1 ESM Phase-1

This phase involves the analytical or experimental determination of the state(s) of a model specimen ($\vec{X}_{ms}$) and product specimen ($\vec{X}_{ps}$), manufactured from the model and product material respectively, to empirically abstract a geometry independent material

transformation matrix [*M*] (see Fig. 3.9.). The material transformation matrix [*M*] is also referred to as a *scale* matrix as a result of the identical geometrical shape, but potentially variable scale, of the specimen pair.

3.3.1.2 ESM Phase-2

This phase involves the analytical or experimental determination of the state(s) of a model specimen ($\vec{X}_{ms}$) and a product replica model ($\vec{X}_{m}$), both manufactured from the model material, to empirically abstract a material independent geometrical transformation matrix [*G*] (see Fig. 3.9.). The geometrical transformation matrix [*G*] is also referred to as a *form* matrix as a result of the intent of the matrix to capture the purely geometrical characteristics of the transformation. The ESM has resulted in the derivation of the following developed methods for the prediction of a product's performance (Cho et al., 1998):

- Psuedo-Inverse Method
- Circulent Matrix Method

3.3.1.3 Solution Paths

The Psuedo-Inverse and Circulent Matrix methods each contain two variant solutions that correspond to the two possible solution paths, Paths A and B, shown in Fig. 3.10.

Path A represents the process of using the phase-1 derived specimen *scale* transformation matrix [M] as an approximation for the desired *scale* transformation

matrix [M']. This transformation is applied to the model state vector ($\bar{X}_m$) for the prediction of the product state vector ($\bar{X}_p$) as follows:

$$\bar{X}_{ps} = [M]\bar{X}_{ms} \tag{3.1}$$

$$[M] = \bar{X}_{ps}\bar{X}_{ms}^{-1} \tag{3.2}$$

$$\bar{X}_p = [M']\bar{X}_m \tag{3.3}$$

$$\bar{X}_p \cong [M]\bar{X}_m \tag{3.4}$$

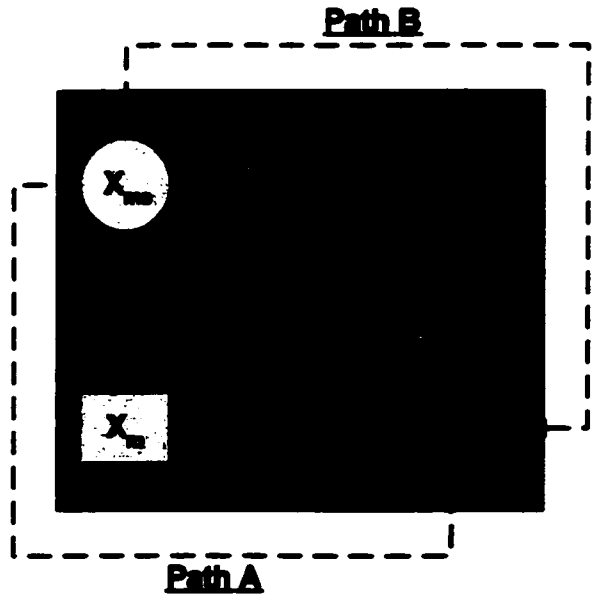

Fig. 3.10. Possible Solution Paths from $\bar{X}_{ms}$ to $\bar{X}_p$

Path B represents the process of using the phase-2 derived model *form* transformation matrix [G] as an approximation for the desired *form* transformation matrix [G']. This

transformation is applied to the product specimen state vector ($\vec{X}_{ps}$) for the prediction of the product state vector ($\vec{X}_p$) as follows:

$$\vec{X}_m = [G]\vec{X}_{ms} \tag{3.5}$$

$$[G] = \vec{X}_m \vec{X}_{ms}^{-1} \tag{3.6}$$

$$\vec{X}_p = [G']\vec{X}_{ps} \tag{3.7}$$

$$\vec{X}_p \cong [G]\vec{X}_{ps} \tag{3.8}$$

With this background as a foundation we now proceed to derive each of the methods and attempt an evaluation of each based upon their own merits, limitations, and ability to accurately predict the state of a product.

3.3.2 Psuedo-Inverse Matrix Approach:

As described above, two paths exist to numerically get from the state vector of the model specimen ($\vec{X}_{ms}$) to the state vector of the product ($\vec{X}_p$) as shown in Fig. 3.10. Equations (3.2) and (3.6) above provide the following derivations for the material and geometry transformations from the known vector states:

$$[M] = \vec{X}_{ps} \vec{X}_{ms}^{-1}$$

$$[G] = \vec{X}_m \vec{X}_{ms}^{-1}$$

However, the state vector $\bar{X}_{ns}$ is most often an n x 1 vector for which the inverse is not defined unless $n = 1$. We therefore propose a substitution for the inverse $[\bar{X}_{ns}^{-1}]$ with the psuedo-inverse $[\bar{X}_{ns}^{+}]$ defined as the n x 1 Moore-Penrose pseudo inverse (Strang, 1988) of $\bar{X}_{ns}$ where $\bar{X}_{ns}^{+} \equiv \left(\bar{X}_{ns}^{T}\bar{X}_{ns}\right)^{-1}\bar{X}_{ns}^{T}$. This substitution results in the following modified transformations:

$$[M] = \bar{X}_{ps}\bar{X}_{ns}^{+} \tag{3.9}$$

$$[G] = \bar{X}_{ns}\bar{X}_{ns}^{+} \tag{3.10}$$

Substitution of $\bar{X}_{ps}$ from eqn. (3.1) and $\bar{X}_{ns}$ from eqn. (3.5) into eqn. (3.8) and (3.4) respectively results in the following expressions representing the two solution paths A and B:

$$\bar{X}_{p} \cong [G]\cdot[M]\bar{X}_{ns}$$

$$\bar{X}_{p} \cong [M]\cdot[G]\bar{X}_{ns}$$

In order to maximize our confidence in the above equations predicting the solution state vector $\bar{X}_{p}$, as swell as verifying the initial assumptions of orthogonality between [M] and [G], the above expressions should provide equal results. Failure to provide equal results is a strong indicator that distortion in one or both of the paths, and thus in [M] or [G], is preventing convergence of the solution. In contrast, if the above equations provide the same result, the following expression will be true:

$$[G]\cdot[M]=[M]\cdot[G]$$

As a result the following transformation matrices are said to be approximately equal and the overall procedure, capturing the two possible solution paths, is presented in Fig. 3.11.:

$$[M]=[M']$$

$$[G]=[G']$$

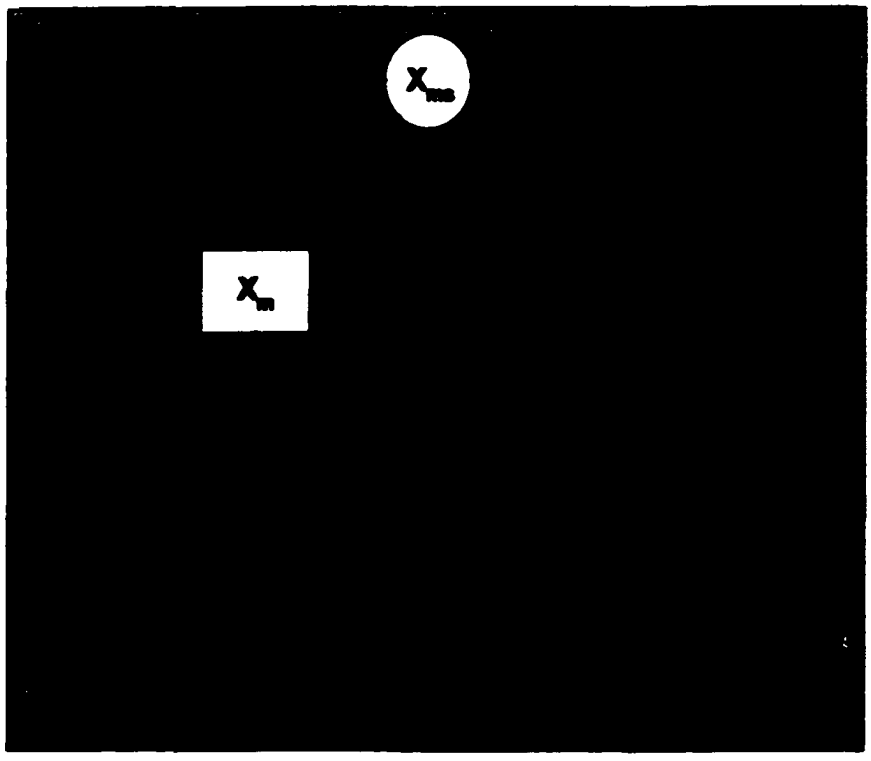

Fig. 3.11. Graphical Derivation of Product State Vector ($\bar{X}_p$)

This equality of transformation matrices indicates that either the specimen pair and the model-product pair have been designed in accordance with the same similarity laws

([M] = [M']) or they exhibit an equal degree of distortion. The chance that two different systems exhibit an equal degree of distortion is extremely unlikely due to the variations in geometry and loading conditions. Likewise the model family and the product family have also either been designed in accordance with the same similarity laws ([G] = [G']) or they also exhibit an equal degree of distortion, again, not likely. If we proceed with the derivation on this assumption we are soon faced with another problem characteristic of the Psuedo-Inverse method. Equations (3.2) and (3.6) define the *scale* and *form* matrices [M] and [G]. However, given state vectors $\bar{X}_{ms}$, $\bar{X}_{ps}$, and $\bar{X}_{m}$, each containing n elements or data points; we are presented with [M] and [G] matrices containing n^2 unknowns with only n equations available for their solution. The resulting matrices are not unique when n > 1 unless the number of columns in the state vectors $\geq$ the number of rows. The number of rows in the state vectors (designated n) typically represents the number of test points for the specimens and model and the number of points being predicted on the product. The number of columns in the state vectors (designated m) represents the number of specimens or individual specimen tests conducted. Up to this point we have assumed m = 1 and will continue with this assumption in the evaluation of each method to provide an equal basis for comparison.

To demonstrate this non-uniqueness consider the following derivation of the *scale* matrix [M] given arbitrary test data representing the temperature at corresponding points on the specimens:

$$\bar{T}_{ms} = \begin{bmatrix} 450 \\ 400 \\ 365 \end{bmatrix} \qquad \bar{T}_{ps} = \begin{bmatrix} 600 \\ 500 \\ 428 \end{bmatrix}$$

$$[M] = \vec{T}_{ps}\vec{T}_{ms}^{+} \qquad \text{where: } \vec{T}_{ms}^{+} \equiv \left(\vec{T}_{ms}^{T}\vec{T}_{ms}\right)^{-1}\vec{T}_{ms}^{T} \qquad \text{Reference: (Strang, 1988)}$$

$$[M] = \begin{bmatrix} 0.545 & 0.484 & 0.442 \\ 0.454 & 0.403 & 0.368 \\ 0.389 & 0.345 & 0.315 \end{bmatrix}$$

However, the following scale matrix is also a solution as are many others:

$$[M] = \begin{bmatrix} 0.5 & 0.5 & 0.476 \\ 0.1 & 1.0 & 0.15 \\ 0.5 & 0.5 & 0.0082 \end{bmatrix}$$

Thus far we have shown that the Psuedo-Inverse method is unable to derive unique *scale* and *form* transformation matrices from a single set of data points due to the undetermined nature of the derived transformation matrices. In order to satisfy the uniqueness criteria we would be forced to either add further problem constraints or require the optimization of an objective function. In addition, empirical tests conducted using this method have shown sensitivity to distortion which manifests itself in significant differences between the transformation matrices [*M*] and [*M'*] as well as [*G*] and [*G'*] from Fig. 3.10.

The ability of the method to predict the product state is dependent upon the similarity of these transformation matrices and any differences will have a direct impact on the accuracy of the prediction method. This leads to the conclusion that this method is susceptible to errors in predicting the state of a product. One way the issue of uniqueness could be alleviated is with additional sets of specimen and model test data. As we have seen, in order to obtain a unique solution the number of tests required would be equal to

or greater than the number of data points being investigated which would significantly reduce the efficiency of the method.

The inability to derive a unique form and scale matrix from a single set of data points is a significant hindrance of the Psuedo-Inverse method. As a result, a method is sought that will provide a unique transformation matrix from a single set of data.

3.3.3 Circulent Matrix Approach:

Cho, et al. proposed a modification to the state vectors ($\vec{X}_{ms}$, $\vec{X}_{ps}$, and $\vec{X}_{n}$) that converts them to their equivalent circulent matrices. There are two initial benefits to be gained in using this method based solely upon the mathematical formulation. First, the resulting derived transformation matrices [*M*] and [*G*] will be uniquely determined. Secondly, since the circulent state matrices are, by definition, square, the psuedo-inverse is no longer required as the matrix inverse is applicable in all cases where cir($\vec{X}_{ms}$) is invertible. The special properties of the circulent matrix result in a transformation matrix limited to just *n* unknown coefficients that can be solved uniquely. The circulent matrix is defined as follows:

$$\vec{X}=\begin{bmatrix} X_1 \\ X_2 \\ X_3 \\ \vdots \\ X_n \end{bmatrix} \rightarrow cir\left(\vec{X}\right)=\begin{bmatrix} X_1 & X_n & X_{n-1} & \cdots & X_2 \\ X_2 & X_1 & X_n & \cdots & X_3 \\ X_3 & X_2 & X_1 & \cdots & X_4 \\ \vdots & \vdots & \vdots & \ddots & \vdots \\ X_n & X_{n-1} & X_{n-2} & \cdots & X_1 \end{bmatrix}$$

By way of example, applying this to the state vector for the model specimen results in the following matrix:

$$cir\left(\bar{X}_{ms}\right)=\begin{bmatrix} X_{ms,1} & X_{ms,n} & X_{ms,n-1} & \cdots & X_{ms,2} \\ X_{ms,2} & X_{ms,1} & X_{ms,n} & \cdots & X_{ms,3} \\ X_{ms,3} & X_{ms,2} & X_{ms,1} & \cdots & X_{ms,4} \\ \vdots & \vdots & \vdots & \ddots & \vdots \\ X_{ms,n} & X_{ms,n-1} & X_{ms,n-2} & \cdots & X_{ms,1} \end{bmatrix}$$

By converting the state vectors to their equivalent circulent matrices we derive the *scale* matrix [*M*] as follows:

$$cir\left(\bar{X}_{ps}\right)=[M]cir\left(\bar{X}_{ms}\right) \tag{3.11}$$

$$[M]=cir\left(\bar{X}_{ps}\right)cir\left(\bar{X}_{ms}\right)^{-1} \tag{3.12}$$

A closer look into the coefficient manipulation provided by the circulent matrix application will increase understanding of the method and reveal how it is able to reduce the number of unknowns by a factor of *n*. We begin with generic state vectors for the model and product specimens and proceed through the formulation.

$$\bar{X}_{ms}=\begin{bmatrix} a \\ b \\ c \end{bmatrix} \qquad cir\left(\bar{X}_{ms}\right)=\begin{bmatrix} a & c & b \\ b & a & c \\ c & b & a \end{bmatrix}$$

$$\bar{X}_{ps}=\begin{bmatrix} d \\ e \\ f \end{bmatrix} \qquad cir\left(\bar{X}_{ps}\right)=\begin{bmatrix} d & f & e \\ e & d & f \\ f & e & d \end{bmatrix}$$

Substitutions of the above expressions into eqn. (3.11) leads to the following:

$$cir\left(\bar{X}_{ps}\right)=[M]\,cir\left(\bar{X}_{ms}\right)$$

$$\begin{bmatrix} d & f & e \\ e & d & f \\ f & e & d \end{bmatrix} = \begin{bmatrix} M_{11} & M_{12} & M_{13} \\ M_{21} & M_{22} & M_{23} \\ M_{31} & M_{32} & M_{33} \end{bmatrix} \begin{bmatrix} a & c & b \\ b & a & c \\ c & b & a \end{bmatrix}$$

Solving the above simultaneous equations for the coefficients of [*M*] reveals that the following equalities exist:

$$M_{11} = M_{22} = M_{33}$$

$$M_{21} = M_{13} = M_{32}$$

$$M_{31} = M_{12} = M_{23}$$

Through substitution of the above relations the following matrix formulation, consisting of 3 unknown coefficients in [*M*] and 3 equations available for their solution, is derived:

$$\begin{bmatrix} d \\ e \\ f \end{bmatrix} = \begin{bmatrix} M_{11} & M_{31} & M_{21} \\ M_{21} & M_{11} & M_{31} \\ M_{31} & M_{21} & M_{11} \end{bmatrix} \begin{bmatrix} a \\ b \\ c \end{bmatrix}$$

Returning to the previous example solved using the Psuedo-Inverse method; a solution is attempted using the Circulent Matrix method. Recall:

$$\vec{T}_{ms} = \begin{bmatrix} 450 \\ 400 \\ 365 \end{bmatrix} \qquad \vec{T}_{ps} = \begin{bmatrix} 600 \\ 500 \\ 428 \end{bmatrix}$$

$$cir\left(\vec{T}_{ms}\right) = \begin{bmatrix} 450 & 365 & 400 \\ 400 & 450 & 365 \\ 365 & 400 & 450 \end{bmatrix}$$

$$cir(\bar{T}_{ps}) = \begin{bmatrix} 600 & 428 & 500 \\ 500 & 600 & 428 \\ 428 & 500 & 600 \end{bmatrix}$$

From eqn. (3.12) above we derive the following transformation matrix:

$$[M] = \begin{bmatrix} 1.767 & -0.264 & -0.246 \\ -0.246 & 1.767 & -0.264 \\ -0.264 & -0.246 & 1.767 \end{bmatrix}$$

We have now derived a unique expression for the scale matrix [*M*] that represents a transformation from cir($\bar{X}_{ms}$) to cir($\bar{X}_{ps}$). Notice this [*M*] also satisfies the expression provided in eqn. (3.9), which used the Psuedo-Inverse method. Another benefit to the Circulent Matrix method is the flexibility to interchange the rows of the state matrices provided the correlation between elements of the two matrices is maintained. One other extremely important characteristic of the approach is that the two solution paths represented in Fig. 3.10. and Fig. 3.11. produce the same results. The mathematical basis for this observation is included below.

$$[M] = cir(\bar{X}_{ps})\, cir(\bar{X}_{ms})^{-1}$$

$$\bar{X}_p = [M](\bar{X}_m) = cir(\bar{X}_{ps})\, cir(\bar{X}_{ms})^{-1}(\bar{X}_m)$$

$$[G] = cir(\bar{X}_m)\, cir(\bar{X}_{ms})^{-1}$$

$$\bar{X}_p = [G](\bar{X}_{ps}) = cir(\bar{X}_m)\, cir(\bar{X}_{ms})^{-1}(\bar{X}_{ps})$$

$$\rightarrow cir(\bar{X}_{ps})\,cir(\bar{X}_{ms})^{-1}(\bar{X}_{m}) = cir(\bar{X}_{m})\,cir(\bar{X}_{ms})^{-1}(\bar{X}_{ps})$$

Multiplying each side of the equation by $cir(\bar{X}_{ms})$ results in the following expression:

$$\rightarrow cir(\bar{X}_{ps})(\bar{X}_{m}) = cir(\bar{X}_{m})(\bar{X}_{ps})$$

$$\bar{X}_{m} = \begin{bmatrix} a \\ b \\ c \end{bmatrix} \qquad cir(\bar{X}_{m}) = \begin{bmatrix} a & c & b \\ b & a & c \\ c & b & a \end{bmatrix}$$

$$\bar{X}_{ps} = \begin{bmatrix} d \\ e \\ f \end{bmatrix} \qquad cir(\bar{X}_{ps}) = \begin{bmatrix} d & f & e \\ e & d & f \\ f & e & d \end{bmatrix}$$

$$\rightarrow \begin{aligned} d(a)+f(b)+e(c) &= a(d)+c(e)+b(f) \\ e(a)+d(b)+f(c) &= b(d)+a(e)+c(f) \\ f(a)+e(b)+d(c) &= c(d)+b(e)+a(f) \end{aligned}$$

We can therefore conclude that the Circulent Matrix approach automatically satisfies the conditions required for the two transformations to converge upon the same solution. The accuracy of the method has yet to be addressed.

In contrast to the Psuedo-Inverse method, the Circulent Matrix method has demonstrated the ability to derive unique transformation matrices using a single set of data points. In addition, it has also been demonstrated that the method has an inherent ability to meet the conditions required for convergence of the two solution paths. The Circulent Matrix approach does require more complex matrix manipulations and a loss in intuitive comprehension of the process as a result.

3.3.4 Example Applications

Two examples of the above methods are presented. The first example provides a numerical study of the predicted deflection of a tapered cantilevered beam. The value of this example lies in the ability to exactly determine the actual deflections and thus provide an absolute measure of the accuracy of the methods. In this example the TSM is also analyzed for comparison with the advanced similarity methods. In the second example, empirical data for all four variants (model and product specimens, model and product) is presented for relative comparison of the advanced similarity methods. Due to the empirical nature of the presented data, the TSM is not considered.

3.3.4.1 Deflection of a Tapered Cantilevered Beam

This example provides a direct comparison between the prediction capabilities of the TSM and ESM. The example is provided to demonstrate both the limitations of the TSM as well as the potential of the ESM to overcome those limitations. The goal in this example is to predict the deflection of an aluminum, tapered, cantilevered beam, supporting both the weight of the beam and a transverse load acting in the vertical direction applied to the end of the beam as shown in Fig. 3.12. The specimens used for this problem are straight, cantilevered beams with similar loading configurations as shown in Fig. 3.13.

The geometry, loading conditions, and material properties for the model specimen (ms), the product specimen (ps), the model (m), and the product (p) are listed in Table 3.2.

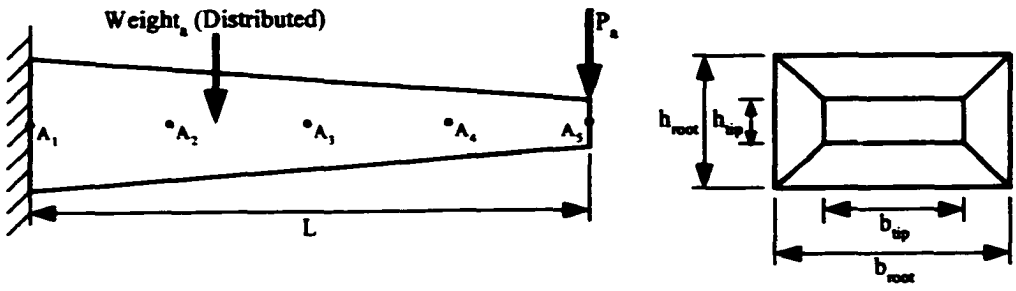

Fig. 3.12. Tapered Cantilevered Beam Geometry & Measurement Points

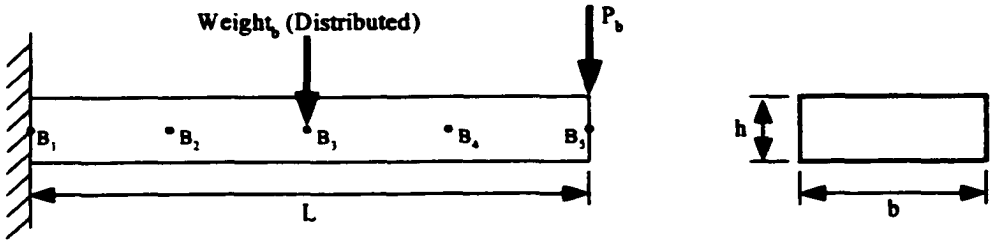

Fig. 3.13. Specimen Beam Geometry & Measurement Points

Table 3.2. Geometry, Loading, and Material Properties

	Model Spec	Product Spec	Model	Product
Load (N)	.54	50	.54	50
Modulus (GPa)	3.1	72.3	3.1	72.3
Density (kg/m^3)	1200	2783	1200	2783
Length (m)	.2	.2	.4	.4
Root Height – h_{root} (m)	.0032	.0032	.0095	.0095
Root Width – b_{root} (m)	.025	.025	.05	.05
Tip Height – h_{tip} (m)	.0032	.0032	.005	.005
Tip Width – b_{tip} (m)	.025	.025	.025	.025

Note the simplified geometry of the specimen beams shown in Fig. 3.13., which satisfies the goal of using specimens that are more easily manufactured than the often

geometrically complex model and product counterparts. The model family (model specimen and model) is fabricated using a representative rapid-prototyped polymeric material and process, again to suggest the potential of greatly reduced time and expense as compared to fabrication of a full-scale material and process specific product. The product family (product specimen and product) is fabricated using a material and process representative of the anticipated final design, machined aluminum in this example.

The parameters contained in Table 3.2 are not totally arbitrary but have been chosen in such a way as to maximize the similarity in the system subject to the constraints presented by the selection of the modeling material. Previous analysis has provided the following π term relationship among the geometry, material properties, and loading conditions for the model and product:

$$\pi_1|_m = \pi_1|_p \quad \rightarrow \quad \left[EL^2/P\right]_m = \left[EL^2/P\right]_p \tag{3.13}$$

Substitution of the material modulus of elasticity (E) and beam length (L) for both the model and product, and the transverse load applied to the product, results in the following specified load requirement for the model which has been included in the example:

$$P_m = P_p\left(\frac{E_m L_m^{\,2}}{E_p L_p^{\,2}}\right) = 50N\left(\frac{3.1x10^9\,Pa(0.2m)^2}{73.2x10^9\,Pa(0.4m)^2}\right) = 0.54\,N$$

The deflection of the beams will result from a combination of the applied loading and the distributed weight of the beam. From the information provided in Table 3.2. above, we can numerically calculate the theoretical deflection at any point along the length of

the beam through direct integration of the following moment and distributed load equations:

$$\frac{d^2y}{dx^2} = \frac{M(x)}{EI}$$
$$\frac{d^4y}{dx^4} = \frac{-w(x)}{EI}$$

where: $M(x)$ = Internal moment acting on the beam's cross section

$w(x)$ = Distributed load due to the beam weight

By arbitrarily selecting five equally spaced points along the neutral axis of the beams (see Fig. 3.12. and Fig. 3.13.) we derive state vectors representing discretized deflections for each of the four beam configurations as follows:

$$\bar{X}_{ms} = \begin{bmatrix} 0 \\ -0.59 \\ -2.16 \\ -4.37 \\ -6.89 \end{bmatrix} \qquad \bar{X}_{ps} = \begin{bmatrix} 0 \\ -18.6 \\ -67.6 \\ -137.0 \\ -216.0 \end{bmatrix}$$

$$\bar{X}_{m} = \begin{bmatrix} 0 \\ -0.014 \\ -0.059 \\ -0.141 \\ -0.257 \end{bmatrix} \qquad \bar{X}_{p} = \begin{bmatrix} 0 \\ -0.419 \\ -1.81 \\ -4.35 \\ -7.96 \end{bmatrix}$$

The predicted beam deflections as a function of the distance along the length of the beam using the TSM, Psuedo-Inverse (both path-A and Path-B solutions), and the Circulent Matrix methods are shown in Fig. 3.14. in relation to the theoretical beam deflection. The relative errors in each method, using the Chi-Square error measurement

method (Dally and Riley, 1991), are shown in Fig. 3.15 in comparison to the theoretical solution.

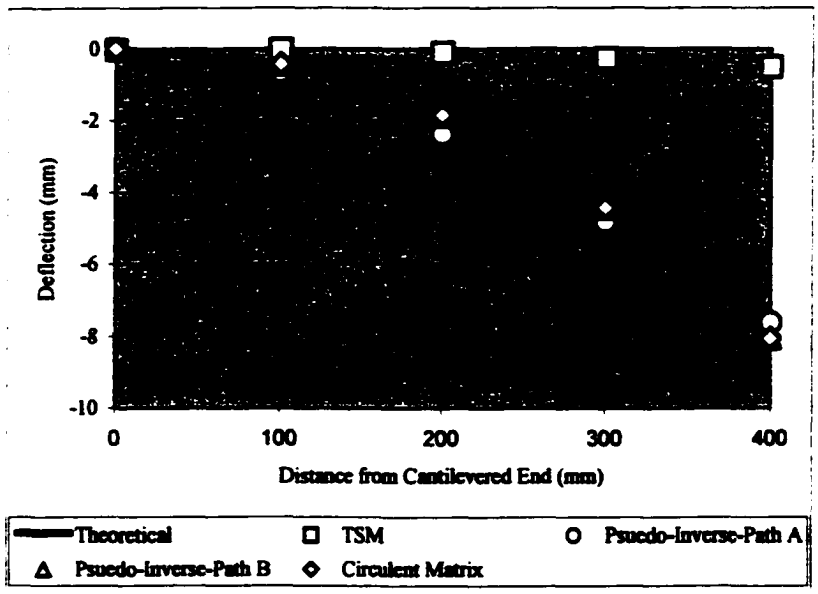

Fig. 3.14. Predicted Beam Deflection using TSM and Psuedo-Inverse Methods

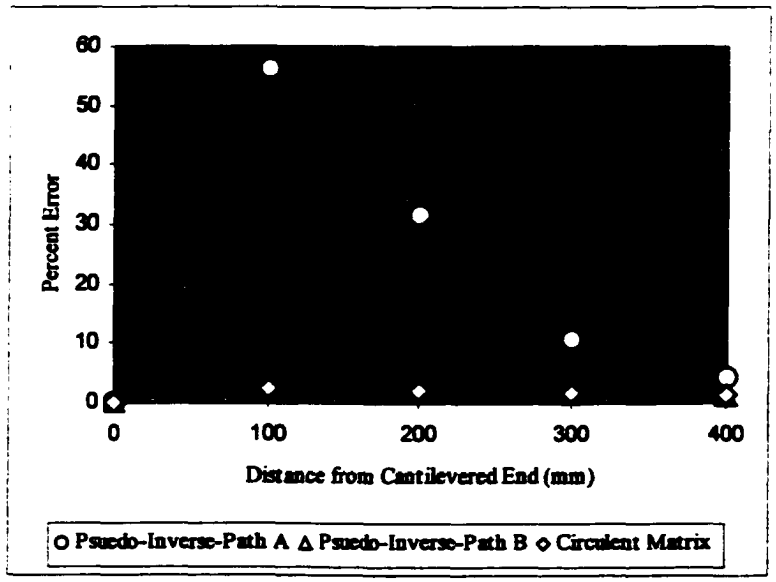

Fig. 3.15. Error in Predicted Beam Deflection

The relative error of the TSM was not included in Fig. 3.15. due to the large magnitude relative to the other methods as can be seen from the TSM predicted deflection curve of Fig. 3.14. As the figure clearly shows, the prediction of the beam deflection using the TSM results in substantial errors and is, therefore, not a valid approach for the solution of this problem. The Psuedo-Inverse method using the Path-A approach, although significantly better than the TSM, also results in significant errors. The Psuedo-Inverse Path-B and the Circulent Matrix approaches both show extremely good correlation with the theoretical deflection of the beam.

The error in the TSM can be attributed to distortion in the system caused by failure of the tests to satisfy the similarity constraints of eqn. (2.3). The source of the distortion could have been anticipated by considering the 2nd π term derived in the previous TSM analysis:

$$\pi_2|_m = \pi_2|_p \quad \rightarrow \quad \left[\rho L^3 / P\right]_m = \left[\rho L^3 / P\right]_p \tag{3.14}$$

Manipulation of the equalities presented in eqns. (3.13) and (3.14) leads to the following constraining ratios required for similarity between the model and product:

$$\left[E / \rho L\right]_m = \left[E / \rho L\right]_p$$

Given a model and a product with the same scale, the above constraints cannot be satisfied with the materials selected for this example due to the inequality of E/ρ for the model versus the product. The error was, therefore, anticipated. In contrast, the ESMs provide increased prediction accuracy with the Circulent Matrix method resulting in the least error.

In the development of the current ESMs, it is recognized that two paths exist to get from the state of the model specimen ($\bar{X}_{ms}$) to the state of the product ($\bar{X}_p$) as shown in Fig. 3.10. It is assumed that the paths produce identical results based upon the assumption that the specimen pair and the model-product pair are designed according to the same similarity constraints and, therefore, that $[M] = [M']$ and $[G] = [G']$. As the above example has shown, satisfying all the similarity constraints is often not feasible and the inclusion of polymeric materials and complex geometry only serves to increase the difficulty in obtaining a non-distorted system. The recognized distortion in a system invalidates the assumption that $[M] = [M']$ and $[G] = [G']$ and, therefore, the assumption that the two solution paths produce identical results. Research to date has shown varying degrees of inconsistency in the degree of accuracy capable with the different ESMs (Cho, 1999).

3.3.4.2 Steady-State Thermal Conduction Problem

In this experimental example, conducted by Cho (Cho, 1999), the results of an empirical study of the prediction of the thermal conduction of a product is presented. The prediction is based upon the measured temperatures of a model and specimen pair at corresponding points within the objects as shown in Fig. 3.16. The state vectors representing the measured temperatures of the four variants (model specimen, product specimen, model, and product) are shown below. The prediction results for the Psuedo-Inverse method (both Path-A and Path-B solutions), and the Circulent Matrix method are shown in Fig. 3.17. The relative error in each of the methods compared to the actual measured temperatures of the product is shown in Fig. 3.18.

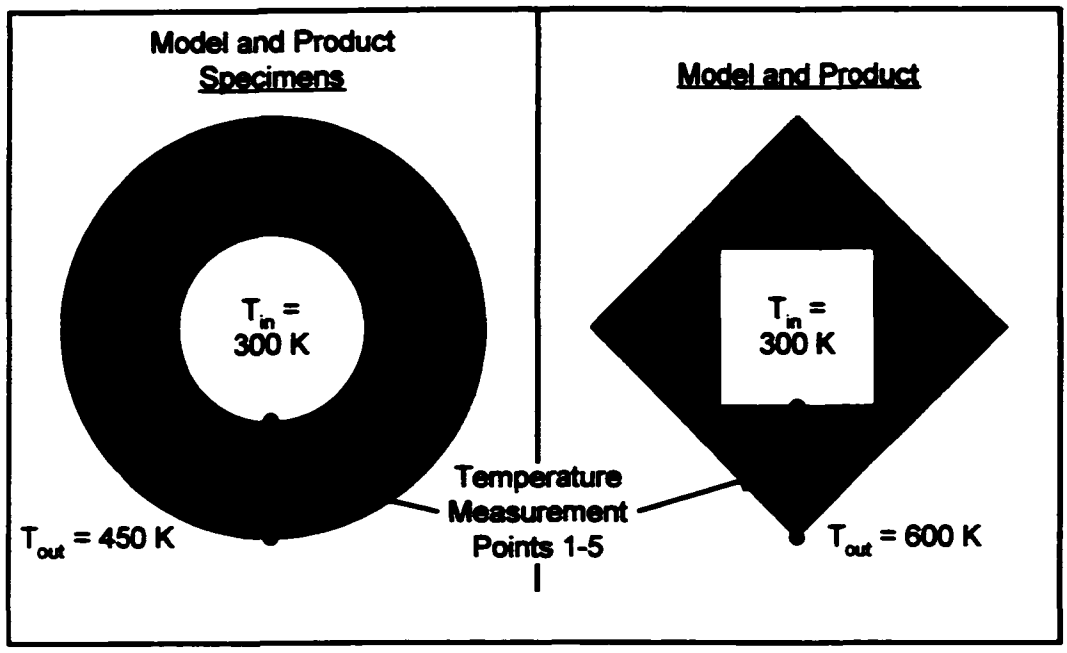

Fig. 3.16. Specimen, Model, and Product Test Conditions

$$\bar{T}_{ms} = \begin{bmatrix} 300 \\ 330 \\ 365 \\ 400 \\ 450 \end{bmatrix} \quad \bar{T}_{ps} = \begin{bmatrix} 300 \\ 360 \\ 428 \\ 500 \\ 600 \end{bmatrix}$$

$$\bar{T}_{m} = \begin{bmatrix} 300 \\ 306 \\ 333 \\ 378 \\ 450 \end{bmatrix} \quad \bar{T}_{p} = \begin{bmatrix} 300 \\ 312 \\ 365 \\ 460 \\ 600 \end{bmatrix}$$

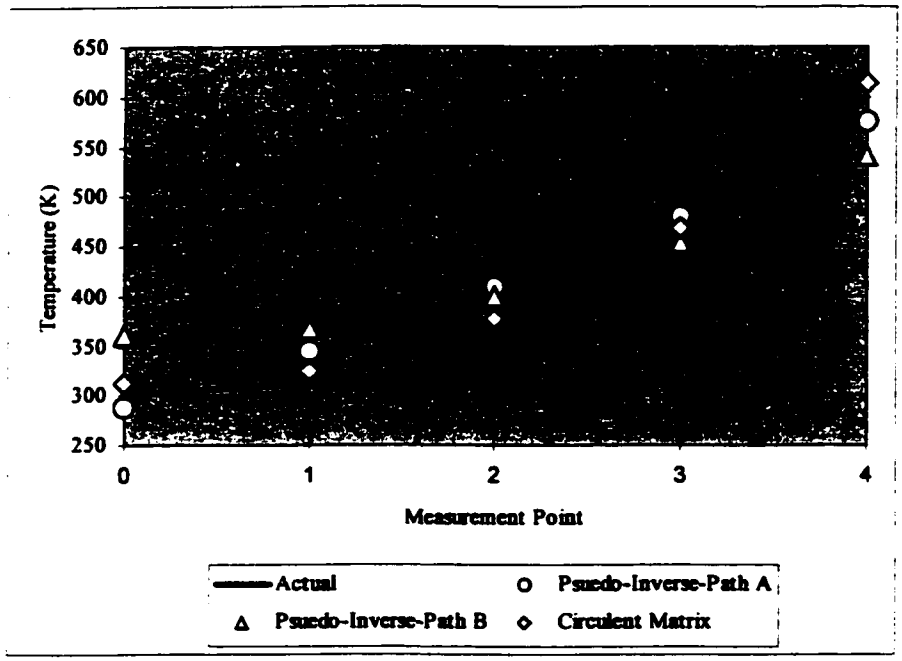

Fig. 3.17. Product Temperature Predictions

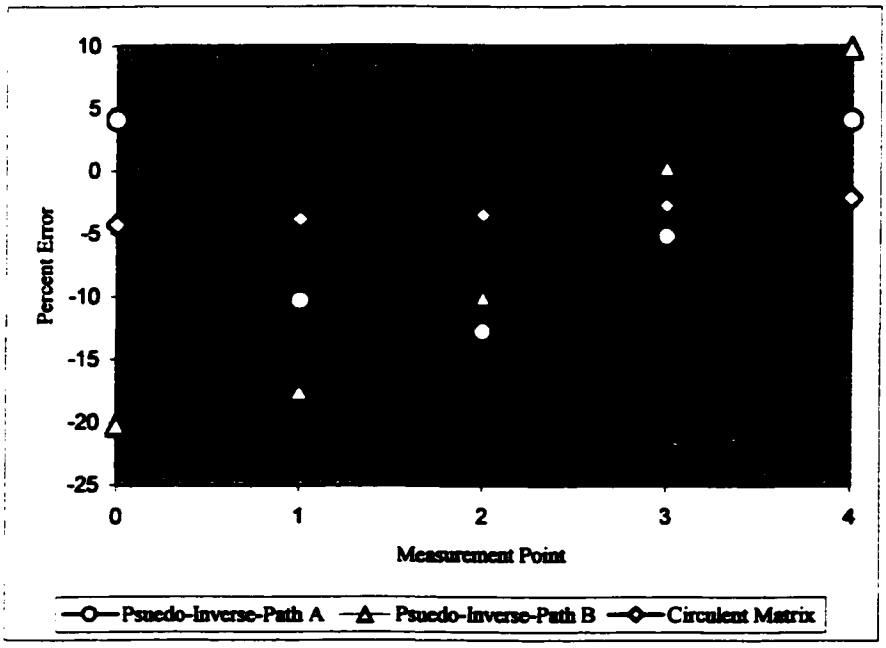

Fig. 3.18. Error in Prediction Methods

As Fig. 3.17. and Fig. 3.18. demonstrate, the temperatures predicted by the Circulent Matrix method are significantly more accurate than either of the Psuedo-Inverse methods. In addition, from this example we again see that the two solution paths for the Psuedo-Inverse method do not converge to the same solution indicating the method suffers from an inability to adequately deal with the system distortion. The Circulent Matrix approach, while proving to be the most accurate of the methods shown, suffers from complex and less than insightful mathematical formulations. While distortion in the system is recognized, we seek a method that will allow a quantification of the degree of distortion to enable the determination of the accuracy of the prediction results without *a priori* knowledge of the product performance.

Chapter 4

Effort Flow Analysis

4.1 Introduction

Effort flow analysis (EFA) is a graphically based design methodology that leads to the directed evolution of products. This is accomplished through the application of design guidelines that are developed specifically to promote product component combinations. Design evolution, in the context of this study, is defined as a change in the design of a product characterized by a reduction in the number of components comprising the original product.

Observation of the products investigated in the course of this research has concluded that the reduction in components is often accompanied by the inclusion of compliant materials in place of rigidly connected components. The compliant replacement is often required to maintain component relative motion without sacrificing product functionality. Component combination opportunities are identified by the EFA method through the graphical modeling of products using an effort flow diagram (EFD). An EFD is a graphic representation of the product components and connecting interfaces as a function of the operations performed by the product.

Solutions to the identified component combination opportunities come predominantly from the domain of compliant mechanisms, but rigid body mechanisms are also considered. Effort flow analysis involves using the EFD in combination with established and derived design guidelines to effect potential changes in the product resulting in an "evolved" design.

4.2 Background

The fundamental goal of product development is to create a product that satisfies the needs of a customer. The drive to continue satisfying customer needs leads to efforts toward product improvement. Even mature designs change to meet new customer needs, to attract new customers, or to take advantage of new materials (Ullman, 1997). This improvement process is a part of the life cycle of the product. The Theory of Inventive Problem Solving (TIPS) suggests that the product life cycle consists of birth, growth, maturity, and decline, or more simply, evolution (Altschuller, 1984). Effort flow analysis is a methodology geared toward the task of directed product evolution in the birth, growth, and maturity phases of this life cycle.

The successful design of an evolutionary product could conceivably be achieved by other design methods as well. There are many design process avenues that could provide results equivalent to that of the EFA methodology presented herein. Modern design methods provide a formal process involving steps or phases aimed at breaking down the design process into manageable and identifiable sub-tasks. Ullman (Ullman, 1997) identifies the following five-steps in his design process:

- Understanding the Problem/ Development of Engineering Specifications

- Concept Generation
- Concept Evaluation
- Product Generation
- Product Evaluation

Ulrich, et al. (Ullrich and Eppinger, 1995) proposes the following similar steps in his Concept Development phase of design:

- Identify Customer Needs
- Establish Target Specifications
- Analysis of Competitive Products
- Concept Generation
- Concept Selection

Other engineering design authors (Dieter, 1991; Otto and Wood, 2001; Paul and Beitz, 1996; Pugh, 1991; Schregenberger, 1998) propose similar structured approaches to design. The uniqueness of the EFA approach comes from its graphical decomposition of both the components and the connecting interface links. The method could rightfully be promoted as a specific method of concept generation for the redesign of existing products. The specificity comes from the directed evolution of products based solely upon the reduction of components through combination and the infusion of compliant materials and structures to effect the successful combination. The efficiency of the EFA method lies in the ability to derive concepts from the graphical component representation of the baseline product.

4.3 Effort Flow Analysis Methodology

Effort flow analysis is a systematic method for facilitating directed product evolution. Product evolution is accomplished by identifying component combination opportunities made available through the substitution of both rigid body and compliant mechanisms for existing product components. The products of interest for this research come from the domain of mechanical effort transmissions. In this study, the term mechanical transmission is defined to be any device that transmits mechanical force or torque. Effort flow analysis is the evolution of a technique originally known as force flow analysis (Jensen et al., 2000; Lefever, 1995; Lefever and Wood, 1996; Otto and Wood, 2001). The overall EFA process is graphically represented in Fig. 4.1. through Fig. 4.3.

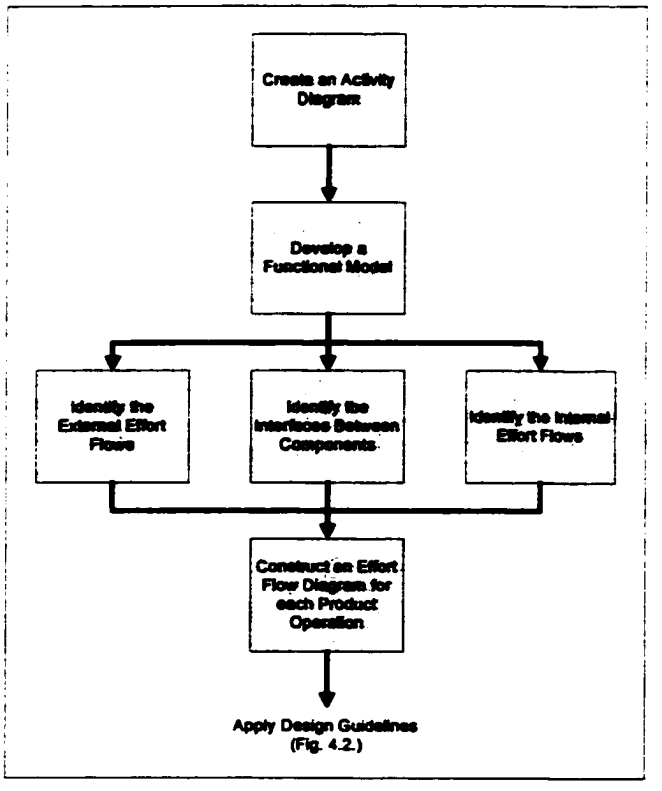

Fig. 4.1. Effort Flow Analysis Diagram Construction

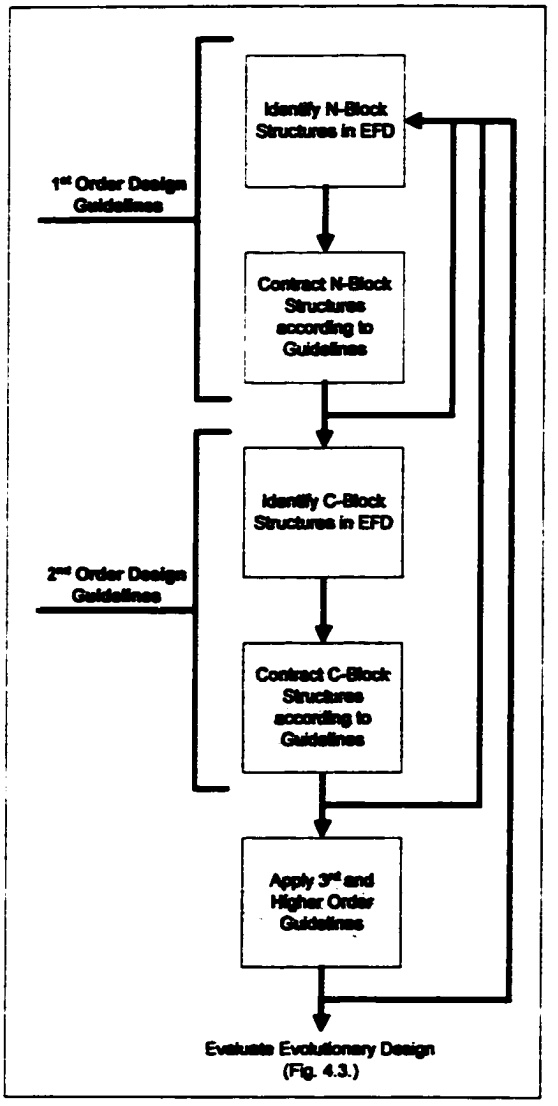

Fig. 4.2. Effort Flow Analysis Design Guideline Application

The process begins with identification of influential product operations through the construction of an activity diagram. Functional modeling of the product components follows this in an attempt to capture the functionality contained in the baseline product component architecture. Finally we proceed with the information derived from the activity diagram and functional model to the development of an EFD.

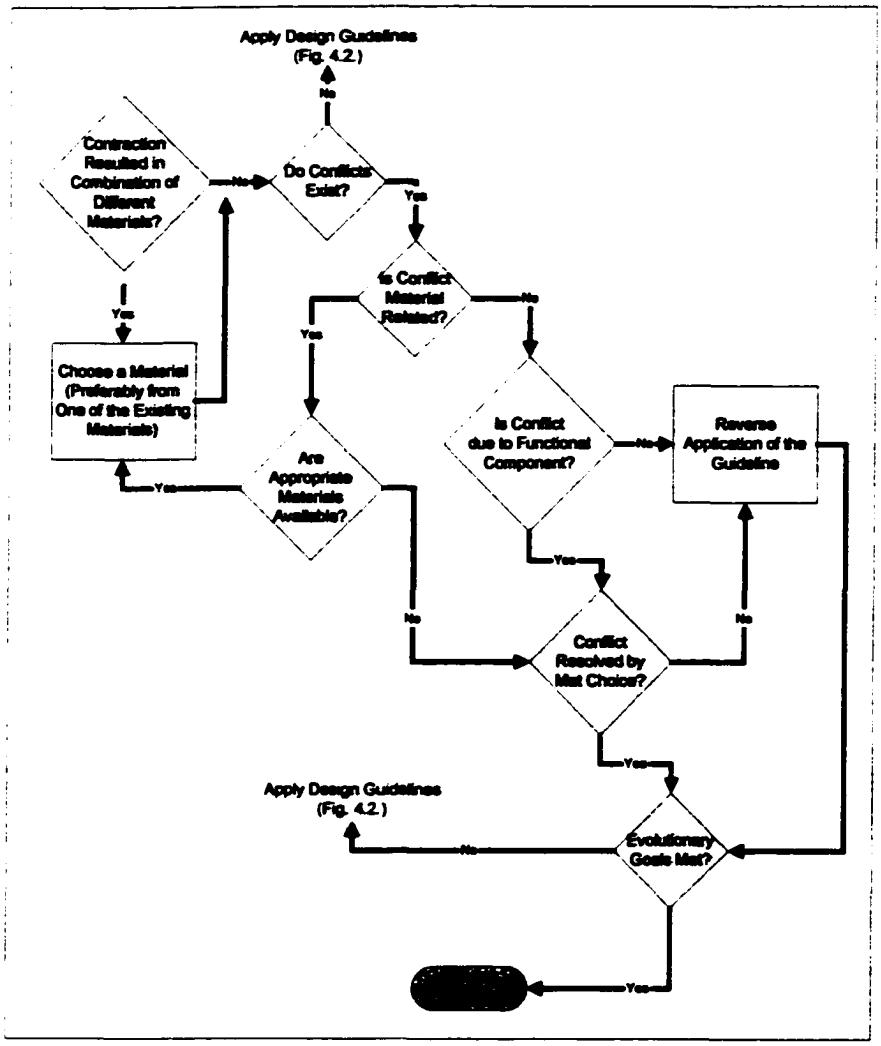

Fig. 4.3. Effort Flow Analysis Evolutionary Design Evaluation

Once the product is modeled in an EFD, potential component combination opportunities can be identified. These opportunities become apparent during characterization of the relative motion at the interfaces between components. These interface characterizations; coupled with the structure of the graph, lead the designer to apply particular design guidelines for the evolutionary design of the product of interest. Effort flow analysis uses an effort flow diagram to model the transfer of effort (force and/or torque) through the components of a product. The EFD is a semantic network

composed of nodes and links that are described using the fundamentals of graph theory (Harary, 1969; TSAI, 2000).

To facilitate the description of the EFA methodology we introduce a wire stripper product pair, consisting of a baseline design and an evolved design as shown in Fig. 4.4. Each of these product variants performs the same primary function of removing the external insulated coating from a wire. The purpose of this example is to demonstrate the utility of the method in identifying component combination opportunities based upon the graphical structures of the components and connecting interfaces. The example is not exhaustive in terms of presenting a complete EFA leading to the evolved product but does provide the basic structure and process of the method.

Fig. 4.4. Original (Baseline) and Evolved Wire Stripper Products

4.3.1 Activity Diagram

Operation of the different functions of the products and knowledge of the logistical aspects involved in bringing the product to the market allows the generation of an operational activity diagram. An activity diagram identifies the specific ways in which the product will be used, or operated, and leads to identification of the operations to be modeled in the EFD. An activity diagram for the wire stripper is shown in Fig. 4.5. where the shaded activities denote infrequent operations, which do not have significant influence over the design of the product and, as such, are not included in the EFD and subsequent EFA.

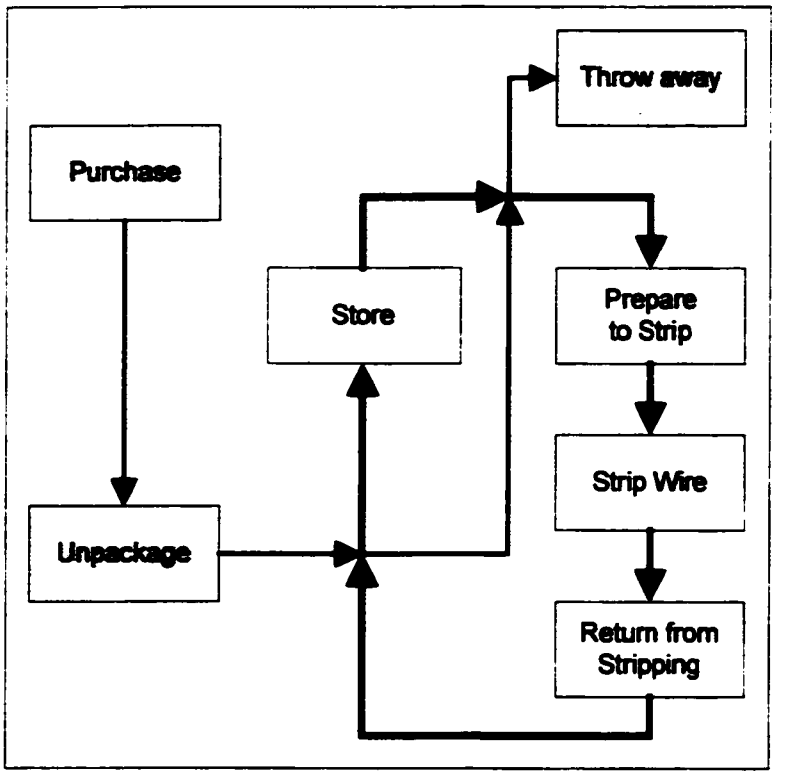

Fig. 4.5. Wire Stripper Activity Diagram

4.3.2 Functional Model

Development of a functional model, or function structure, for the baseline product can be an invaluable tool for understanding the component-level functions that are required for the product to function in its intended capacity. One or more of the components making up the product must perform each of the functions shown in a function structure. The functional elements of a product are the individual operations and transformations that contribute to the overall performance of the product (Ullrich and Eppinger, 1995).

Through functional modeling we gain confidence in our comprehension of the multi-layer functionality of the baseline product and assurance that through the evolutionary design process no loss in functionality will result. For further discussion of the insights afforded through functional modeling the reader is referenced to Otto (Otto and Wood, 2001). The functional model for the baseline wire stripper is shown in Fig. 4.6.

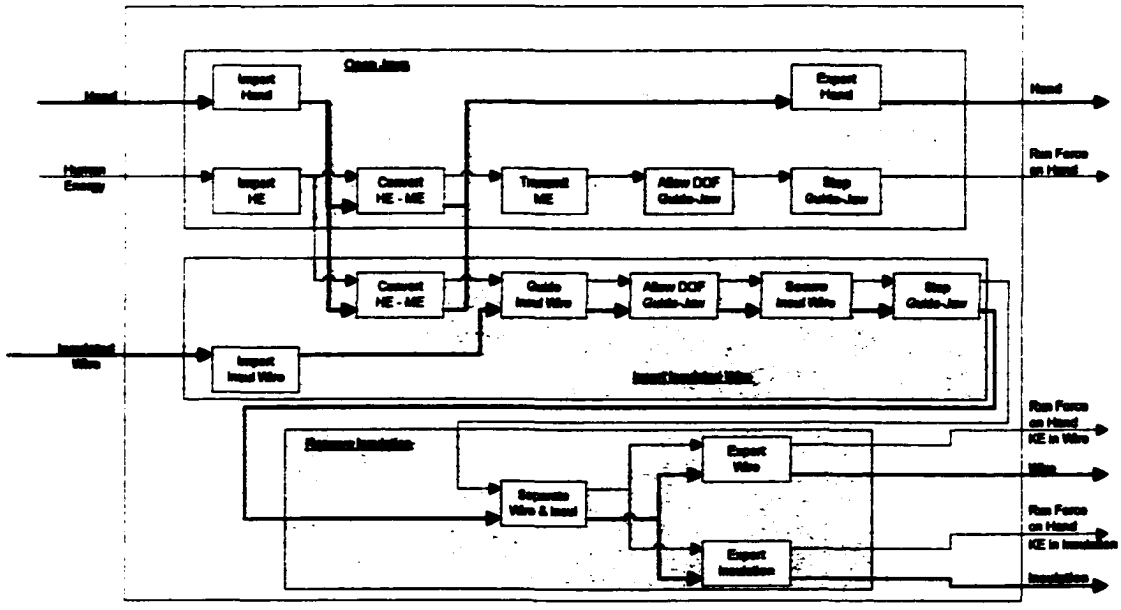

Fig. 4.6. Wire Stripper Functional Model

4.3.3 Effort Flow Diagrams

4.3.3.1 Component Nodes

Nodes on the EFD represent the components of the product. Whenever possible, nodes are organized in such a manner that they mimic the general topology of the product. While less critical for products with relatively few components, this technique has proven exceedingly beneficial as the number of components increases. The nodes for the baseline wire stripper are shown, organized in this fashion, in Fig. 4.7.

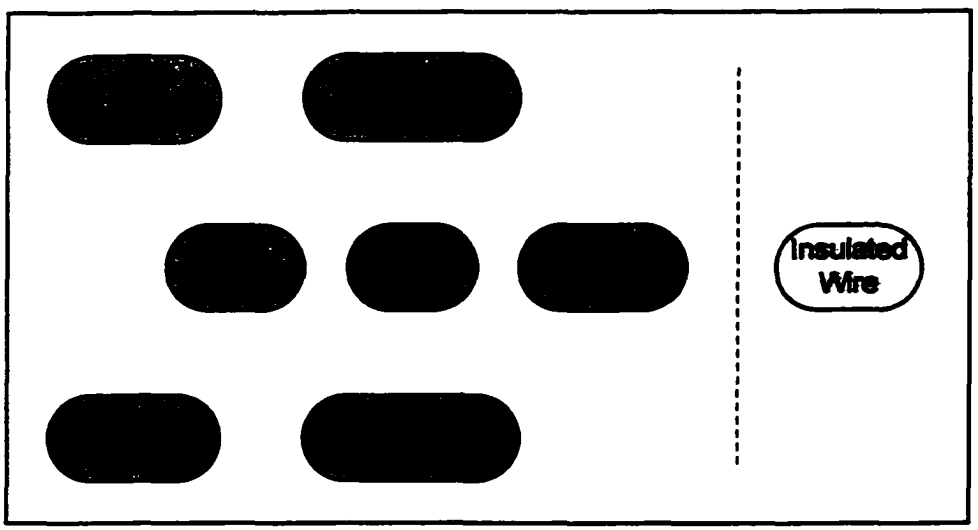

Fig. 4.7. Wire Stripper Node Configuration

As the diagram shows, the baseline design is comprised of seven individual components. For completeness, the object the product is operating on is also shown, the insulated wire in this example. The reason for this is to avoid loosing insight into the relationship existing between the product components and the interface(s) with the external environment.

4.3.3.2 Interface Links

The diagram links represent the interfaces between the product components. An EFD maps the flow of effort from the input interface(s), through all the affected components, to the output interface(s) for each of the product's operations. The links connecting the components act as the conduit to graphically represent this transfer of effort between components. The fundamental information needed to carry out effort flow analysis on a product is captured in the interface description contained in the links and in their designations. This information set includes, at a minimum, the type of relative motion, the direction of the effort flow, and the operation with which the effort is associated. For example, the link designation $R_{1\text{-}2}C_3$ between two components signifies an R-Link with a positive direction for operation 1, an R-Link with a negative direction for operation 2, and a C-Link with a positive direction for operation 3. The interfaces are characterized based upon the absence, presence, or degree of relative motion that exists between the connected components. The set of possible relative motion types as well as the naming convention adopted to describe each possibility is shown in Table 4.1.

Table 4.1. Table of Relative Motion Permutations

	Relative Motion Location		
Link Type	Between Interfaces	Between Components	Description
N-Link	0	0	No relative motion either at the interface or between the components
C-Link	0	1	Relative motion between the extents of the components but not at the interface
R-Link	1	1	Relative motion both at the interface and between the components
I-Link	1	0	Relative motion at the interface only

Because this set spans all possible combinations of relative motion in mechanical transmissions, and because the members of this set are orthogonal, the set is referred to as a *basis for relative motion* in EFA. The next step in constructing the EFD is the inclusion of these connecting links in the node diagram of Fig. 4.7. The links are assigned according to the relative motion between respective components for the operation under consideration. In this study, an interface is defined as:

A spatial region where energy and/or material flow between components or between a component and the external environment. (Van wie et al., 2001).

This definition of an interface does not include the spatial or structural aspects that have been used by other researchers (Howell, 2001). In EFA, the focus is on the energy flow; one of the triad of fundamental functional flows: material, energy, and information (Otto and Wood, 2001). While a complete description of an interface is important in general design analysis, it is not necessary, nor is it warranted, to meet the goal of EFA, which is to describe as simply as possible the existence and fundamental relative motion characteristics of an interface. The link types possess a hierarchy of relative complexity. This hierarchy becomes critical during procedures performed on the EFDs to effect component combinations based upon the link designations in the graph structures. A recognized value of EFA is in the understanding and manipulation afforded by the characteristics of the links as described below.

N-Link

The N-Link is characterized by the absence of relative motion between the components connected by the link. In other words, the two components are prevented from moving with respect to each other by some aspect of the design. Fasteners, friction,

or a number of other constraining mechanisms could be responsible for the constraint of the components. This link type represents the least complex combination opportunity since the connected components exhibit no relative motion. As such, the N-Link is considered the lowest in the link hierarchy and considered a 1st order combination opportunity.

C-link

The C-Link is characterized by the absence of relative motion at the link interfaces with the components but exhibiting relative motion between the components themselves. The most common example of a C-Link is a spring. A spring is typically secured to each of the components but allows the components to move with respect to each other. Components connected by C-Links are prime candidates for combination through the infusion of compliant members, which can act to preserve the functionality provided by the C-Link in the original design. This link type represents a more complex combination since the connected components do require relative motion to perform their intended function. As such, the C-Link is considered higher, or more functionally restrictive, than an N-Link in the link hierarchy. This means components connected by both N and C-Links must meet the requirements of the original C-Link to be candidates for successful combination. C-Links are considered 2nd order combination opportunities.

R-Link

The R-Link is characterized by relative motion both at the link interface with the components and also between the components themselves. A common example of an R-Link is a hinge where the two hinge halves move with respect to each other including the

interface where the two are connected. Components connected by R-Links are candidates for combination through the creative use of compliant materials and structures which can act to preserve the functionality provided by the R-Link in the original design. This link type represents a complex combination, dependent on the degree of relative motion required, since the connected components do require relative motion to perform their intended function. As such, the R-Link is considered higher, or more functionally restrictive, than either the N or C-Link in the link hierarchy. This essentially means that components connected by both R and C or N-Links must meet the requirements of the original R-Link to be candidates for successful combination. R-Links are considered 3rd order combination opportunities.

I-Link

Relative motion at the link interface with the components but no relative motion between the components themselves characterizes the I-Link. During the course of this study, including a thorough review of supporting literature, a product containing an I-Link interface has yet to be found. The reason is clear if one considers the relative motion that would be required to justify the I-Link designation. The link is included here for the purpose of completing the basis set of all possible relative motion configurations.

4.3.3.3 Operations Modeled in an Effort Flow Diagram

The analysis of the wire stripper continues by considering the activity diagram of Fig. 4.5. where three operations are identified that are critical to the EFA of the product:

Activity	Operation
Prepare to Strip Wire	1. Insert and Secure Insulated Wire

Strip Wire	2. Strip Insulation from Wire
Return from Stripping	3. Release Jaws and Insulation

For the first operation of "Insert and Secure Insulated Wire" the EFD shown in Fig. 4.8. is derived. As the figure shows, the link designations include a subscript which relates the link to the specific operation. Note that in addition to the interfaces existing between the components there are also interfaces included from both the input effort source and to the external environment. Next the analysisWe now proceed with the addition of the second operation, "Strip Insulation from Wire", to the EFD as shown in Fig. 4.9. The link designations are now changed to include the component relative motion specified by the second operation. In the case where the link type is the same for more than one operation, an additional subscript is added to the link designation for each additional operation.

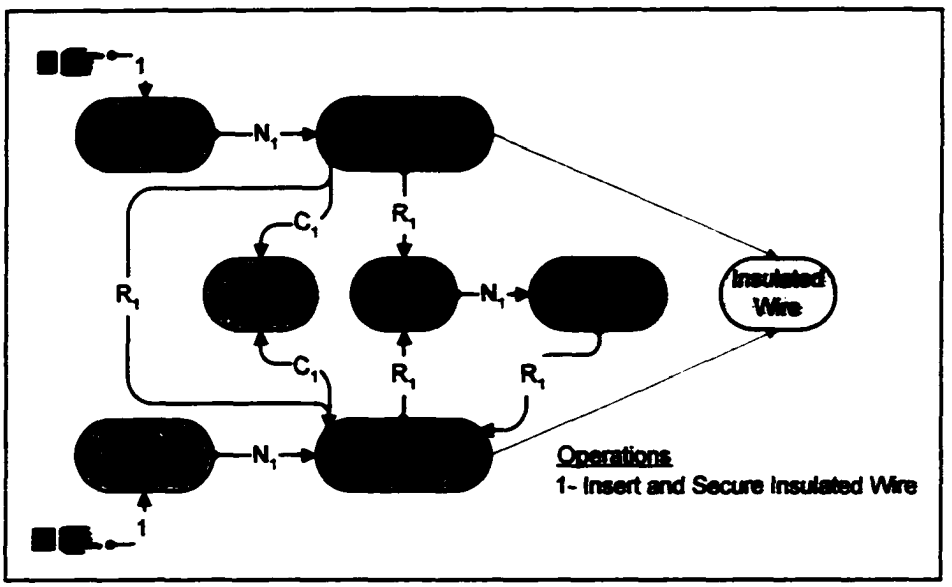

Fig. 4.8. Wire Stripper Effort Flow Diagram for Operation 1

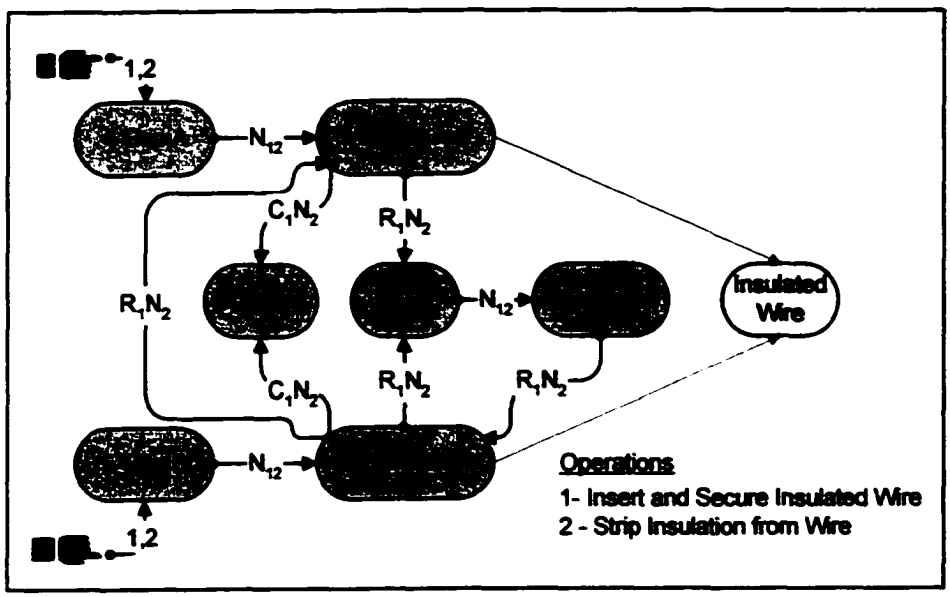

Fig. 4.9. Wire Stripper Effort Flow Diagram for Operation 1 & 2

Finally the component relative motion links for the third operation, "Return from Stripping", are included in the EFD as shown in Fig. 4.10. The link designations are modified to include the relative motion specified by inclusion of the third operation.

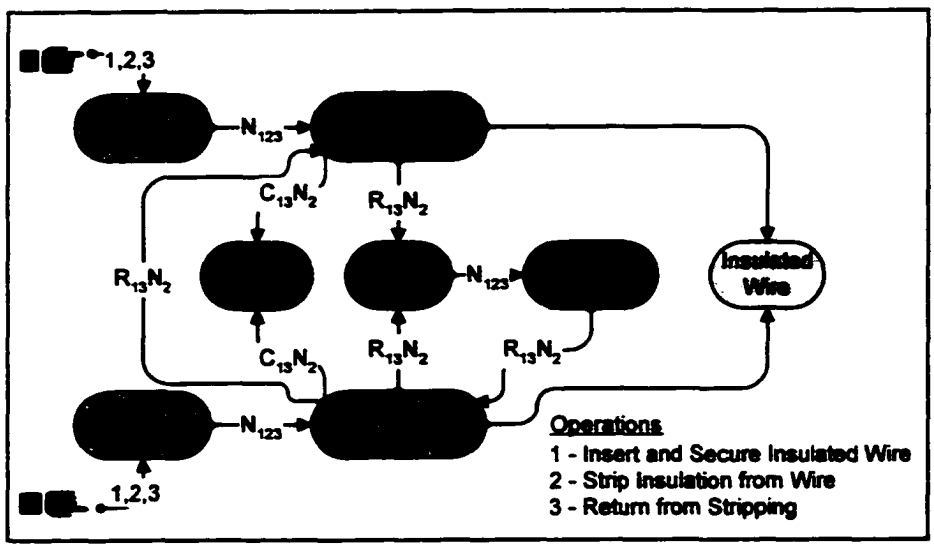

Fig. 4.10. Wire Stripper Effort Flow Diagram for Operation 1, 2 & 3

From this introductory example, it should be clear that interfaces are a critical element in EFA. Also evident is the fact that as the number of operations considered increases the complexity of the diagram and resulting analysis also increases.

Periodically the analysis of a product through the EFA process requires the separation of a single component into its equivalent functional components as shown in Fig. 4.11. This possibility exists only when a component performs more than a single function. This need arises when the functional separation affords the opportunity for product evolution not possible based upon the standard EFD architecture and existing design guidelines. By separating the component into its functional equivalent components, the relative motion link interface connectivity is changed in accordance with the applicable operations and additional evolution opportunities can be presented.

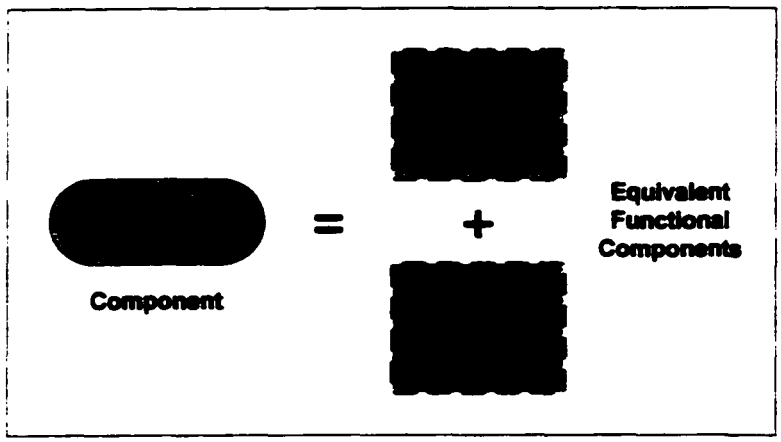

Fig. 4.11. Wire Stripper Functional Components

4.4 Design Guidelines

Once the baseline product is completely and accurately modeled in an EFD, potential component combination opportunities can be identified and design guidelines (see

Chapter 5) can be applied to effect the evolutionary design. These opportunities are dependent on the relative motion designations at the interfaces between components. These interface characterizations; coupled with the structure of the graph, lay the foundation for the evolutionary design work to begin.

4.4.1 1st Order Graph Structure Combinations

Successful application of evolutionary design guidelines begins with the identification of potentially combinable graph structures from the EFD as outlined in Fig. 4.2. The process begins by identifying 1st order combination opportunities; that is, graph structures connected only by N-Links. The EFA of the wire stripper continues by identifying 1st order combination opportunities as shown in the shaded boxes in Fig. 4.12.

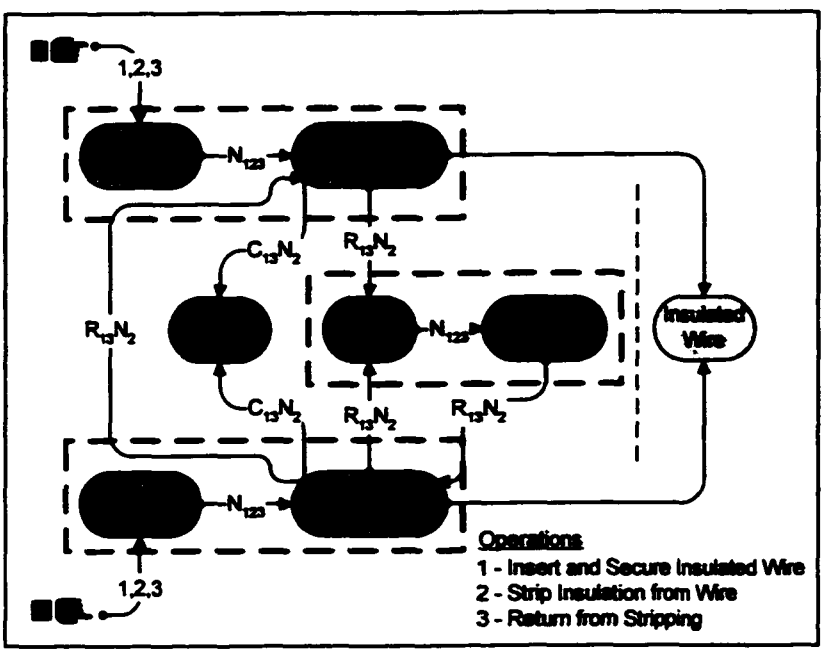

Fig. 4.12. First Order Combination Opportunities

By contracting these graph structures and the associated interface links between the affected components we evolve the EFD into that of Fig. 4.13. Through contraction of these 1st order combination opportunities the number of components has been reduced from seven to four.

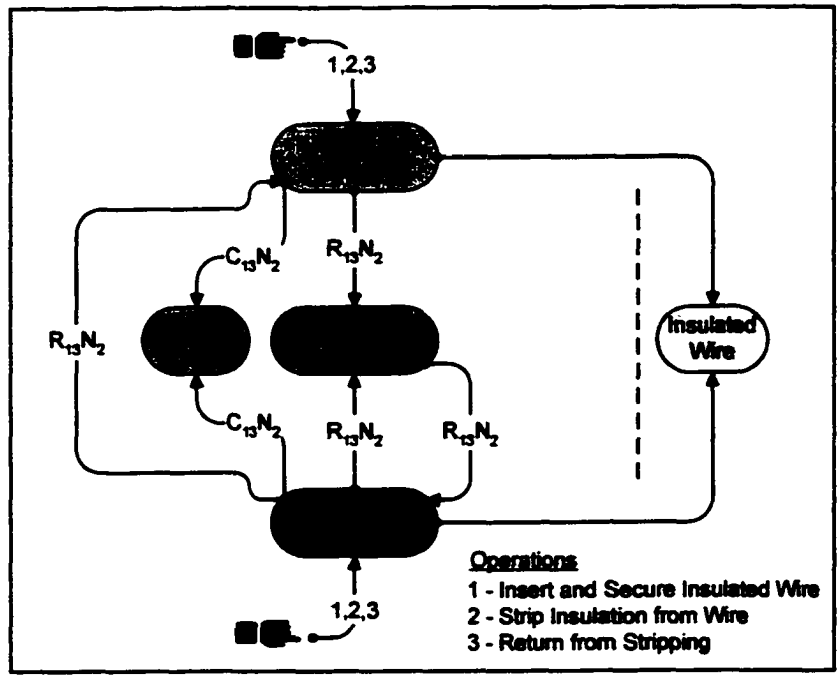

Fig. 4.13. First Order Component Combinations

4.4.2 2nd Order Graph Structure Combinations

The analysis continues by identifying 2nd order combination opportunities; that is, graph structures connected by C-Links or a combination of a C-Link(s) and N-Link(s), as shown in the shaded box in Fig. 4.14. Inspection of Fig. 4.14. reveals another link that satisfies the criteria for 2nd order combination; the interface between the Spring (Component #6) and the combined Lower Jaw (Component #2) and Grip B (Component

#5). However, we are forced to arbitrarily choose only one of the above links for the resulting combination of the Spring component with either the Upper Jaw/Grip A component or the Lower Jaw/Grip B component. By contracting these graph structures and the associated interface links between the affected components the product has further evolved into the product represented by the EFD shown in Fig. 4.15. By contracting the 2nd order combination opportunities the number of components has been further reduced from four down to three.

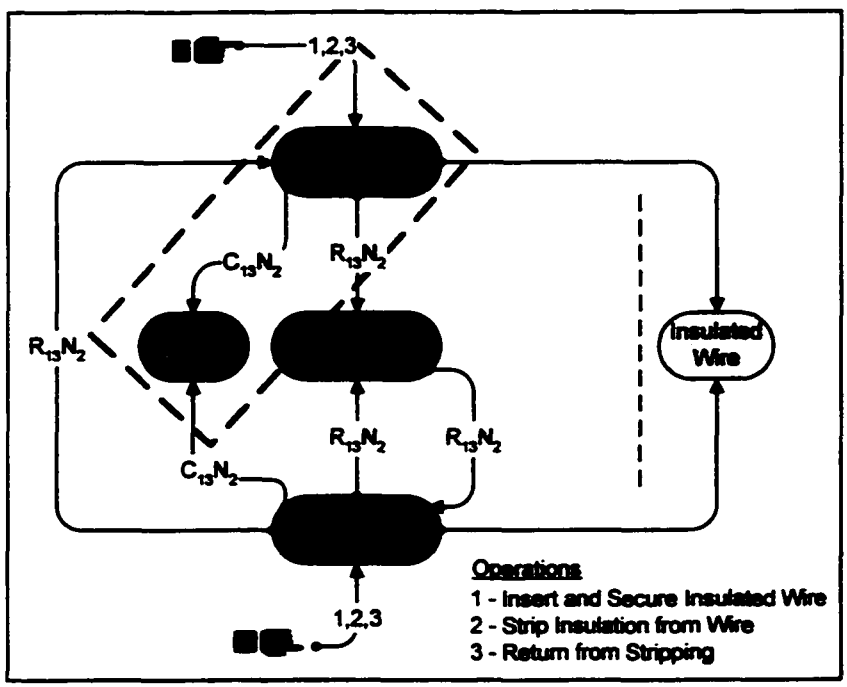

Fig. 4.14. Second Order Combination Opportunities

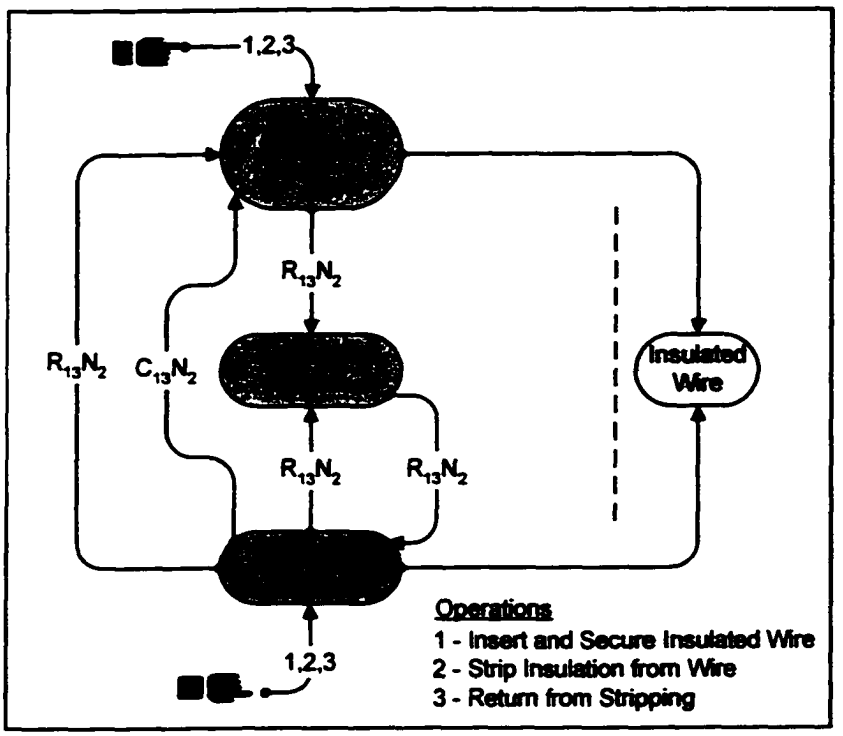

Fig. 4.15. Second Order Component Combinations

4.4.3 Higher Order Graph Structure Combinations

The process continues in this fashion, identifying potential graph structure combinations and applying appropriate design guidelines, until the desired degree of evolution is achieved or the evolution is halted due to material or other constraints.

The state of evolution depicted in Fig. 4.15. represents only a partially evolved product. Further design evolution would require more advanced manipulation of the links and graph structures in the EFD in conjunction with application of higher order design guidelines. A complete analysis of this product is included in Appendix A.

Chapter 5

Empirical Product Study

5.1 Introduction

The empirical study of mechanical domain products was undertaken to form an evaluation control group as a means of developing directed product evolution design guidelines. The guidelines are developed for subsequent use in the conceptual development of evolved products using combined components and material and structural compliance. The design guidelines presented herein are based upon the observed evolution of products that capitalize on the incorporation of compliant mechanisms and other part combination opportunities in their design. The process of extracting design guidelines mirrors that of reverse engineering design. In this process evolved products are reverse engineered with the sole purpose of identifying a path and purpose that led from the baseline design to a successful, and existing, evolved design. The result of this study is a set of product evolution design guidelines that are integral to the effort flow analysis methodology. The design guidelines provide a structured methodology with specific direction in the systematic generation of component combination concepts in product design and redesign.

The product control group used for this study is comprised mainly of typical consumer products. This sample domain is selected since it represents a significant aspect of design focus in industry (McAdams et al., 1998). In addition to being well characterized in terms of the specific functions of the products, these items are also readily available for study. In order to identify a viable path of evolution for a product in the study, each product group is chosen such that there exists a baseline, or original, design and at least one evolved variant of the design. In many cases there exists multiple evolution variants in the group, which offers the ability to identify, more specifically, the evolution path followed in the design of the products. The baseline product is generally characterized by both the absence of significant use of compliance in its construction and a non-optimized reduction in the number of components. In contrast, the evolved product variant(s) does exhibit a significant use of compliance as well as a reduction in the number of components. The baseline product is designated as the original design, and is used as a comparative baseline for observation of the evolution of all subsequent product variants in the group.

5.2 Empirical Study

A block diagram representation of the procedure used in the study is shown in Fig. 5.1. The main process steps are contained in the shaded boxes that are representative of the logical and chronological flow of information during the course of a product study. The unshaded boxes behind the main process steps contain an additional level of detailed process information. Particular interest should be paid to the use of EFA inside the flow of information in the study process.

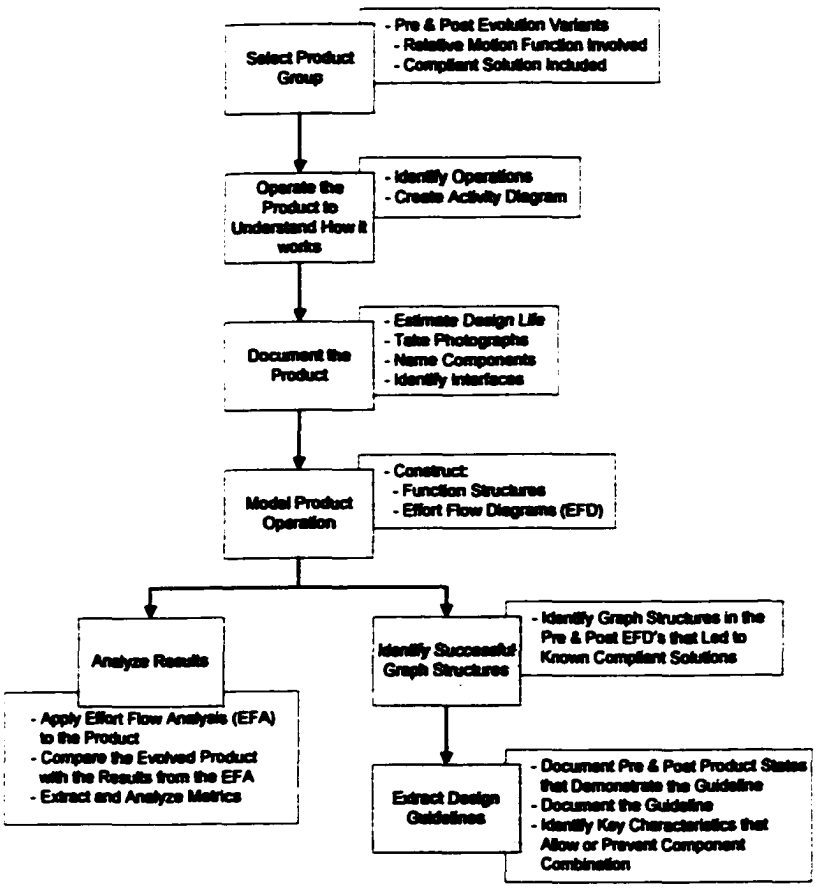

Fig. 5.1. Empirical Study Process

Although not specifically highlighted in the figure, it can be seen that EFA uses the product study to increase the number and quality of the design guidelines contained in the EFA process. In other words, EFA is used within the process of the study to affect its own evolution as a design methodology. The scope of the study has been limited to products contained in the domain of mechanical effort transmissions as a means of providing boundaries on the control group and to sufficiently restrict the variables influencing the problem. The inherent ability of EFA to self-evolve through progressive

development of a design guideline suite in no way prohibits its application to other energy domains.

Guideline extraction and collection for a specific product group begins by first modeling the baseline and evolved products using effort flow diagrams (EFDs). The types of diagram component contractions necessary to achieve the desired evolved product are then determined. Physically, a diagram contraction represents the combining of components, but manifests itself as a contraction of the graph structures in an effort flow diagram as shown in Fig. 5.2. and Fig. 5.3.

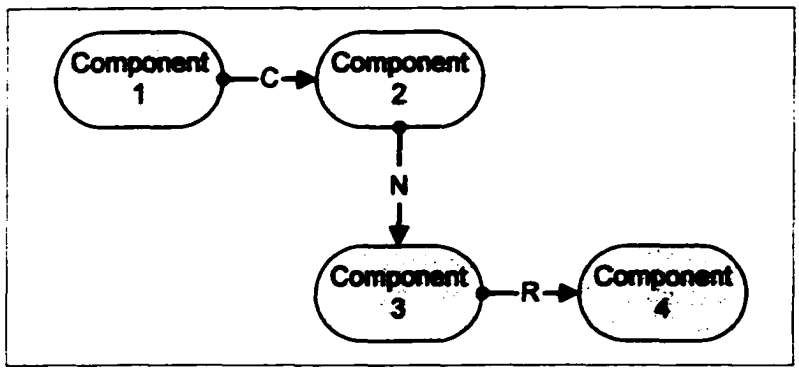

Fig. 5.2. Original Product Graph Structure

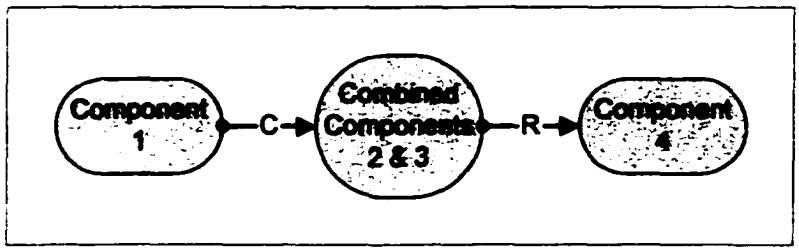

Fig. 5.3. Evolved/Contracted Product Graph Structure

The resulting evolution design guidelines are based on observations of both the physical products and the abstracted representation of the products contained in the

EFDs. In this way, the manipulation of the diagram can be related to the physical components it represents. The guidelines are presented in such a way that they relate physical embodiments to specific arrangements of the links and nodes that repeatedly arise in the graph structures of the diagrams.

To demonstrate the approach taken in the study, a brief example of the overall process is provided for the storage clip product shown in Fig. 5.4. Operation of the different functions of the product and knowledge of the logistical aspects involved in bringing the product to the market allows the generation of the activity diagram of Fig. 5.5. An activity diagram, through a chronological flow of product operations, identifies the specific ways in which the product will be used or operated.

Fig. 5.4. Original and Evolved Storage Clips

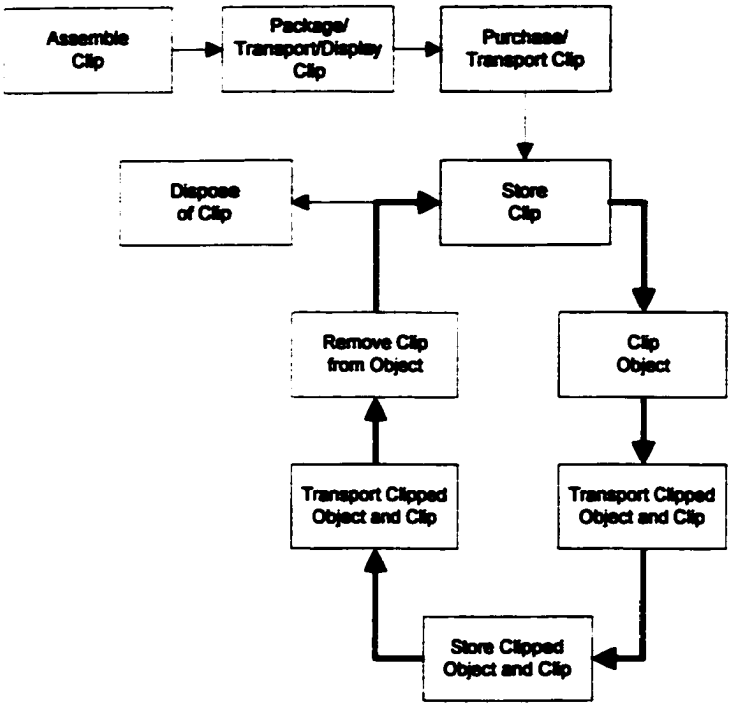

Fig. 5.5. Storage Clip Activity Diagram

These operations are highlighted by the use of bold lines which signify the primary use of the product. It is important to note that certain of the activities included in the diagram (represented by shaded boxes) are not of concern to the research presented herein. These activities are often related to operations, which take place prior to the product being placed into service by the consumer, or are infrequent occurrences, which lessen their importance for consideration in the design evolution of the product.

The activity diagram leads to the identification of operations, which are the user activities that will be modeled in the effort flow diagram (represented by unshaded boxes). Once the operations are fully understood, the product is documented to include assignment of component names, identification of interface types, and photographic documentation. Modeling begins with the generation of a functional model or functional structure as shown in Fig. 5.6.

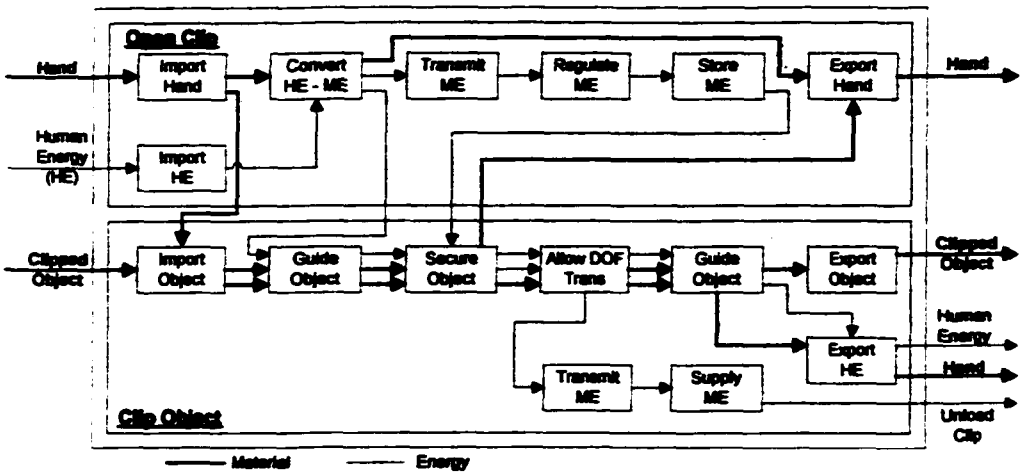

Fig. 5.6. Storage Clip Functional Model

A functional model of the original product allows the designer to fully understand the required functions of the product components based upon the top-level requirements of the product (Otto and Wood, 2001). The functional model graphically maps the flow of material, energy, and information through the components of the product for each of the product functions. By using this method, confidence is gained that the required functions of each of the components has been identified. Next the EFDs for each product operation are developed for both the original product configuration (see Fig. 5.7.) and the evolved product configuration (see Fig. 5.8.).

From these diagrams, which show the beginning and end points on the product evolution path, analysis of the results, identification of successful graph structures, and extraction of guidelines steps are implemented. These three final steps of the empirical study process (see Fig 5.1) are where the design guidelines are eventually extracted from the study.

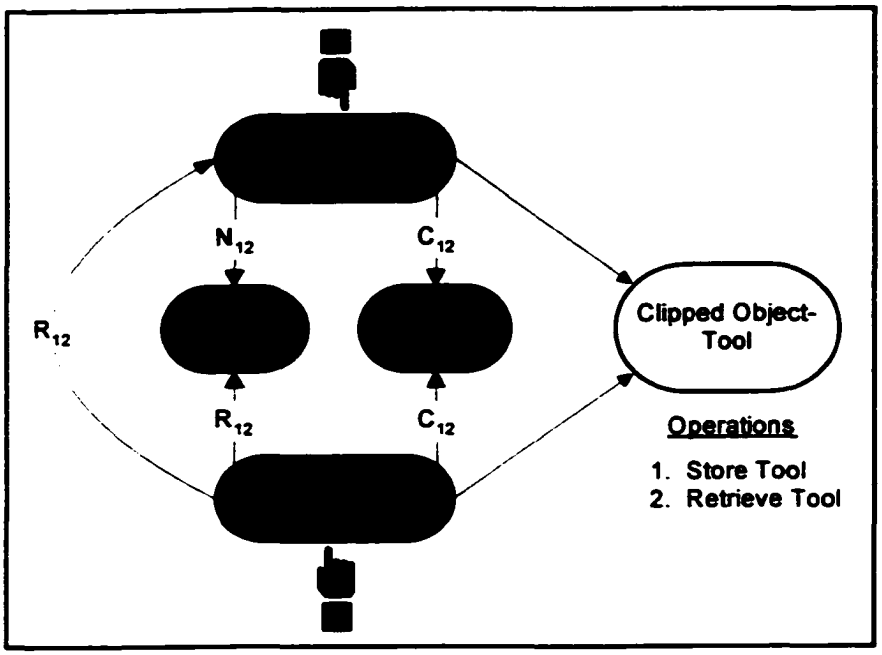

Fig. 5.7. Original Storage Clip Effort flow Diagram

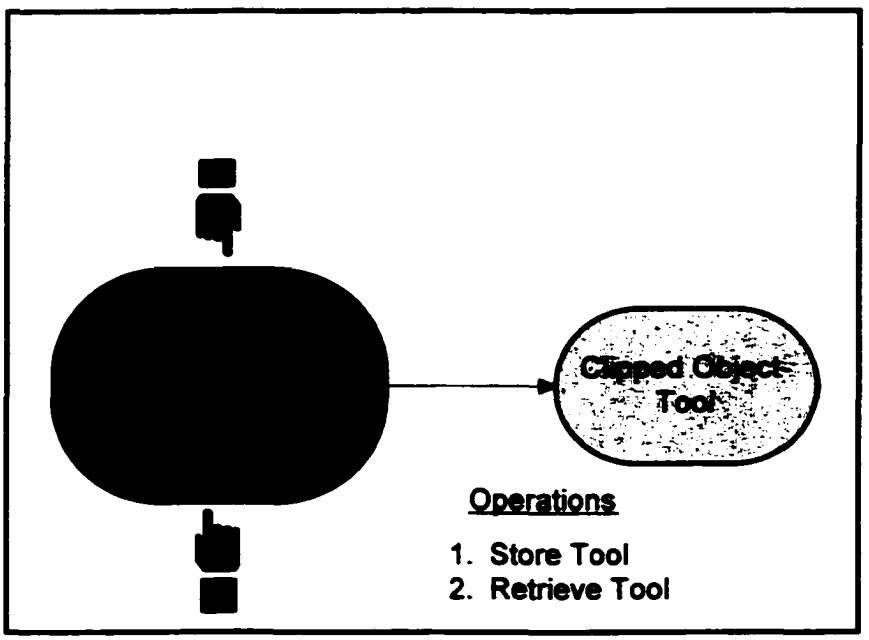

Fig. 5.8. Storage Clip Evolved Effort Flow Diagram

As an example of the process of extracting design guidelines from the observation of the graph structures contained in the baseline and evolved product EFDs, consider the storage clip spring. The primary functional requirement of the storage clip is to secure the clipped object. In the baseline product, this function is accomplished through the stored energy in the spring transferred to the lever arms and acting against the interface between the arms and against the clipped object to product a frictional lock. In the evolved product, securing the clipped object is achieved by stored strain energy in the deformed arms again acting against the clipped object. An extracted design guideline from this product study states that compliant structural members integrally attached to accomplish the same function can replace the function of energy storage in a spring.

Additional design guidelines from this product group and all other product groups studied are contained in the guidelines of the next section. Following the guidelines section is a more comprehensive example of a product group from this study.

The method used to extract guidelines for subsequent use in the evolutionary design of products is validated based upon two premises. First, each of the design guidelines is deduced from the direct observation of the EFD graph structure evolution between the baseline and evolved product variants. It can therefore be concluded that application of the derived design guidelines will lead to the successful evolution of the baseline product. Hence the guidelines are valid at least for the product group used for their derivation. Second, each of the guidelines derived during the course of the study becomes available for use in subsequent product studies. It has been observed that many of the derived guidelines are applicable to nearly all product groups investigated. Validation of the guideline is reinforced each time it is successfully used in the evolution of a product.

While this validation approach is not definitive proof of the global applicability of the specific guidelines, the validity of the study results is sound and reasonable in the framework presented herein.

5.3 Guidelines

In the formal presentation format of the design guidelines, the *imperative form* from English grammar will be adopted based upon the required implementation of the guidelines. In the framework of this method, the context used will be in the form of directions or instructions. This format is consistent with the *action-centered guideline model* used by Nowack, (Nowack, 1997). In the model a typical design cycle begins with an initial *issue*, which prompts an *action* that results in a *consequence*, which in turn must be evaluated to see if the effect on the original issue is satisfactory (see Fig. 5.9.). In the framework of the EFA design methodology, the original graph structures represent the issue of needing to reduce the number of components; the guidelines represent the specific *action* that is taken to attempt to address the *issue*. The result of guideline application is the *consequence*, which must then be evaluated to determine if the result of application of the guideline is a satisfactory evolutionary step in the design of the product.

In order for this set of design guidelines to be useful, a classification scheme must be devised to aid the designer in finding those guidelines that apply to the design problem at hand. One approach to classifying directional or instructional rules relating to the design of compliant mechanisms is given in the work by Berglund *et al* (Berglund et al., 2000).

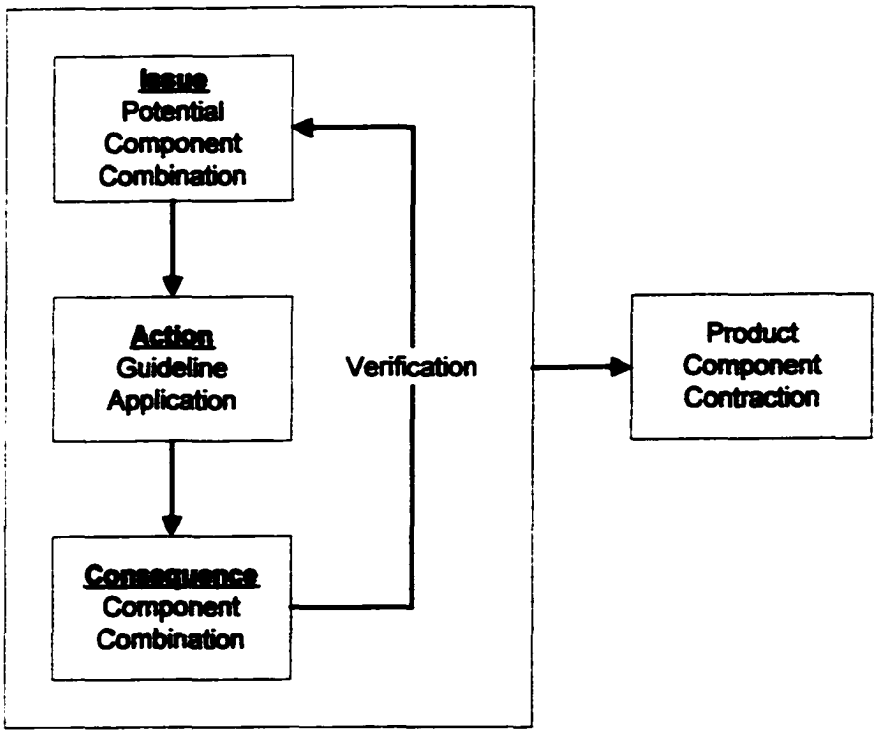

Fig. 5.9. Action-Centered Guideline Model

In his work the design rules for compliant mechanisms are classified according to the area of mechanics where the design rule is either most influential or most constrained and includes the following broad categories:

- Stiffness and Strength
- Material Selection
- Forces, Loads and Motion
- Geometry
- Manufacturing Issues

The main difference between the *design rules* of Berglund and the *design guidelines* presented herein is in the level of detail required for the specific application. Berglund's design rules are much broader in scope covering general details of compliant mechanism

design, while the design guidelines developed here are applicable to specific components and interfaces at the product component architecture level. This difference dictates that we take a different, more specific, approach to classifying the design guidelines. Here, the guidelines are sorted in such a way that they relate to both the domain of applicability of the guideline and the specific graph structures observed in the baseline and evolved product EFDs.

The classification scheme proposed here is to use four broad classes, or domains, to classify the product design guidelines derived from the empirical study:

- Relative Motion Domain
    - *N-Link*
    - *C-Link*
    - *R-Link*
    - *I-Link*
- Graph Structure Domain
    - *Parallel*
    - *Serial*
    - *Mixed*
- Function Domain
- Analysis Domain

The Relative Motion Domain designation refers to the type of component interface addressed by the guideline. The interface types are the NCRI interface types discussed in the previous chapter. Under the Relative Motion Domain classification, the interface specific guidelines are further designated according to their degree or order of difficulty.

An N-Link contraction or combination is considered a 1st order contraction since it does not involve the consideration of any relative motion constraints. Similarly, the C-Link contraction or combination is considered a 2nd order contraction since it does require a consideration of the relative motion between the connecting components. An R-Link contraction or combination is termed a 3rd order contraction since it requires a consideration of the relative motion between both the connecting components and between their interfaces. We can therefore observe the increase in difficulty as the relative motion constraints increase.

The Graph Structure Domain refers to the arrangement of the interface links (N, C, R, & I) and the nodes in the EFD. This domain is analogous to the parallel or serial arrangement of electrical or mechanical components in a system. Guidelines in the Graph Structure Domain specify when and how these configurations can be manipulated to achieve the desired product evolution.

The Function Domain contains design guidelines that are related primarily to the functionality of the combined components and less upon the relationship between them.

Finally, the Analysis Domain contains design guidelines that are related to, or influenced by, the analysis of combined components in both rigid body and compliant mechanisms.

A summary of the design guidelines collected during the course of the study is presented in Table 5.1. through Table 5.4. using the domain classifications suggested above. Several of the guidelines in the table are referenced; these guidelines are extracted from the literature for their applicability and are validated through repeated application but are not the result of the study.

extracted from the literature for their applicability and are validated through repeated application but are not the result of the study.

Implicit in the formulation and application of the guidelines is the assumption that fundamental physical laws such as strain/displacement relations, the material constitutive law, and equilibrium conditions are not violated. In addition, any redesign carried out using these guidelines must continue to satisfy the original product functions. These statements are embedded in the EFA methodology where any change to the model requires that the conditions for successful combination, which include maintenance of original design functionality, be satisfied.

Though each of the guidelines presented here may stand on its own merits, the realization of the full potential of the EFA process results only from the synthesis of the guidelines into a framework within which the successful redesign of products utilizing compliant mechanisms is achieved.

Table 5.1. Relative Motion Domain Design Guidelines

N-Links – 1st Order	
1.	Groups of components connected by N-Links are candidates for combination into rigid body structures. Combination is contingent upon satisfaction of the following constraints: a. Material strength/maximum stress is within acceptable limits. b. Fatigue strength is at an appropriate level for the expected number of loading cycles. c. Assembly/disassembly design features are not compromised with

	d. Original product functions continue to be provided. Maintenance of the original material is desirable, however, material changes are allowed subject to the above constraints (Boothroyd et al., 1994).
2.	When only N-Links are produced by one operation in a multi-operation model, the N-Links that are coincident with other link types can be omitted from the model, as higher order link types will dictate combinability.
C-Links – 2nd Order	
3.	Groups of components connected by C-Links are candidates for combination into compliant mechanisms. Combination is contingent upon the following constraints: a. The degree-of-freedom for the resulting interfaces with uncombined components are maintained. b. Material strength/maximum stress is within acceptable limits. c. Fatigue strength is at an appropriate level for the expected number of loading cycles. d. Relationship between force and deflection is within acceptable limits where appropriate. e. Assembly/disassembly design features are not compromised with respect to interfacing components (Boothroyd et al., 1994). f. Original product functions continue to be provided. Maintenance of the original material is desirable, however, material changes are allowed subject to the above constraints (Boothroyd et al., 1994).

4.	If combination across a C-Link requires relative motion to be confined to a small region, use *Localized* or *Lumped* compliance solutions. Analysis of compliance is best suited to the pseudo rigid-body model method of Howell (Howell, 2001).
5.	If combination across a C-Link dictates that broad regions of a device be compliant, use *Distributed* compliance solutions. Analysis of distributed compliance requires the use of continuum models (Ananthasuresh and Frecker, 2001).
6.	When a C-Link enables a strain energy storage function, the components connected by the C-Link may be combined if the desired strain energy storage can be maintained using a compliant mechanism while still meeting other product functions.
7.	Compliant mechanisms made of polymer materials may need to be augmented by support structures to overcome the effects of creep when subjected to sustained loads. For example, the compliant mechanism in Fig. 5.10. is augmented by a metallic coil spring. The purpose of the spring is deduced to be creep prevention, as the device performs all operations when the spring is removed.

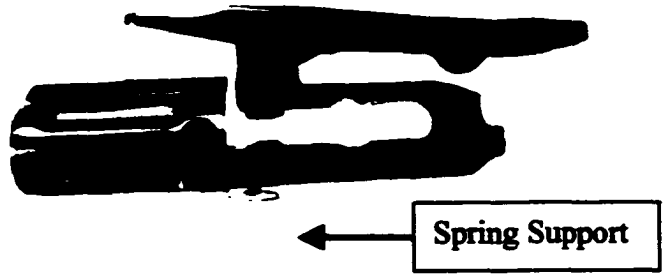

Fig. 5.10. Pilot Pen Clip/Cap/Index and Spring Components

R-Links – 3rd Order or Higher

8. Components connected by R-Links, where the general relative motion is *small*, are candidates for component combination. In this context, small can be determined by the fatigue strength of the material at the point of maximum stress. Combination is contingent upon the following constraints:

   a. Required deflection between the combined components is maintained with the combination, as defined by the R-Link, with deflection requirements applicable at both the component interface and between the components. Deflection based design requirements must also be satisfied.

   b. Material strength/maximum stress is within acceptable limits.

   c. Fatigue strength is at an appropriate level for the expected number of loading cycles.

   d. Relationship between force and deflection is within acceptable limits where appropriate both at the component interface and between the components.

	e. Assembly/disassembly design features are not compromised with respect to interfacing components (Boothroyd et al., 1994). f. Original product functions continue to be provided. Maintenance of the original material is desirable, however, material changes are allowed subject to the above constraints (Boothroyd et al., 1994).
9.	When one R-Link provides relative motion for more than one operation, the components connected by that link may be combined provided the motions are of the same type (translation or rotation) for all operations.
10.	R-Links where the motion is large (up to 359°), and the energy storage in the joint is to be minimized, are candidates for combination if the effort transmission is small (only enough to generate motion) using localized compliance (a single-piece flexible hinge or similar type connection). The single-piece hinge is especially useful in 2D (i.e. planar) motion.

Table 5.2. Graph Structure Domain Design Guidelines

Series - 3rd Order or Higher	
11.	When R-links of the same type (translation or rotation) are in series, those connected components are candidates for combination up until an interface is reached where the required R-Link motions are of another type.
Parallel - 3rd Order or Higher	

12.	When a block of components connected by C-Links contains C-Links that are in parallel with R-Links, the components connected by the C-Links are candidates for component combination if the relative motion at the R-Links can be maintained through the motion generated in the combined C-Block. See Fig. 5.11.

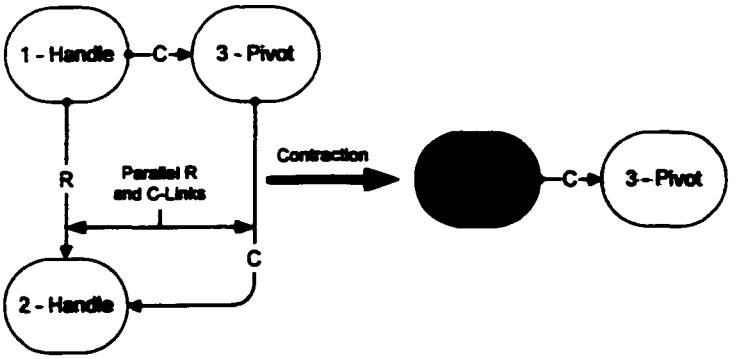

Fig. 5.11. Graph Structure Contraction for Parallel R & C-Links

13.	Components connected by parallel links, which are determined to be functionally identical, are considered **redundant** and as a result can be reduced to a single non-redundant link. For example, two identical hinges result in two identical parallel link structures. By contracting the two links into one, no capability is lost, and complexity of the diagram is reduced. This guideline applies to links of any type.
14.	Components connected by **non-redundant** parallel links are candidates for component combination contingent upon the constraints dictated by the guideline requirements for each specific link configuration.
15.	R-Links in parallel with energy storage C-Links are candidates for component combination using compliant components provided the required

	strength, energy storage and degree-of-freedom is maintained in the contracted compliant component.
Combined R & N-Links - 3rd Order or Higher	
16.	Components connected by RN-Links (i.e. links which are designated as R-Links for one or more operations and N-Links for one or more operations) are candidates for combination. Combination is contingent upon the constraints afforded by both the R and the N-Link as follows: a. Deflection based functions are maintained with the combination, as defined by the R-Link, with deflection requirements applicable at both the component interface and between the components. Deflection based design requirements must also be satisfied. b. Material strength/maximum stress is within acceptable limits. c. Fatigue strength is at an appropriate level for the expected number of loading cycles. d. Relationship between force and deflection is within acceptable limits where appropriate both at the component interface and between the components. e. Assembly/disassembly design features are not compromised with respect to interfacing components (Boothroyd et al., 1994). f. Original product functions continue to be provided. Maintenance of the original material is desirable, however, material changes are allowed subject to the above constraints (Boothroyd et al., 1994).

17.	Components connected by RN-Links (i.e. links which are designated as R-Links for one or more operations and N-Links for one or more operations) are candidates for combination using a **rigid body** if the degree-of-freedom can be successfully moved up or down the flow path from the link of interest.
18.	Components connected by RN-Links (i.e. links which are designated as R-Links for one or more operations and N-Links for one or more operations) are candidates for combination using **compliant mechanisms** when the required degree-of-freedom can be maintained in the combined component.
Combined C & N-Links - 3rd Order or Higher	
19.	Components connected by CN-Links (i.e. links which are designated as C-Links for one or more operations and N-Links for one or more operations) are candidates for combination. Combination is contingent upon achieving the desired degree-of-freedom needed for the N-Link using a compliant member. A link of this type appears to be a combination of the N-Block and C-Block contraction opportunities. This guideline is evidenced in the effort flow diagram structure of Fig. 5.12. where the arms and spring of a baseline product are combined to produce the beams, hinge and latch in the evolved product of Fig. 5.13. In this case, the degree-of-freedom constraint is changed from resisting a compressive load in the original product to resisting a tensile load in the evolved product. In addition, the constraint on out-of-plane motion enforced by the interface between the arms of the

original product is enforced by the hinge and latch of the evolved product.

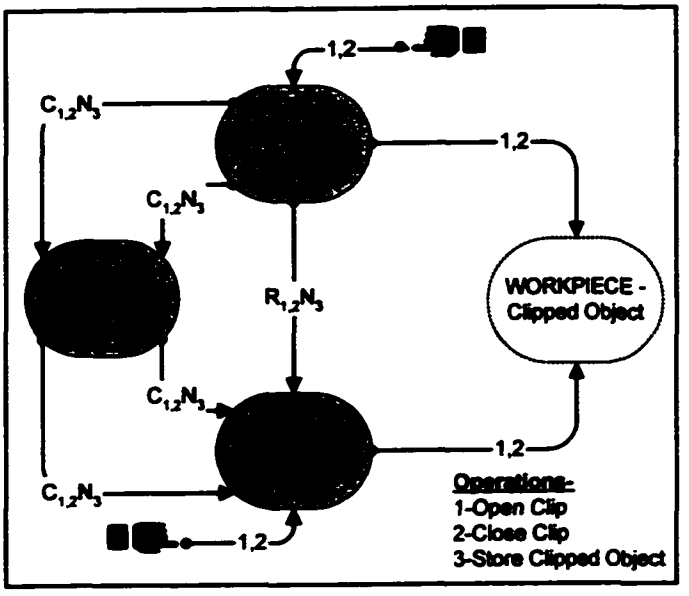

Fig. 5.12. Parallel Structure in Graph for Clip Product

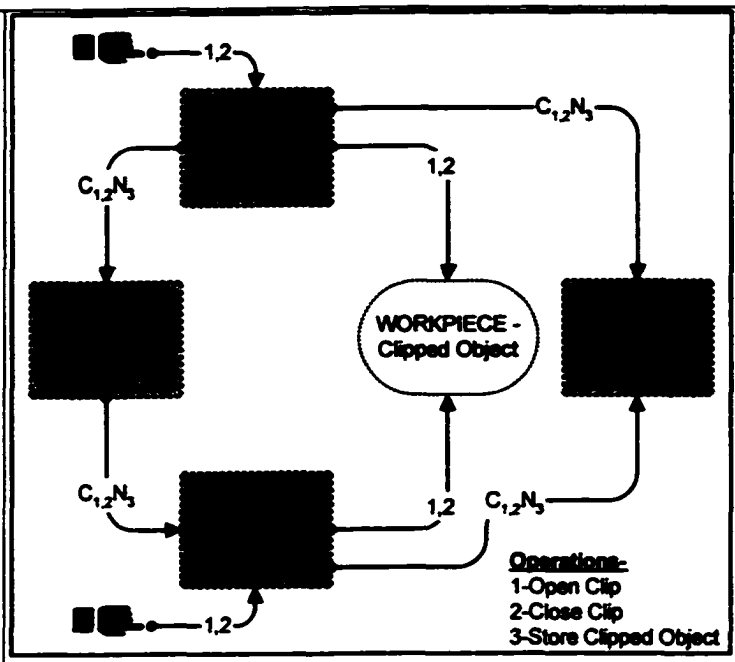

Fig. 5.13. Monolithic Structure shown as Functional Components in Clip Product

The product modeled in Fig. 5.13. is a one-piece product, the rectangular nodes shown are designated functional components and are used to show which portions of the product provide particular functional features.

20. Components connected by CN-Links (i.e. links which are designated as C-links for one or more operations and N-links for one or more operations) are candidates for combination. Combination is contingent upon the constraints afforded by both the C and the N-link as follows:

a. Required deflection between the combined components is maintained with the combination as defined by the C-link.

b. Material strength/maximum stress is within acceptable limits.

c. Fatigue strength is at an appropriate level for the expected number of loading cycles.

	d. Relationship between force and deflection is within acceptable limits where appropriate. e. Assembly/disassembly design features are not compromised with respect to interfacing components (Boothroyd et al., 1994). f. Original product functions continue to be provided. Maintenance of the original material is desirable, however, material changes are allowed subject to the above constraints (Boothroyd et al., 1994)

Table 5.3. Function Domain Design Guidelines

21.	Integral attachment (e.g. a living hinge) accompanied by strain energy (distributed compliance) can be used to replace the energy storage of a spring (Howell, 2001).
22.	The degree-of-freedom afforded by an R-Link may not need to be a part of the product being modeled, the degree-of-freedom may be transferred from the system of interest to the system of an interfacing external system such as the human interface, which is not part of the actual product.
23.	Living hinges can be used in high load applications when the loading is tensile only.
24.	When an effort flow diagram affords multiple choices for possible graph structure contractions (e.g. possibility for combining component A with either component B or component C), each possible solution path should be followed to its maximum evolved state to allow determination of an optimized configuration.

Table 5.4. Analysis Domain Design Guidelines

25.	When bending deflection is specified, reduce the second moment of area (I) to reduce the stress and thus the likelihood of fatigue failure in a compliant mechanism. The mechanics behind this result follow the argument that a desired deflection is specified: $$I = \frac{bh^3}{12} \quad (5.1)$$ $$\delta = \frac{FL^3}{3EI} \quad (5.2)$$ $$\sigma = \frac{My}{I} = \frac{(FL)\left(\frac{h}{2}\right)}{I} \quad (5.3)$$ The maximum or minimum force required to achieve the deflection is specified, and eqn. (5.2) is solved for the force (F) as in eqn. (5.4). Equation (5.4) is then substituted into eqn. (5.5) for F resulting in a relationship for stress as a function of distance from the neutral axis (h) for a given deflection as shown in eqn. (5.6). $$F = \frac{3\delta EI}{L^3} \quad (5.4)$$ $$\sigma = \frac{h}{2}\frac{FL}{I} \quad (5.5)$$

	$\sigma = \frac{3h}{2}\frac{\delta E}{L^2}$ (5.6) Note that as h is reduced, the stress is also reduced, as is the second moment of area (I). To achieve a given deflection with a minimum normal stress due to bending, the objective is to reduce I. The most effective way to do this is to reduce h. This result is related to the guideline proposed by Berglund (Berglund et al., 2000) where it is stated "Avoid adding material to a compliant segment if it experiences static or fatigue failure in bending."
26.	Materials with the highest strength-to-modulus ratio will allow a larger deflection before failure. This ratio is one of the most important factors in selecting a material for a compliant mechanism (Howell, 2001).
27.	In systems with both living hinges and other compliant segments, the rigidity of the living hinges is often sufficiently low compared to the other flexible components that their rigidity and energy storage can be ignored (Howell, 2001).
28.	When the resulting compliant design dictates that the relative motion be confined to a small region then use *Localized* or *Lumped* compliance solutions, such as a living hinge. Analysis of this type of compliant mechanism is best suited to the pseudo rigid-body model method (Howell, 2001).

5.4 Guideline Development Example

An example will illustrate how EFA is used to derive the guidelines presented herein. A tool case product group, used to store and transport lightweight hand tools, is used to demonstrate the methodology. The baseline product is constructed from a combination of 19 separate polymer and metal components. The evolution of the baseline product is charted through three intermediate products (Variants A, B, & C) to a fully evolved product. To understand the operations that need to be modeled for this product group, an activity diagram is constructed as shown in Fig. 5.14.

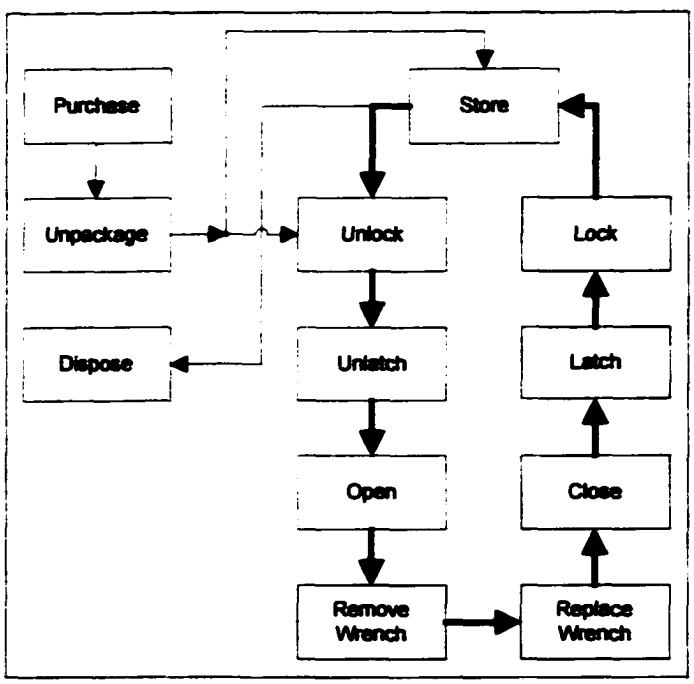

Fig. 5.14. Tool Case Activity Diagram

The operations of concern are as follows: Unlock, Unlatch, Open, Close, Latch, Lock, and Transport. A legend assigning an operation number to designated operations is included in the EFDs of Fig. 5.15. through Fig. 5.19. The subscripts contained in the diagram link designations indicate the operation for which the link is active. Images of

the products modeled in the diagrams are included to enhance understanding of the diagrams. Samples of the guidelines hypothesized through analysis of the tool case product group are now presented.

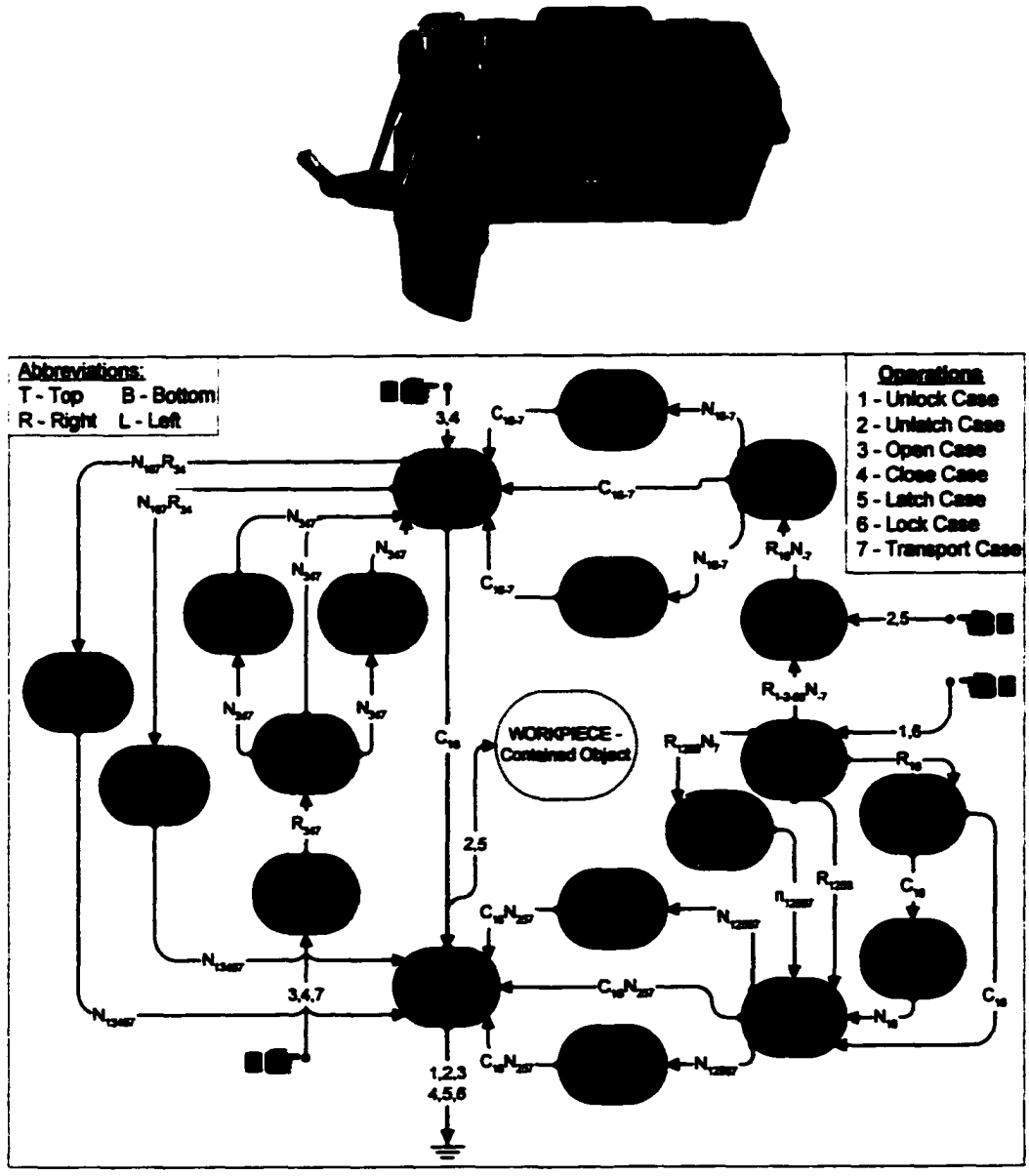

Fig. 5.15. Picture and Effort Flow Diagram for Baseline Tool Box

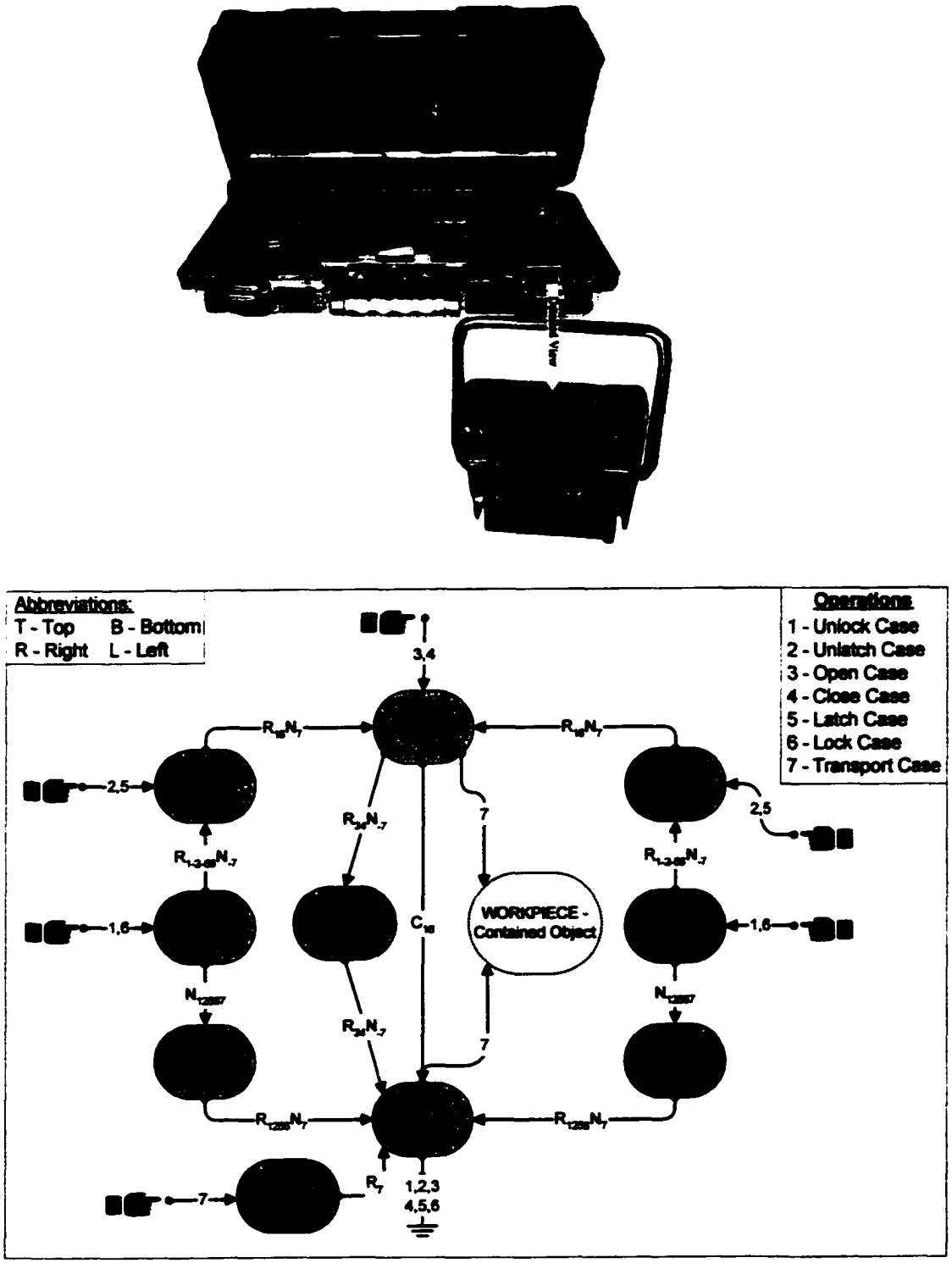

Fig. 5.16. Picture and Effort Flow Diagram for Variant A Tool Box

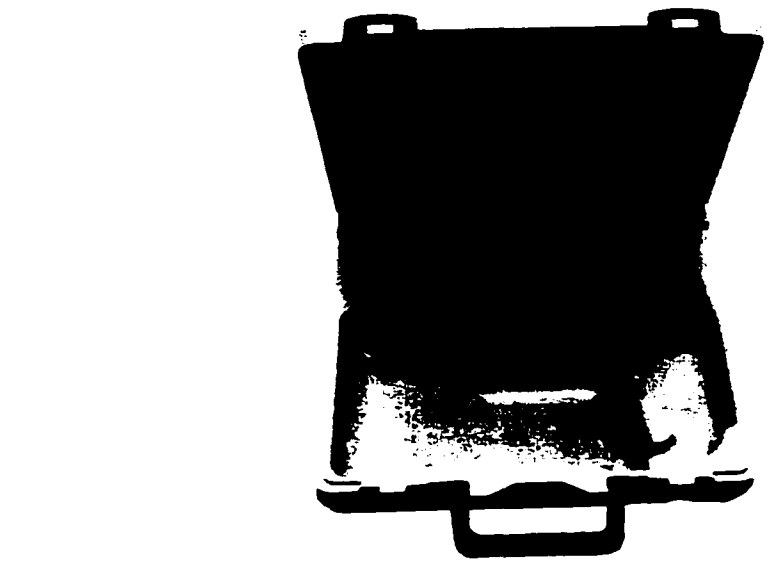

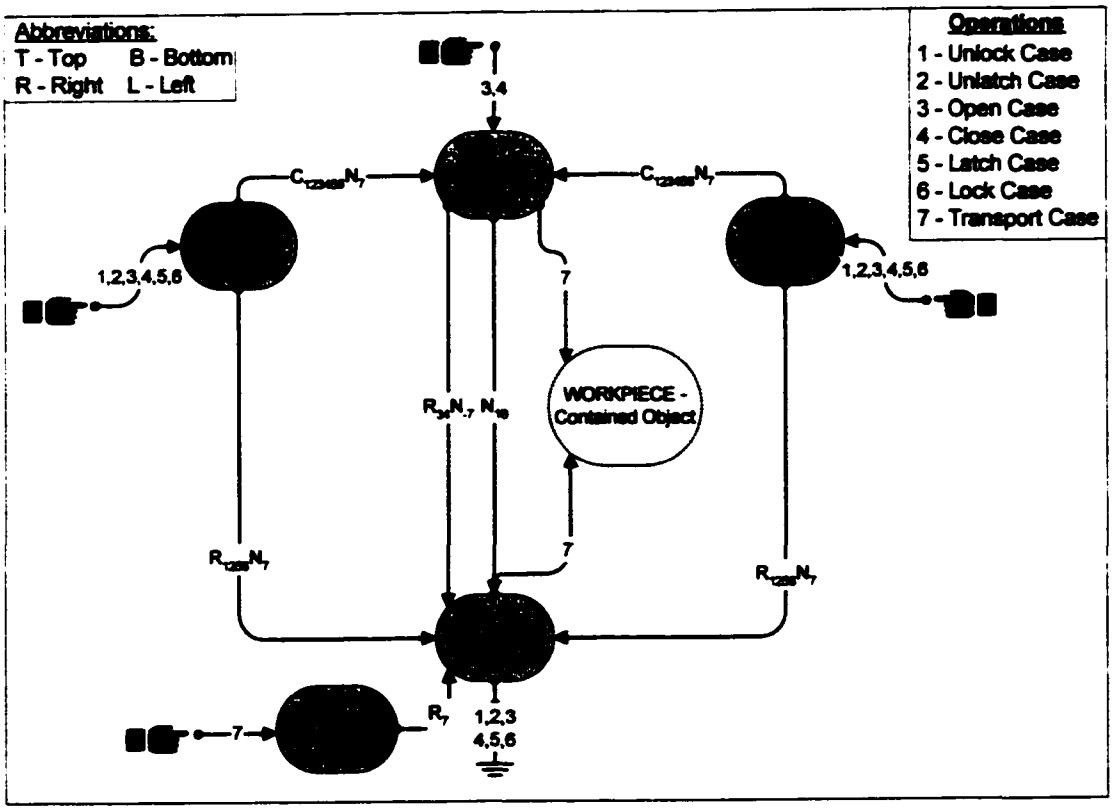

Fig. 5.17. Picture and Effort Flow Diagram for Variant B Tool Box

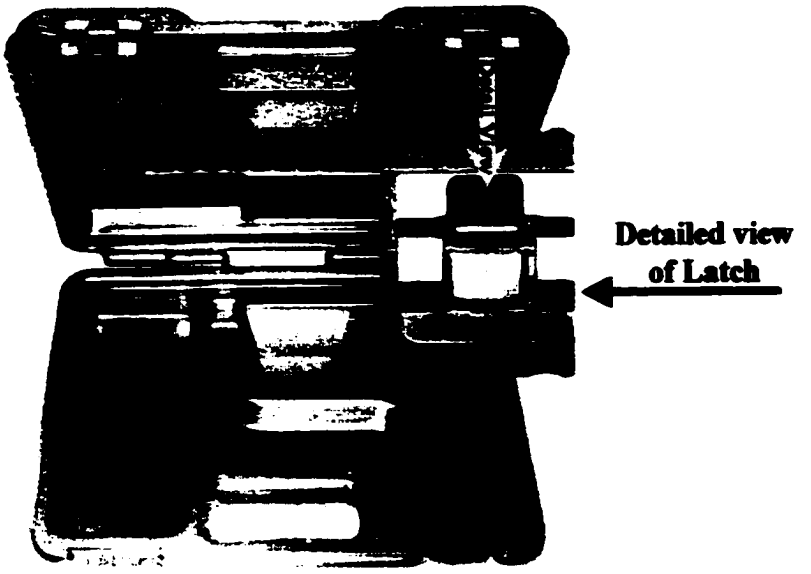

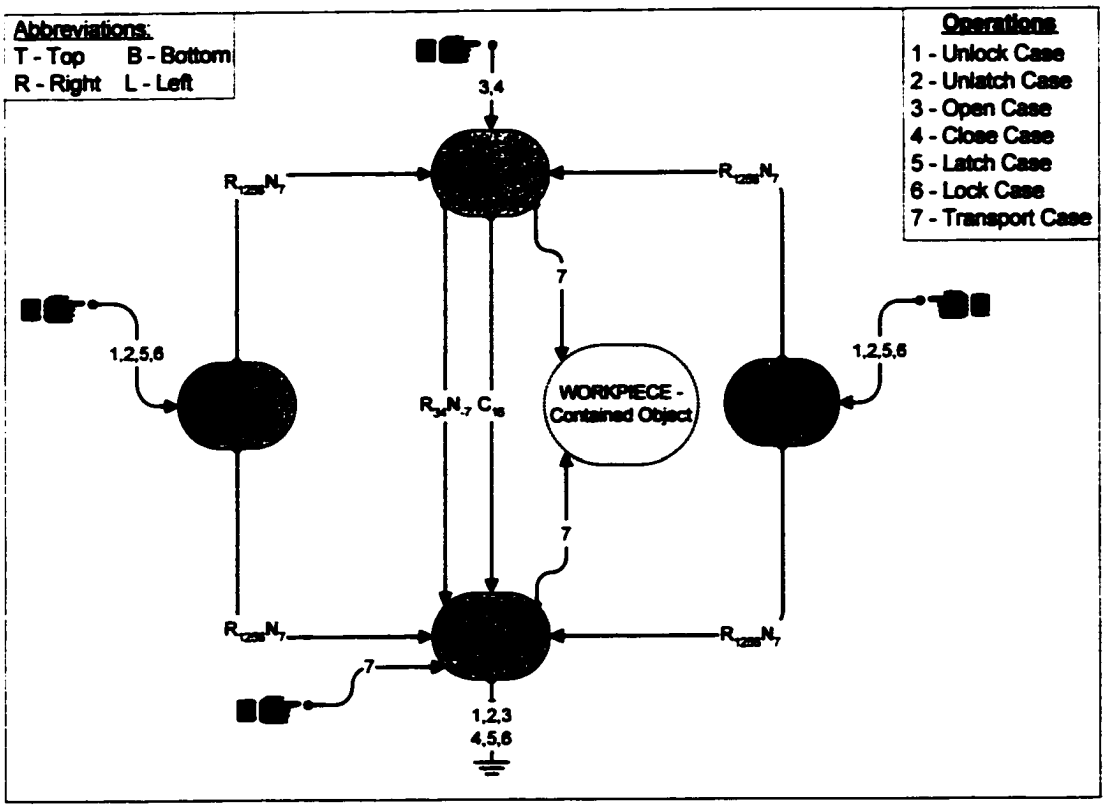

Fig. 5.18. Picture and Effort Flow Diagram for Variant C Tool Box

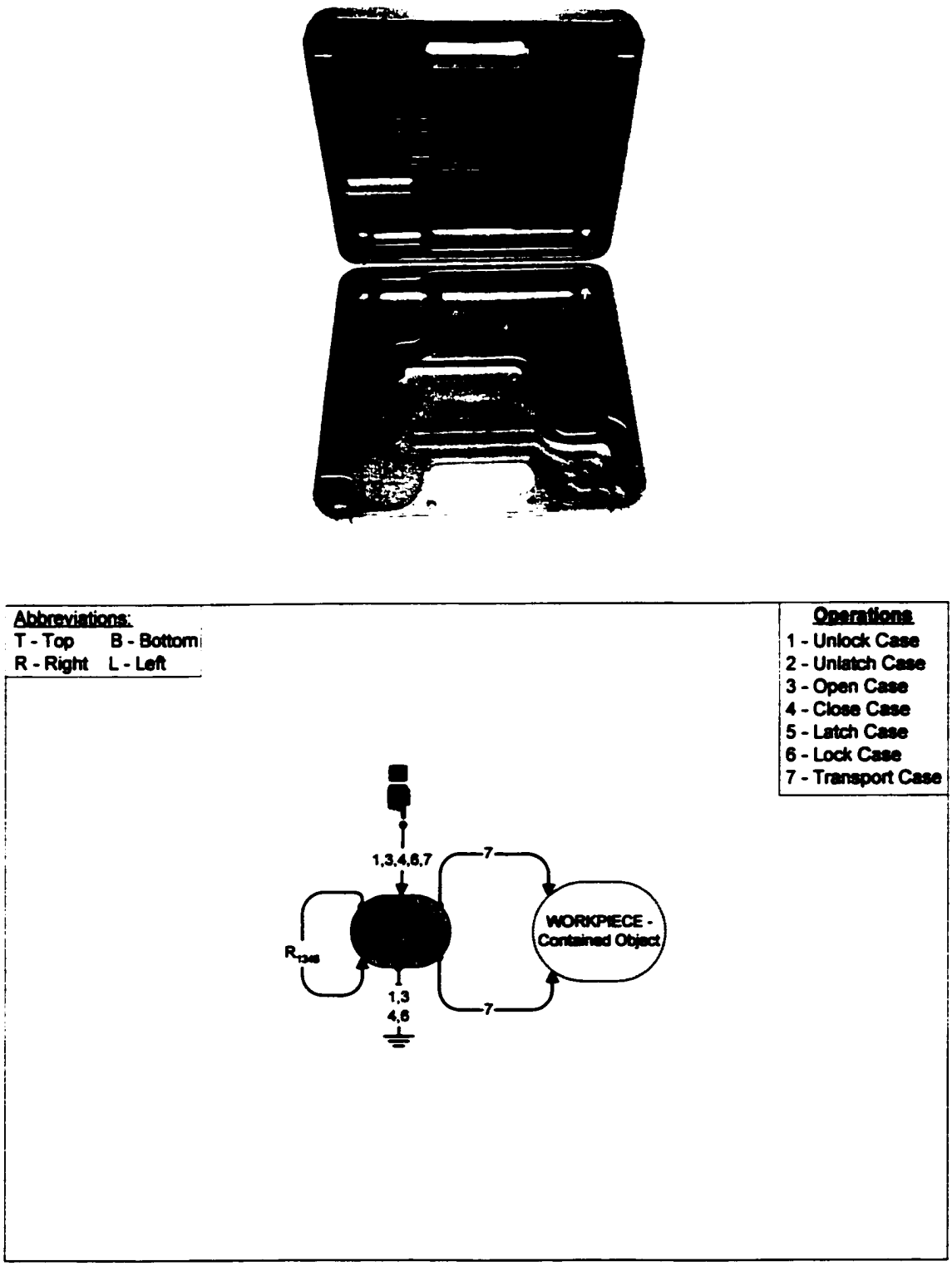

Fig. 5.19. Picture and Effort Flow Diagram for Fully Evolved Tool Box

Examples of three Relative Motion Domain guidelines (Table 5.1.) are represented in the evolution of the baseline tool case.

1. Guideline 1, has four instances:
    a. Combination of Rivets 1 and 2 and the Bracket into the Lid from the Baseline product.
    b. Combination of the Hinge Pins and the Base from Variant A.
    c. Combination of the Latch Pin and Latch Lever evolving from Variant A to Variant C.
    d. Combination of the Latch Hook with Rivets 3 and 4, and combination of the Latch Bracket with Rivets 5 and 6.
2. Guideline 2 has one instance: In Variant C, operation 7 produces only N-Links and can hence be neglected for effort flow analysis of this variant.
3. Guideline 10 has one instance: Combination of the Latch Ring and Latch Lever is possible by moving the relative motion between these two parts to another interface resulting in the combined Latch Lever and Ring of Variant C.

Two Graph Structure Domain guidelines (Table 5.2.) are especially prevalent in the evolution of this product group.

1. Guideline 17, has three instances:
    a. Combination of the Latch Lever, Latch Ring, and Latch Pin from either the Baseline or Variant A results in the compliant Latch Ring of Variant B.

b. Combination of the Lid and Base from either Variant B or Variant C results in the fully evolved product.

c. Combination of the Latch Ring and the Lid of Variant C leads to the integral latch mechanism of the fully evolved product.

2. Guideline 20, has three instances:

a. The combined Latch Hook and Rivets 3 and 4 discussed previously are subsequently combined with the Lid for all products subsequent to the Baseline product.

b. The combined Latch Bracket and Rivets 5 and 6 discussed previously are subsequently combined with the Base for all products subsequent to the Baseline product.

c. Combination of the Latch Rings with the Lid of Variant B produces a single component Lid with integral latches in the fully evolved product.

In addition to the Relative Motion Domain and Graph Structure Domain guidelines addressed above, observations that are more general lead to guidelines in the Function Domain and Analysis Domain as follows:

1. The degree-of-freedom afforded by an R-Link may not need to be a part of the product being modeled. This observation comes from the integration of the movable handle of the Baseline and Variants A and B into the integral Handle of Variant C and the fully evolved product. In this case, the degree-of-freedom has been transferred to the human interface, which is not part of the actual product (reference Guideline 22).

2. Living hinges are appropriate when heavy loads are not involved (reference Guideline 23).
3. When an EFD affords multiple choices for possible graph structure contractions (e.g. possibility for combining component A with either component B or component C), each possible solution path should be followed to its maximum evolved state. Comparisons among the solution paths and results can then be made and the solution that best satisfies the functional requirements chosen (reference Guideline 24).

This discussion on hypothesized guidelines is just a brief overview of the general methodology for applying the collected guidelines gathered from the empirical study to the tool case product group. This example is meant to show the process and highlight only a portion of the results.

5.5 Results and Discussion

During the course of this study, nine product groups consisting of 26 separate products have contributed to the development of the suite of guidelines presented in this chapter. In the example presented herein, the most basic guidelines are applied repeatedly resulting in the number of parts being reduced from 19 in the baseline design to a single compliant component for the fully evolved product. The fundamental guidelines extracted and collected during the course of the empirical product study are responsible for understanding this dramatic evolution, and their application to other product groups are expected to yield similar results.

Development of the process continues with the incorporation of these guidelines into the framework of a product evolution methodology. The methodology that results is EFA, a systematic methodology for the synthesis of designs that incorporate compliant mechanisms in the design and redesign of products from the domain of mechanical transmissions. In this chapter a process has been developed for systematically contracting the EFD graph structures of baseline products and thereby have identified components, which are candidates for combination with other components. Lacking in the methodology at this point is the ability to analyze the proposed combinations to determine if the new design meets the performance requirements of the original product. Development of an interface between EFA and specific analysis tools such as the empirical similitude methods presented herein are the subject of the remaining chapters.

Chapter 6

Advancing the Empirical Similarity Method

6.1 Introduction

Analysis of the performance of a newly designed or redesigned product or component can be an extremely difficult and daunting task. Theoretical analysis of the design often requires simplifying assumptions regarding the definition of boundary conditions, the value of material properties, and perhaps simplifications to complex geometrical characteristics just to name a few. These assumptions result in a decay in the potential accuracy of predictions.

At the other end of the spectrum experimental analysis requires the manufacture of a replica prototype or model, possibly even fabricated from the design specified materials and processing methods to produce an actual product for realistic analysis. This method of testing results in extremely accurate analysis but often lacks the flexibility to sufficiently characterize variations in the design parameters critical to the system design.

A compromise is sought between the applicable theoretical methods and available experimental techniques that offers both flexibility and efficiency while still providing adequate accuracy for the problem at hand. The approach presented herein provides an integral feasibility verification element to the enhanced effort flow analysis (EFA)

methodology. The method will provide a crucial analytical tool for the evolutionary re-design of products by taking advantage of compliant materials and structures to effect successful component combination.

6.1.1 Theoretical Analysis

Theoretical analysis envelopes a variety of numerical techniques that can be used to attempt to characterize how a product will perform when subject to theoretical test conditions. The test conditions are most often aimed at representing conditions, or worst-case conditions, the product will see during the performance of its intended operation(s) with appropriate factors of safety included where appropriate. For this type of analysis the development of a virtual, or mathematical, model is typically required. Theoretical analysis, whether it be finite element analysis, computational fluid dynamics, theoretical based equations, or any other method, has the advantage of an inherent flexibility not constrained by physical boundaries or conditions. Assumptions are often made to simplify complex geometry, approximate loading and/or boundary conditions, approximate material properties, and so on. These simplifying assumptions are often necessary for obtaining an efficient numerical solution but at a cost of reduced accuracy.

6.1.2 Experimental Analysis

Another option for determining the performance of a designed product or component is by means of actual measurements. Using suitable instrumentation the quantities of interest can be measured to obtain the desired test results. Often, efficient and accurate determinations of the values of interest are difficult to obtain analytically and an

experimental evaluation is the only means available (John and Haberman, 1980). Experimental studies can be carried out on full-scale products or on either reduced or inflated scale products to accommodate available experimental testing equipment. However, as is often the case, the manufacture of test products, especially when the geometric characteristics and material and processing methods must be precisely duplicated, can be cost prohibitive. The design or redesign of products based solely upon experimental product testing is an extremely inefficient approach and is therefore rarely used as the only analysis method.

6.1.3 Empirical Analysis

Experimental analysis is the method of choice when the variables and associated mathematics affecting a mechanical problem are too complex for the formulation of adequate expressions to describe the problem at hand. However, the number of variables affecting the problem could render all but the most specific experimental solutions prohibitive. For example, if we were confronted with a problem consisting of four variables (e.g. length, width, density, and load) each with only three possible states, the number of tests required to fully characterize the solution set would be $3^4 = 81$! Empirical analysis, in the framework of similitude-based design and as depicted in Fig. 6.1., serves two primary purposes. First, it serves as a processor for analyzing and manipulating experimental results including designing and organizing the experiments. Secondly it serves as a link between the analytical expressions governing the problem and the variables involved in the process. Both theoretical analysis and experimental analysis methods are critical components to a successful design and together with

empirical methods provide a flexible alternative to strict reliance on either theoretical or experimental solutions.

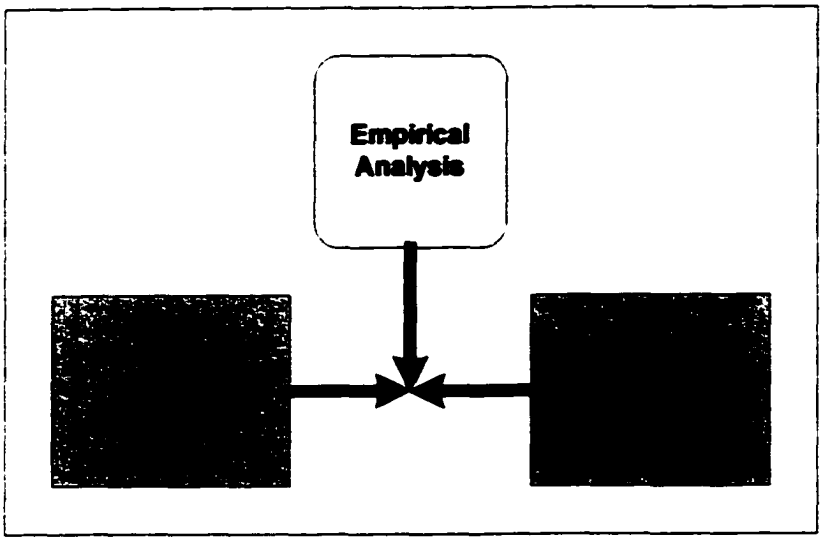

Fig. 6.1. Relationship Between Analysis Methods

6.2 Empirical Similarity Methods

Discussions in previous chapters have eluded to the difficulty in accurately characterizing the performance of a designed product by performing tests on a prototype model. This is largely due to the severe constraints imposed by the required similarity conditions that are often impractical or impossible to completely satisfy. Failure to satisfy the similarity conditions results in a system that lacks the required similarity between the product and the model for an accurate representation. The end result is a distorted system that, in terms of the traditional similarity method (TSM) π terms, is described by the following equation where the subscripts m and p denote the prototype model and product respectively:

$$\pi_{m,i} \neq \pi_{p,i}; \quad \forall i \tag{6.1}$$

With the recognized inability of the TSM to effectively handle distorted model-product systems, an empirical approach is adopted to bridge the gap between numerical and experimental methods. The infusion of empirical test data into the theoretical expressions for variable mapping between the model and product has shown promising results. In this section a method is developed to provide improved prediction accuracy and range of applicability and/or to reduce the constraints required for an accurate prediction. The task, as in TSM, is to determine the transformation required to get from the model state to successful prediction of the product state as shown in Fig. 6.2. While the TSM uses a single multiplication factor (λ) for this transformation (see Chapter 2), the empirical similarity method (ESM) takes advantage of empirical tests results to significantly improve the prediction accuracy achievable.

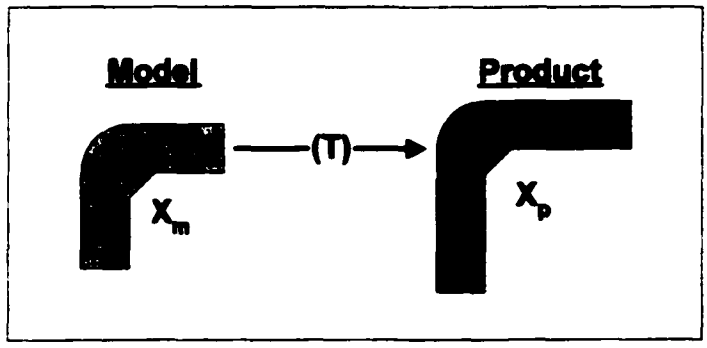

Fig. 6.2. Transformation from Model State to Product State

The goal of the ESM is to be able to accurately predict the state of a product ($\vec{X}_p$) from the measured states of the model specimen, product specimen and model ($\vec{X}_{ms}$, $\vec{X}_{ps}$, $\vec{X}_m$) according to the following generic formulation:

$$\bar{X}_p = f(\bar{X}_{ms}, \bar{X}_{ps}, \bar{X}_m)$$

In Chapter 3 we developed this fundamental relationship and went further to develop the following equations for prediction of the vector state of a product based upon the measured states of the model specimen, product specimen, and model:

$$[M] = \bar{X}_{ps}\bar{X}_{ms}^{+} \tag{3.9}$$

$$[G] = \bar{X}_m\bar{X}_{ms}^{+} \tag{3.10}$$

This leads to the following expressions for the prediction of the product vector state:

$$\bar{X}_p \cong [G]\cdot[M]\bar{X}_{ms} = (\bar{X}_m\bar{X}_{ms}^{+})(\bar{X}_{ps}\bar{X}_{ms}^{+})\bar{X}_{ms}$$

$$\bar{X}_p \cong \bar{X}_m\bar{X}_{ms}^{+}\bar{X}_{ps} \tag{6.2}$$

Initial attempts by Cho (Cho et al., 1998) to develop viable empirical similarity methods based upon the formulation of eqn. (6.2.) have been discussed previously. Each method was shown to have distinct advantages and disadvantages in their respective abilities to predict the performance of a product.

The Psuedo-Inverse method discussed previously provided an easily applied approach to predicting the performance of a product based upon the measured states of a model specimen, product specimen, and a model. Although relatively straightforward to apply, investigation into the method revealed that the derived scale and form transformation matrices were not unique representations of the transformations. In order to satisfy the uniqueness criteria further problem constraints or the application of an objective function

would be required. In addition, empirical tests conducted using this method have shown sensitivity to distortion, which manifests itself in significant differences between the transformation matrices [*M*] and [*M'*] from Fig. 3.9. The ability of the method to predict the product state is dependent upon the similarity of these transformation matrices and any differences will directly impact the accuracy of the prediction results. This observation led to the conclusion that this method is susceptible to errors in predicting the state of a product and, as a result, should not be used without further characterization of the limitations of the method.

In contrast to the Psuedo-Inverse method, the Circulent Matrix method was able to derive unique *material* [M] and *geometry* [G] transformation matrices using a single set of data points. The Circulent Matrix approach does require significantly more complex matrix manipulations and there is a severe loss in intuitive comprehension of the transformation process as a result.

In an effort to improve upon the predictive capability and intuitive representation of the transformation process of previous methods, the Compensation Matrix method is introduced. The method shows extremely promising results in the efficiency of its application, prediction accuracy, and advanced insight into the degree of model distortion and anticipated error in product performance prediction.

6.3 Compensation Matrix Approach:

The mechanical domain specificity used to constrain the development of the ESM in Chapter 3 is now relaxed. This allows the replacement of the previously used material transformation matrix [*M*] with a scale transformation matrix [*S*], which represents the

non-geometric state transformation which captures the state vector changes resulting from variations in material, fluid properties, temperature, etc. Similarly the geometry transformation matrix [*G*] is replaced with a form transformation matrix [*F*]. This serves to generalize the transformation through a de-emphasis of strict reliance on only the physical dimensions of the model specimen and model respectively. The goal of the ESM remains to empirically derive accurate scale [*S*] and form [*F*] transformation matrices from the measured states of the model specimen, product specimen, and model as shown in Fig. 6.3. The derived scale transformation matrix will be used as an approximation to the transformation matrix [*S'*] to predict the performance of the product from the measured state of the model. Representations of the four vector states involved in the method are shown below.

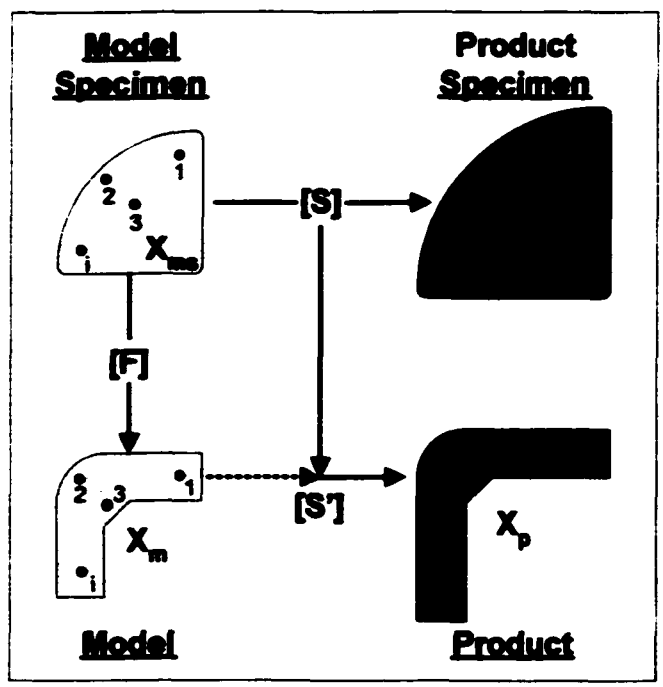

Fig. 6.3. Transformation Matrices and Vector Data Points

$$\bar{X}_{ms} = \begin{bmatrix} X_{ms,1} \\ X_{ms,2} \\ \vdots \\ X_{ms,J} \end{bmatrix} \qquad \bar{X}_{ps} = \begin{bmatrix} X_{ps,1} \\ X_{ps,2} \\ \vdots \\ X_{ps,J} \end{bmatrix}$$

$$\bar{X}_{m} = \begin{bmatrix} X_{m,1} \\ X_{m,2} \\ \vdots \\ X_{m,J} \end{bmatrix} \qquad \bar{X}_{p} = \begin{bmatrix} X_{p,1} \\ X_{p,2} \\ \vdots \\ X_{p,J} \end{bmatrix}$$

In this section a method is developed that provides a unique transformation matrix as well as vastly improved insights into the characteristics affecting the transformation matrices. Of particular interest is the characterization of the distortion in the model specimen-product specimen system. This approach uses the form matrix representation only indirectly through the application of the scale matrix formulation to the measured state of the model. Although the form transformation could be mathematically derived in a fashion similar to that of the scale transformation, the derivation is not required for application of the method.

Given a distorted system, it is advantageous to attempt to construct a scale transformation matrix [*S*] that maximizes the contribution of the similarity characteristics inherent in the two systems; model specimen and product specimen. It is also advantageous to attempt to separate the similarity characteristics from the dissimilar, or distorted, characteristics to the maximum extent possible to allow a direct determination of the degree of distortion in the system. The Compensation Matrix method achieves both of these goals simultaneously, a process which is graphically depicted in Fig. 6.4. The method accomplishes this through the combination of a scaled identity matrix [S_0], to

account for the similarity, and a matrix perturbation [δS], to account for the distortion in the system.

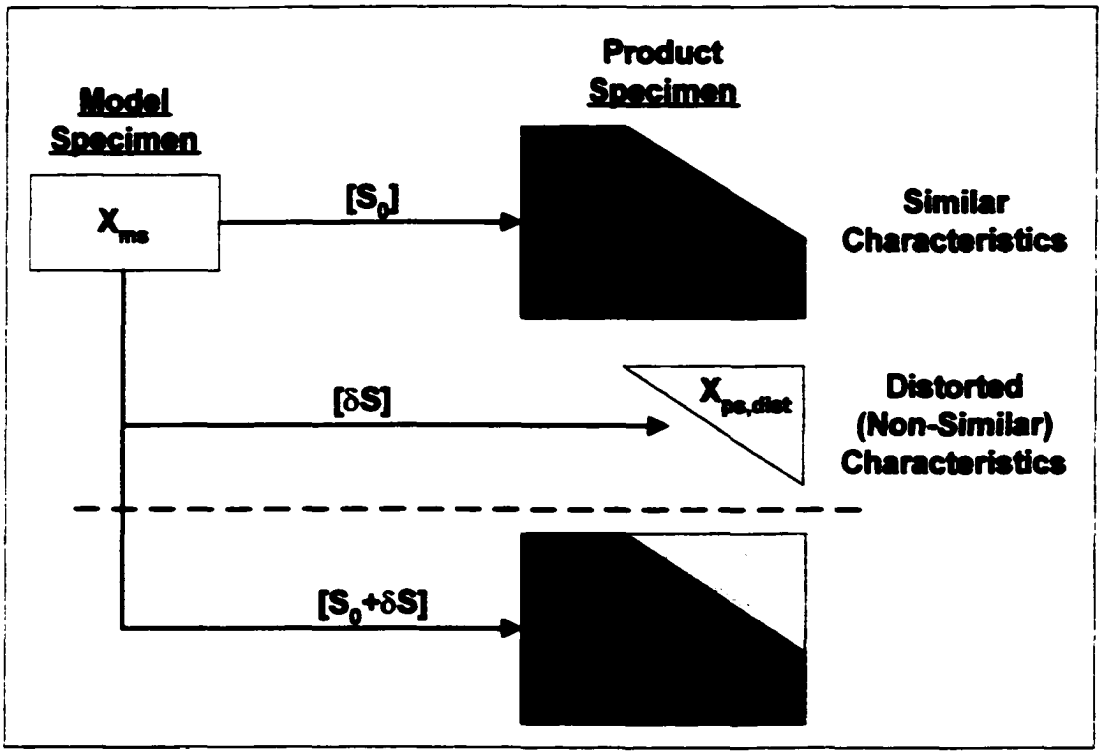

Fig. 6.4. Graphical Depiction of the Compensation Matrix Method

6.3.1 Capturing the System Similarity

Capturing 100 percent of the similarity and zero percent of the dissimilarity in a distorted model-product system is an extremely difficult, if not impossible, task due to the complex interrelationships between the parameters characterizing the problem. With an acceptance of this phenomenon a procedure is sought that will extract the maximum similarity in the system. The approach begins with the assumption that the scale transformation matrix [S] from Fig. 6.3. is a linear function. It is recognized that for the

special case where the relationship between the two state vectors, $\bar{X}_{ms}$ and $\bar{X}_{ps}$, is not distorted due to similarity constraints (i.e. no dissimilarity), the transformation matrix between the two systems can be represented as a scaled identity matrix as shown below.

$$\begin{aligned} X_{ps,1} &= \lambda X_{ms,1} \\ X_{ps,2} &= \lambda X_{ms,2} \\ &\vdots \\ X_{ps,n} &= \lambda X_{ms,n} \end{aligned}$$

where λ represents a scalar quantity

In matrix format the relations are expressed as follows:

$$\bar{X}_{ps} = \begin{bmatrix} \lambda & 0 & \cdots & 0 \\ 0 & \lambda & \cdots & 0 \\ \vdots & \vdots & \ddots & \vdots \\ 0 & 0 & \cdots & \lambda \end{bmatrix} \bar{X}_{ms}$$

$$\bar{X}_{ps} = \lambda [I] \bar{X}_{ms}$$

$$[S_0] = \lambda [I]$$

$$\Rightarrow \bar{X}_{ps} = [S_0] \bar{X}_{ms} \tag{6.3}$$

As previously stated, it is advantageous to derive a transformation matrix that maximizes the similarity characteristics inherent in the two systems, captured in this formulation in the $[S_0]$ scale matrix. If two systems are completely similar, the transformation is expected to yield exact results with no error. It is therefore hypothesized that maximizing the similarity in a distorted system will reduce the prediction error to the maximum extent possible. In an attempt to accomplish this a first

order least squares solution is derived as a best approximation to the transformation matrix $[S_0]$. This in effect produces a single linear function between the vector $\bar{X}_{ps}$ and the vector $\bar{X}_{ms}$. This least squares function represents a best-fit line through the data points contained in the state vectors in which the Chi-Square error is minimized (Nakos and Joyner, 1998).

The derivation begins with the state vectors for the model and product specimens as shown below.

$$\bar{X}_{ms} = \begin{bmatrix} X_{ms,1} \\ X_{ms,2} \\ \vdots \\ X_{ms,i} \end{bmatrix} \qquad \bar{X}_{ps} = \begin{bmatrix} X_{ps,1} \\ X_{ps,2} \\ \vdots \\ X_{ps,i} \end{bmatrix}$$

These state vectors can be written in the form of a linear equation as follows:

$$\begin{aligned} X_{ps_1} &= a + bX_{ms_1} \\ X_{ps_2} &= a + bX_{ms_2} \\ &\vdots \\ X_{ps_n} &= a + bX_{ms_n} \end{aligned} \qquad \rightarrow \begin{bmatrix} X_{ps_1} \\ X_{ps_2} \\ \vdots \\ X_{ps_n} \end{bmatrix} = \begin{bmatrix} 1 & X_{ms_1} \\ 1 & X_{ms_2} \\ \vdots & \vdots \\ 1 & X_{ms_n} \end{bmatrix} \begin{bmatrix} a \\ b \end{bmatrix}$$

$$\bar{X}_{ps} = [Z]\bar{v} \tag{6.4}$$

where: $$[Z] = \begin{bmatrix} 1 & X_{ms_1} \\ 1 & X_{ms_2} \\ 1 & \vdots \\ 1 & X_{ms_n} \end{bmatrix}, \qquad \bar{v} = \begin{bmatrix} a \\ b \end{bmatrix} \tag{6.5}$$

If the set of points $(X_{ms_1}, X_{ps_1})(X_{ms_2}, X_{ps_2})\ldots(X_{ms_n}, X_{ps_n})$ are not collinear, it will be impossible to find coefficients a & b to satisfy eqn. (6.4) exactly. Recognizing the unlikely possibility of a collinear relationship between $\bar{X}_{ms}$ and $\bar{X}_{ps}$ a solution, $\bar{v}^*$, is sought which will minimize the overall error in the straight-line approximation. That error is defined by:

$$\left|\bar{X}_{ps} - [Z]\bar{v}\right|$$

A first order least squares solution takes the following form:

$$\bar{v} = \bar{v}^* = \begin{bmatrix} a^* \\ b^* \end{bmatrix}$$

This expression provides the best fit through the data points defined by the line:

$$X_{ps_i} = a^* + b^* X_{ms_i} \quad \forall\, i = 1,2,\ldots,n$$

The values of a^* and b^* are determined from the following equation:

$$\bar{v}^* = \left(Z^T \cdot Z\right)^{-1} \cdot Z^T \cdot X_{ps} \tag{6.6}$$

$$\bar{v}^* = \begin{bmatrix} v_0 \\ v_1 \end{bmatrix}$$

It can be shown that the equation for $\bar{v}^*$ is always consistent and always produces a least squares straight line fit to the data (Hill, 1986). The solution provided is unique if, and only if; the values in the $\bar{X}_{ms}$ state vector are all different (e.g. no two or more

elements of the vector have the same value). The equation of the least squares line through the data points is then written as follows where $\hat{e}$ represents a unit vector with the same dimensions as the state vectors, $\bar{X}_{ms}$ & $\bar{X}_{ps}$:

$$\bar{X}_{ps} = (\nu_1)\bar{X}_{ms} + (\nu_0)\hat{e} \tag{6.7}$$

This equation provides the diagonal values of the $[S_0]$ matrix from the ν_1 term and also provides an additional correction term in the form of the ν_0 term, synonymous with the y-intercept in the above equation for the line. The first order least squares derived $[S_0]$ matrix is now presented as follows:

$$[S_0] = \begin{bmatrix} \nu_1 & 0 & \cdots & 0 \\ 0 & \nu_1 & 0 & 0 \\ \vdots & \vdots & \ddots & \vdots \\ 0 & 0 & \cdots & \nu_1 \end{bmatrix} \tag{6.8}$$

The linear transformation from $\bar{X}_{ms}$ to $\bar{X}_{ps}$ now takes the following form from eqn. (6.7):

$$\Rightarrow \bar{X}_{ps} = [S_0]\bar{X}_{ms} + \nu_0\hat{e} \tag{6.9}$$

6.3.2 Isolating the System Dissimilarity

The vast majority of modeled systems do contain a degree of distortion arising from material, geometry, loading conditions, or a number of other sources. Still, the above derivation provides a good foundational starting point as the only assumption made to

this point is one of linearity of the transformation between the two considered specimen systems. As a point of departure we now seek an adjustment to the scale matrix [S_0], by way of a matrix perturbation, [δS], to the approximation described above which would allow the consideration of distorted systems in addition to similar systems. As previously stated, it is advantageous to derive a transformation matrix that both maximizes the similarity characteristics inherent in the two systems, captured in the [S_0] matrix, and also isolates the distortion in the system [δS] to the maximum extent possible. The following formulation satisfies these objectives:

$$\vec{X}_{ps} = [S_0 + \delta S]\vec{X}_{ms} + v_0\hat{e} \tag{6.10}$$

In this expression the term $[S_0 + \delta S]$ is designated as the compensation transformation matrix due to its constituents of the scaled identity matrix component and the perturbed matrix component. A perturbation to the scale matrix [S_0] is sought, which will result in a maximization of the diagonal norm of the combined matrix $[S_0 + \delta S]$. Maximizing the diagonal norm is equivalent to perturbing the Compensation Matrix in such a way as to maximize the similarity and thereby minimize the distortion in the transformation between the two state vectors. Using this approach increases the confidence that the error in the transformation has been minimized. The diagonal norm of an n x n matrix [S] is defined as follows (Noble and Daniel, 1988):

$$\|S\|_{Diag} = \sum_{i=1}^{n} s_{ii}^{\,2} \qquad \text{where: } i = 1,2,\ldots,n, \text{ and m is an element of } [S] \tag{6.11}$$

It can be seen that for a completely similar system the diagonal norm will always be maximal due to the absence of any off-diagonal terms.

By way of an illustrative example, as well as a preview of the new Compensation Matrix method, consider the following state vectors and the resulting transformation matrices derived from the Psuedo-Inverse, the Circulent Matrix, and the Compensation Matrix methods:

$$\bar{X}_{ms} = \begin{bmatrix} 0 \\ -0.204 \\ -0.742 \\ -1.500 \\ -2.368 \end{bmatrix} \qquad \bar{X}_{ps} = \begin{bmatrix} 0 \\ -0.086 \\ -0.313 \\ -0.635 \\ -1.002 \end{bmatrix}$$

Psuedo-Inverse Method (reference procedure described in Chapter 3):

$$[M]_{Psuedo\_Inverse} = \begin{bmatrix} 0 & 0 & 0 & 0 & 0 \\ 0 & 2.084E-3 & 7.568E-3 & 0.015 & 0.024 \\ 0 & 7.577E-3 & 0.028 & 0.028 & 0.088 \\ 0 & 0.015 & 0.056 & 0.113 & 0.178 \\ 0 & 0.024 & 0.088 & 0.178 & 0.281 \end{bmatrix}$$

Circulent Matrix Method (reference procedure described in Chapter 3):

$$[M]_{Circulent} = \begin{bmatrix} 0.295 & -0.024 & -8.233E-3 & 3.5E-3 & 2.399E-3 \\ 2.399E-3 & 0.295 & -0.024 & -8.233E-3 & 3.5E-3 \\ 3.5E-3 & 2.399E-3 & 0.295 & -0.024 & -8.233E-3 \\ -8.233E-3 & 3.5E-3 & 2.399E-3 & 0.295 & -0.024 \\ -0.024 & -8.233E-3 & 3.5E-3 & 2.399E-3 & 0.295 \end{bmatrix}$$

Compensation Matrix Method (derivation provided in the following section):

$$[S]_{Compensation} = \begin{bmatrix} 0.423 & 6.099E-6 & 2.214E-5 & 4.479E-5 & 7.071E-5 \\ 0 & 0.423 & 8.171E-7 & 1.653E-6 & 2.609E-6 \\ 0 & -6.552E-6 & 0.423 & -4.811E-5 & -7.596E-5 \\ 0 & -4.922E-6 & -1.787E-5 & 0.423 & -5.706E-5 \\ 0 & 5.15E-6 & 1.87E-5 & 3.782E-5 & 0.423 \end{bmatrix}$$

Table 6.1. provides a comparison of the diagonal norms of the transformation matrices for the three methods presented above. As the table clearly shows, the Compensation Matrix method is much more effective at separating the similar contributions from the dissimilar contributions based upon the diagonal norm of the matrices. It is mathematically possible, and even probable, to fail to account for all the similarity in the matrix and thereby have it present itself as distortion components. The accuracy of this approach hinges on several criteria including a determination of the best similarity matrix $[S_0]$ for the approximation. A first order least squares solution maximizes the similarity in a linear system isolating the remaining distortion.

Table 6.1. Diagonal Norm of Matrices A, B, & C

Matrix	Derivation Method	Diagonal Norm
A	Psuedo-Inverse	0.092
B	Circulent Matrix	0.435
C	Compensation Matrix	0.896

6.3.3 Developing the Method

In addition to improving the accuracy of the prediction, the Compensation Matrix approach also offers a greater degree of insight into the characteristics of the system distortion than previous methods, which offers the potential to analyze the anticipated

error in the prediction. From eqn. (6.10) we can rearrange terms and solve for the matrix perturbation [δS] as follows:

$$[\delta S] = \left(\bar{X}_{ps} - v_0\hat{e} - [S_0]\bar{X}_{ms}\right)\bar{X}_{ms}^{+} \tag{6.12}$$

This expression again requires the use of the psuedo-inverse of $\bar{X}_{ms}$ (Strang, 1988) as opposed to the inverse since the state vector is normally not square and thus not invertible. From this expression, given that [S_0] is uniquely determined as shown above, the value of [δS] is also uniquely determined.

The expression for the prediction of the product state vector ($\bar{X}_p$) can now be derived from eqn. (6.10) as shown below and as shown graphically in Fig. 6.5.

$$\bar{X}_p \cong [S_0 + \delta S]\bar{X}_m + v_0\hat{e} \tag{6.13}$$

The interrelationship between the scaled identity matrix [S_0], derived from the least squares approximation, and the perturbed matrix [δS], can best be expressed as a function of system distortion. The distortion, a numerical measure of the dissimilarity in the system, is defined as the ratio of the sum of the squares of the perturbed matrix elements to that of the scaled identity matrix elements. The higher the value of distortion, the more dissimilar the two state vectors are and the more influence the perturbed matrix has on the mapping between the state vectors. In equation form the distortion is defined as shown in eqn. (6.14).

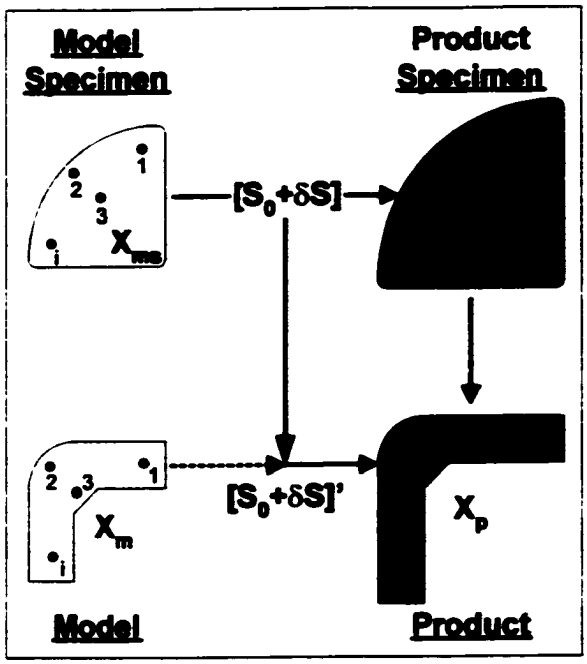

Fig. 6.5. Compensation Matrix Method Transformation Matrix

$$Distortion = \frac{\sum_{i=1}^{n}\sum_{j=1}^{n}\delta S_{ij}^{\,2}}{\sum_{i=1}^{n} S_{ii}^{\,2}} \tag{6.14}$$

A generic example will serve to demonstrate the fundamental characteristics of the derived scale and perturbed matrices. We begin the example with arbitrary state vectors defined in eqn. (6.15) and shown graphically in Fig. 6.6.

$$\bar{X}_{ms} = \begin{bmatrix} 0 \\ 1 \\ 2 \\ 3 \\ 4 \end{bmatrix} \quad \bar{X}_{ps-1} = \begin{bmatrix} 10 \\ 15 \\ 20 \\ 25 \\ 30 \end{bmatrix} \quad \bar{X}_{ps-2} = \begin{bmatrix} 10 \\ 15 \\ 19 \\ 22 \\ 24 \end{bmatrix} \quad \bar{X}_{ps-3} = \begin{bmatrix} 10 \\ 19 \\ 24 \\ 24 \\ 20 \end{bmatrix} \tag{6.15}$$

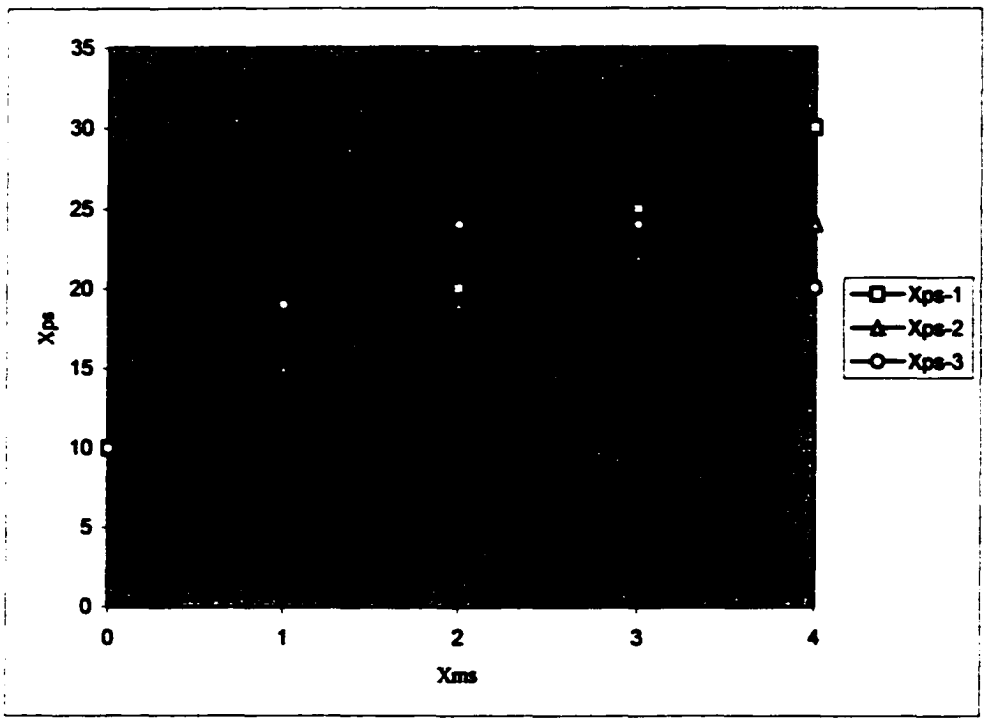

Fig. 6.6. Hypothetical Measured States of $\bar{X}_{ps-1}$, $\bar{X}_{ps-2}$, *and* $\bar{X}_{ps-3}$ in Relation to $\bar{X}_{ms}$

As is evident from both the state vectors and the figure, the degree of non-linearity introduced into the vectors increases from $\bar{X}_{ps-1}$, a linear function, to $\bar{X}_{ps-3}$, a highly non-linear function. This was done purposely to demonstrate the flexibility of the method to accommodate distortion, due to non-linearity in this case, in the predictive capability of the method.

The functional relationship between $\bar{X}_{ms}$ and $\bar{X}_{ps-1}$ is completely linear and, therefore, no distortion is expected in the derivation of the transformation matrix [*S*]. The functional relationship between $\bar{X}_{ms}$ and $\bar{X}_{ps-2}$ is slightly non-linear and the relationship between $\bar{X}_{ms}$ and $\bar{X}_{ps-3}$ is highly non-linear. These two state vectors are expected to

introduce distortion in the derivation of the transformation matrix [*S*]. These characteristics will be demonstrated in the derivation that follows.

For each state vector analyzed the least squares solution will be presented followed by the formulation of the equation of the resulting line. Next the compensated transformation matrices [*S*] will be presented followed by decomposition into the similarity matrices (or scaled identity matrices) [S_0] and the perturbed matrices [δS]. Finally the calculated diagonal norm, distortion (see eqn. (6.14)), absolute error, and the predicted values of the state vector will be presented. This will allow the changes in the matrices to be observed as distortion is introduced into the system.

1) $\bar{X}_{ps-1}$:

Equation of best-fit line through data points: $\bar{v}_1^* = \begin{bmatrix} v_0 \\ v_1 \end{bmatrix} = \begin{bmatrix} 10 \\ 5 \end{bmatrix}$

$$\bar{X}_{ps-1} = (5)\bar{X}_{ms} + (10)$$

Compensation Matrix: $[S_1] = \begin{bmatrix} 5 & 0 & 0 & 0 & 0 \\ 0 & 5 & 0 & 0 & 0 \\ 0 & 0 & 5 & 0 & 0 \\ 0 & 0 & 0 & 5 & 0 \\ 0 & 0 & 0 & 0 & 5 \end{bmatrix}$

Similarity Matrix: $[S_{0_1}] = \begin{bmatrix} 5 & 0 & 0 & 0 & 0 \\ 0 & 5 & 0 & 0 & 0 \\ 0 & 0 & 5 & 0 & 0 \\ 0 & 0 & 0 & 5 & 0 \\ 0 & 0 & 0 & 0 & 5 \end{bmatrix}$

Perturbed Matrix: $[\delta S_1] = \begin{bmatrix} 0 & 0 & 0 & 0 & 0 \\ 0 & 0 & 0 & 0 & 0 \\ 0 & 0 & 0 & 0 & 0 \\ 0 & 0 & 0 & 0 & 0 \\ 0 & 0 & 0 & 0 & 0 \end{bmatrix}$

Diagonal Norm ($\bar{X}_{ps-1}$): 125.0

Distortion ($\bar{X}_{ps-1}$): 0.0

Prediction Accuracy ($\bar{X}_{ps-1}$): 100 %

State Vector Prediction ($\bar{X}_{ps-1}$): $\bar{X}_{ps-1}|_{Pred} = \begin{bmatrix} 10 \\ 15 \\ 20 \\ 25 \\ 30 \end{bmatrix}$

2) $\bar{X}_{ps-2}$:

Equation of best-fit line through data points: $\bar{v}_2^* = \begin{bmatrix} v_0 \\ v_1 \end{bmatrix} = \begin{bmatrix} 11 \\ 3.5 \end{bmatrix}$

$$\bar{X}_{ps-2} = (3.5)\bar{X}_{ms} + (11)$$

Compensation Matrix: $[S_2] = \begin{bmatrix} 3.5 & -0.033 & -0.067 & -0.1 & -0.133 \\ 0 & 3.517 & 0.033 & 0.05 & 0.067 \\ 0 & 0.033 & 3.567 & 0.1 & 0.133 \\ 0 & 0.017 & 0.033 & 3.55 & 0.067 \\ 0 & -0.033 & -0.067 & -0.1 & 3.367 \end{bmatrix}$

Similarity Matrix: $[S_{0_2}]=\begin{bmatrix} 3.5 & 0 & 0 & 0 & 0 \\ 0 & 3.5 & 0 & 0 & 0 \\ 0 & 0 & 3.5 & 0 & 0 \\ 0 & 0 & 0 & 3.5 & 0 \\ 0 & 0 & 0 & 0 & 3.5 \end{bmatrix}$

Perturbed Matrix: $[\delta S_2]=\begin{bmatrix} 0 & -0.033 & -0.067 & -0.1 & -0.133 \\ 0 & 0.17 & 0.033 & 0.05 & 0.067 \\ 0 & 0.033 & 0.067 & 0.1 & 0.133 \\ 0 & 0.017 & 0.033 & 0.05 & 0.067 \\ 0 & -0.033 & -0.067 & -0.1 & -0.133 \end{bmatrix}$

Diagonal Norm ($\bar{X}_{ps-2}$): 61.275

Distortion ($\bar{X}_{ps-2}$): 1.905×10^{-3}

Prediction Accuracy ($\bar{X}_{ps-2}$): 100 %

State Vector Prediction ($\bar{X}_{ps-2}$): $\bar{X}_{ps-2}|_{Pred}=\begin{bmatrix} 10 \\ 15 \\ 19 \\ 22 \\ 24 \end{bmatrix}$

3) $\bar{X}_{ps-3}$:

Equation of best-fit line through data points: $\bar{v}_3^* = \begin{bmatrix} v_0 \\ v_1 \end{bmatrix} = \begin{bmatrix} 14.4 \\ 2.5 \end{bmatrix}$

$$\bar{X}_{ps-3} = (2.5)\bar{X}_{ms} + (14.4)$$

Compensation Matrix: $[S_3]=\begin{bmatrix} 2.5 & -0.147 & -0.293 & -0.44 & -0.587 \\ 0 & 2.57 & 0.14 & 0.21 & 0.28 \\ 0 & 0.153 & 2.807 & 0.46 & 0.613 \\ 0 & 0.07 & 0.14 & 2.71 & 0.28 \\ 0 & -0.147 & -0.293 & -0.44 & 1.913 \end{bmatrix}$

Similarity Matrix: $[S_{0_3}]=\begin{bmatrix} 2.5 & 0 & 0 & 0 & 0 \\ 0 & 2.5 & 0 & 0 & 0 \\ 0 & 0 & 2.5 & 0 & 0 \\ 0 & 0 & 0 & 2.5 & 0 \\ 0 & 0 & 0 & 0 & 2.5 \end{bmatrix}$

Perturbed Matrix: $[\delta S_3]=\begin{bmatrix} 0 & -0.147 & -0.293 & -0.44 & -0.587 \\ 0 & 0.07 & 0.14 & 0.21 & 0.28 \\ 0 & 0.153 & 0.307 & 0.46 & 0.613 \\ 0 & 0.07 & 0.14 & 0.21 & 0.28 \\ 0 & -0.147 & -0.293 & -0.44 & -0.587 \end{bmatrix}$

Diagonal Norm ($\bar{X}_{ps-3}$): 31.737

Distortion ($\bar{X}_{ps-3}$): 0.073

Prediction Accuracy ($\bar{X}_{ps-3}$): 100 %

State Vector Prediction ($\bar{X}_{ps-3}$): $\bar{X}_{ps-3}|_{Pred}=\begin{bmatrix} 10 \\ 19 \\ 24 \\ 24 \\ 20 \end{bmatrix}$

The results of this example are summarized in Fig. 6.7., Fig. 6.8., and Fig. 6.9. which shows the value of the diagonal norm, the calculated distortion, and the prediction accuracy of the three state vectors respectively, using the Compensation Matrix method.

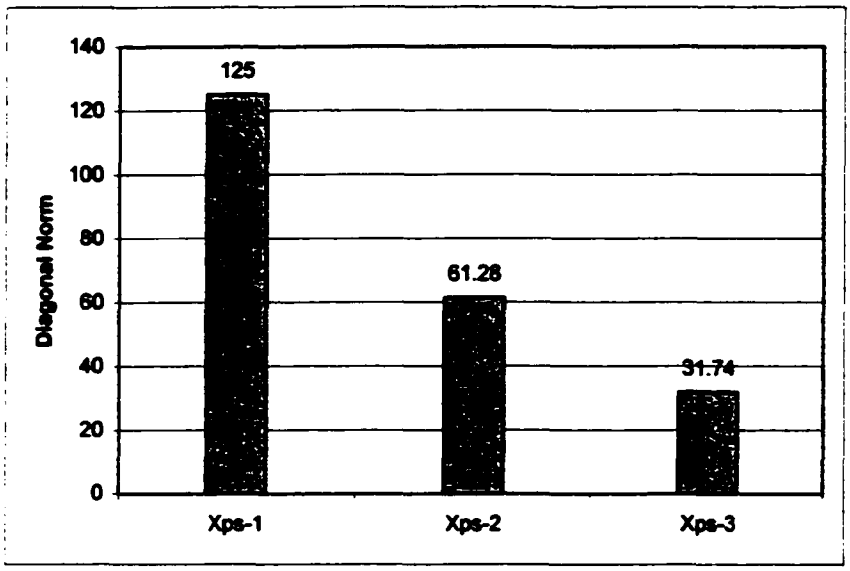

Fig. 6.7. Comparison of Diagonal Norms for $\bar{X}_{ps-1}$, $\bar{X}_{ps-2}$, *and* $\bar{X}_{ps-3}$

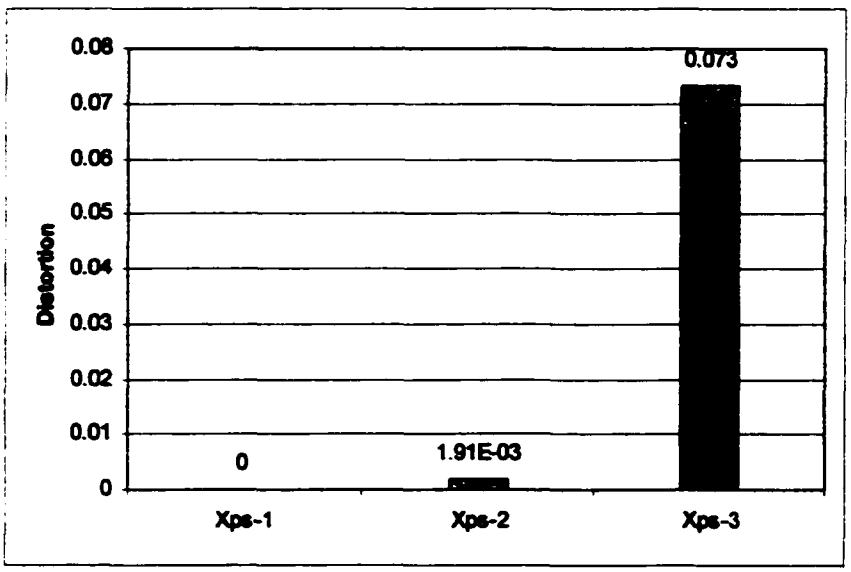

Fig. 6.8. Comparison of System Distortion for $\bar{X}_{ps-1}$, $\bar{X}_{ps-2}$, *and* $\bar{X}_{ps-3}$

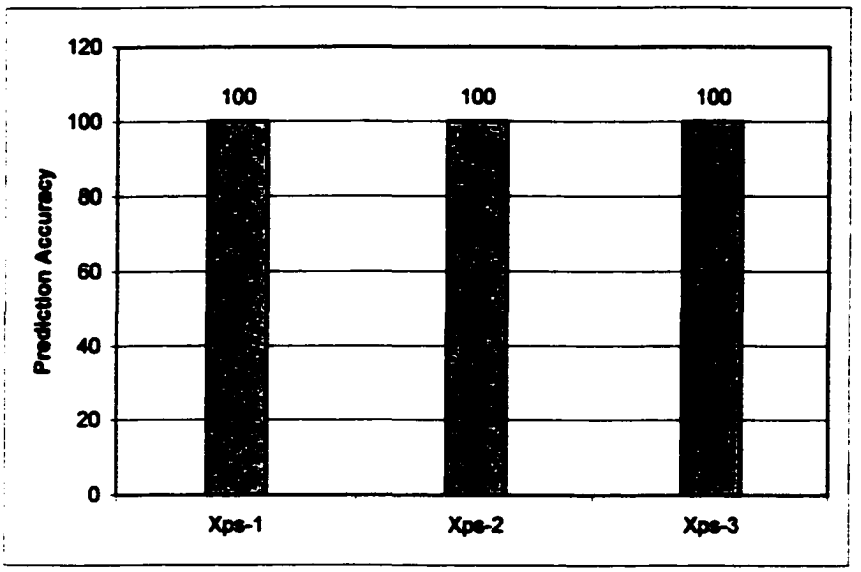

Fig. 6.9. Comparison of Prediction Accuracy for $\bar{X}_{ps-1}$, $\bar{X}_{ps-2}$, *and* $\bar{X}_{ps-3}$

As the figures clearly demonstrate, at least for this generic example, the perturbation matrix compensates the overall transformation matrix for any distortion in the system.

The Compensation Matrix approach has demonstrated the ability to derive unique transformation matrices and presents itself in a form that allows straightforward observation of the matrix manipulations required in order to achieve a solution. A separation of the similarity contribution, provided by $[S_0]$, from the distorted contributions, provided by $[\delta S]$, also allows further analysis of the degree of distortion in the approximation. It is hypothesized that the degree of accuracy in any of the methods presented thus far can be relatively determined by an examination of the magnitude of the diagonal norm of the transformation matrix. A higher value of the diagonal norm is indicative of an improved optimization of the similarity characteristics in the system. This hypothesis will be discussed further in the example that follows.

6.4 Example Application - Compensation Matrix Method

The tapered cantilevered beam example presented in Chapter 3 for the verification of the original ESMs is repeated here as a demonstration of the improved capabilities of the Compensation Matrix method. In addition to providing an accurate basis for comparison with previous methods, the example also captures the mechanics of materials phenomena most often used by products incorporating compliance in their design, the bending of beams. During the course of the empirical product study documented in Chapter 5, the preponderance of products investigated used the bending of a flexible member to achieve the degree of relative motion required to maintain functionality of the original product. The study verified that very few products using compliant members or structures in their design subject the members to either axial or torsional loading. With this evidence in hand a continuance of this example proceeds.

The product predictive capability of the newly developed Compensation Matrix method is compared to both the Circulent Matrix method and the theoretical or empirically derived actual product performance. The results are presented as both a direct comparison of the prediction results and as a measure of the respective error of the two methods in comparison to the baseline product.

Various methods have been investigated to attempt to accurately characterize the error in the performance prediction without giving bias to the method. The error method chosen for this example is a median-based relative error formulation (Gerald and Wheatley, 1989). This method is a modified version of the Chi-Square relative error approach (Dally and Riley, 1991) which is shown below in eqn. (6.16). Using the Chi-Square method without modification resulted in extremely large errors with only small differences between the predicted and actual values. This occurs at points where the

value of the denominator, Xp_{Pred_i}, is very close to zero such as the predicted deflection at the cantilever support end of the beam or the normal stress at the free end of a beam.

$$Error_i = \left[\frac{\left(Xp_{Pred_i} - Xp_{Act_i} \right)^2}{Xp_{Pred_i}^2} \right]^{0.5} \quad \forall i \tag{6.16}$$

A modification is sought to the above equation, which will not skew the calculated errors at these critical, or any other measurement points. By substituting the mean value of Xp_{Pred_i} into the denominator of eqn. (6.16) a mean-based relative calculated error is derived as shown in eqn. (6.17) below.

$$Mean\ Error_i = \left[\frac{\left(Xp_{Pred_i} - Xp_{Act_i} \right)^2}{\overline{Xp}_{Pred}^2} \right]^{0.5} \quad \forall i \tag{6.17}$$

This example provides a numerical study of the predicted deflection, angle of rotation, and maximum normal stress of a tapered cantilevered beam. The value of this example lies in the ability to theoretically determine the correct values and thus provide an absolute measure of the accuracy of the methods. This example provides a direct comparison between the prediction capabilities of the Compensation Matrix and Circulent Matrix methods. The goal in this example is to predict the performance of an aluminum, tapered, cantilevered beam, supporting both the beam weight (calculated as a function of the beam geometry and specified material density) and a transverse load acting in the vertical direction and applied to the end of the beam as shown in Fig. 6.10.

The specimens used for this problem are straight, cantilevered beams with similar loading configurations as shown in Fig. 6.11.

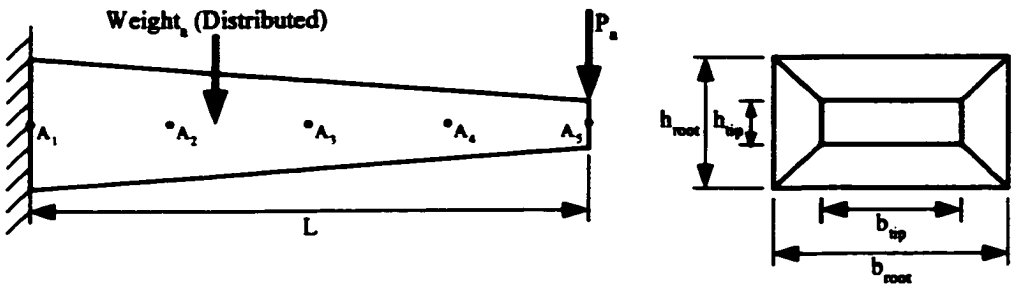

Fig. 6.10. Tapered Cantilevered Beam Geometry & Measurement Points

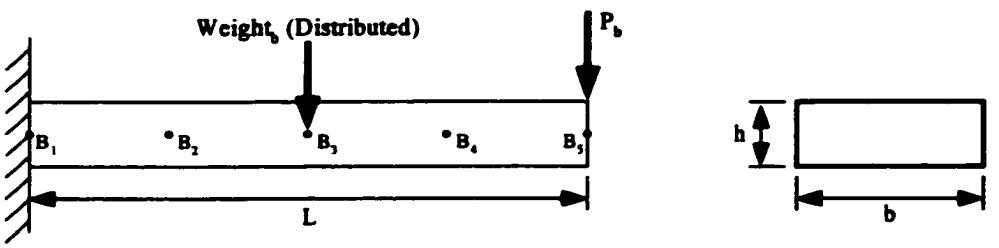

Fig. 6.11. Specimen Beam Geometry & Measurement Points

The geometry, loading conditions, and material properties for the model specimen (ms), the product specimen (ps), the model (m), and the product (p) are listed in Table 6.2. Note the simplified geometry of the specimen beams, which are more easily manufactured than the often geometrically complex model and product counterparts. The model family (model specimen and model) is fabricated using a representative rapid-prototyped polymeric material and process, again to suggest the potential of greatly reduced time and expense as compared to fabrication of full-scale material and process

specific products. The product family (product specimen and product) is fabricated using a material and process representative of the anticipated final design.

Table 6.2. Geometry, Loading, and Material Properties

	Model Spec	Product Spec	Model	Product
Load (N)	.54	50	.54	50
Modulus (GPa)	3.1	72.3	3.1	72.3
Density (kg/m^3)	1200	2783	1200	2783
Length (m)	.2	.2	.4	.4
Root Height – h_{root} (m)	.0032	.0032	.0095	.0095
Root Width – b_{root} (m)	.025	.025	.05	.05
Tip Height – h_{tip} (m)	.0032	.0032	.005	.005
Tip Width – b_{tip} (m)	.025	.025	.025	.025

The above parameters, in conjunction with the differential equations expressing the deflection, angle of rotation, and normal stress of the beam, represent a non-linear system. This non-linearity was introduced purposely to demonstrate the ability of the methods to overcome this source of dissimilarity. The non-linearity is a result of the following:

1. Geometry – The geometrical shape of the specimen beams does not linearly map to the shape of the model/product beams as a result of the taper introduced into the latter beams.
2. Material Properties – In the review of the TSM it was shown that for two systems of this type to be similar, the ratio of (ρ/E) had to be equal. From the parameters in the above table the following ratios are calculated which show significant differences and are, as a result, a source of non-linearity in this example:

$$\left(\frac{\rho}{E}\right)_{Model} = \left(\frac{1200}{3.1x10^9}\right) = 0.387x10^{-6}$$

$$\left(\frac{\rho}{E}\right)_{Product} = \left(\frac{2783}{72.3x10^9}\right) = 0.0384x10^{-6}$$

3. Stiffness – Although not modeled in this example, certain materials can exhibit variations in stiffness properties (e.g. modulus of elasticity, modulus of rigidity) due to strain hardening under load, material processing influence, or other factors. These can also be a source of non-linear behavior between the states of two systems.

The linear and angular deformation as well as the stress in the beams result from a combination of the applied concentrated loading and the distributed weight of the beam. From the information provided in Table 6.2. the theoretical deflection, angle of rotation, and maximum normal stress in the beam are numerically calculated at any point along the length of the beam through direct integration of the following moment and distributed load equations:

$$\frac{d^2y}{dx^2} = \frac{M(x)}{EI}$$

$$\frac{d^4y}{dx^4} = \frac{-w(x)}{EI}$$

where: M(x) = Internal moment acting on the beam's cross section

w(x) = Distributed load due to weight

Complete derivations of the deflections and stresses are included in Appendix B.

6.4.1 Beam Deflection

By arbitrarily selecting five equally spaced points along the neutral axis of the beams (see Fig. 6.10. and Fig. 6.11.) state vectors representing discretized deflections for each of the four beam configurations are numerically derived with the following results:

$$\bar{X}_{mv} = \begin{bmatrix} 0 \\ -0.5943 \\ -2.159 \\ -4.367 \\ -6.895 \end{bmatrix} \qquad \bar{X}_{pv} = \begin{bmatrix} 0 \\ -2.322 \\ -8.445 \\ -17 \\ -27 \end{bmatrix}$$

(values shown in mm)

$$\bar{X}_{m} = \begin{bmatrix} 0 \\ -0.1145 \\ -0.4889 \\ -1.163 \\ -2.112 \end{bmatrix} \qquad \bar{X}_{p} = \begin{bmatrix} 0 \\ -0.4192 \\ -1.809 \\ -4.347 \\ -7.958 \end{bmatrix}$$

The predicted beam deflections using the Compensation Matrix and Circulent Matrix methods are shown in Fig. 6.12. The relative errors in each method are shown in Fig. 6.13. in comparison to the theoretical solution. As the figures clearly show, the prediction of the beam deflection using both approaches shows extremely good correlation with the theoretical deflection of the beam. From the error graphs of Fig. 6.13. it can be seen that the error in the Compensation Matrix method is slightly less and thus the overall prediction accuracy improved over the Circulent Matrix method. Table 6.3. shows a summary of the error summation for each of the five points and a calculation of the diagonal norm for each of the methods. The table verifies that the Compensation Matrix method is superior for predicting the product beam deflection.

Table 6.3. Total Mean Error and Diagonal Norm Comparisons for Beam Deflection

	Circulent	Compensation
Total Mean Error	7.66%	4.46%
Diagonal Norm	6.86×10^{-3}	4.92×10^{3}

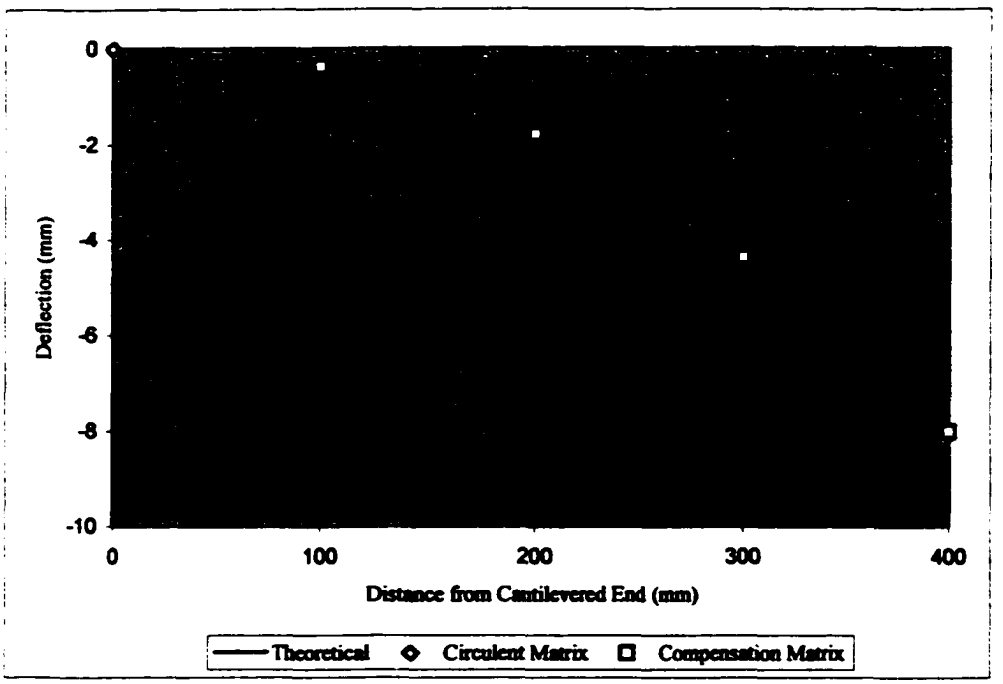

Fig. 6.12. Predicted Deflection using Circulent and Compensation Matrix Methods

The transformation matrices derived by each of the methods are drastically different as is evident from the respective calculated diagonal norms. As previously discussed, the degree of accuracy in any of the methods presented thus far can be relatively determined by an examination of the magnitude of the diagonal norm of the transformation matrix. A higher value of the diagonal norm is indicative of an improved optimization of the similarity characteristics in the system. The transformation matrices are provided below for further inspection.

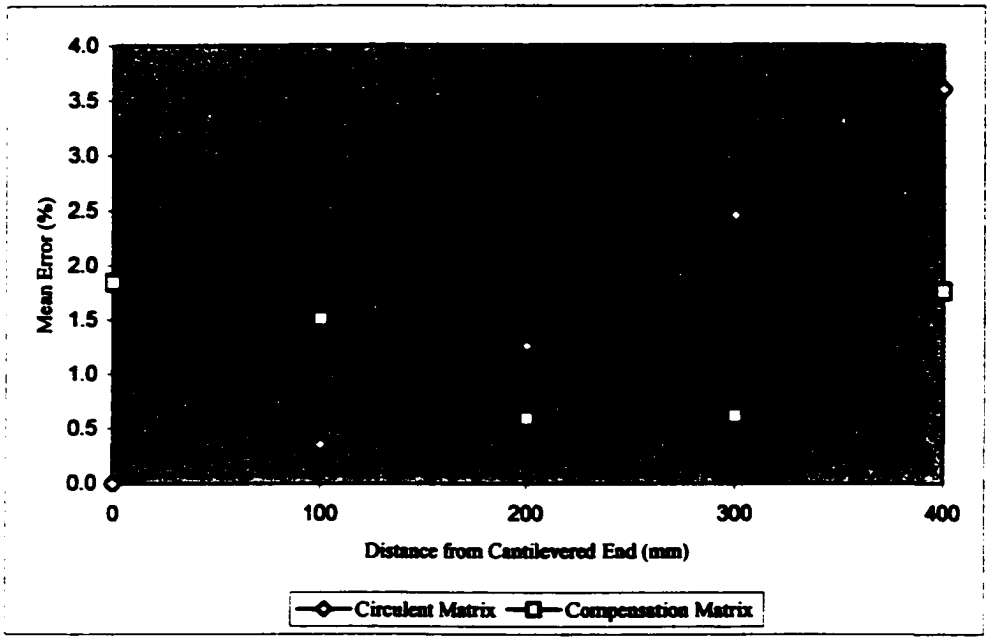

Fig. 6.13. Error in Predicted Beam Deflection

$$[M]_{Circulant} = \begin{bmatrix} 0.037 & -3.139E-3 & -1.078E-3 & 4.666E-4 & 3.126E-4 \\ 3.126E-4 & 0.037 & -3.139E-3 & -1.078E-3 & 4.666E-4 \\ 4.666E-4 & 3.126E-4 & 0.037 & -3.139E-3 & -1.078E-3 \\ -1.078E-3 & 4.666E-4 & 3.126E-4 & 0.037 & -3.139E-3 \\ -3.139E-3 & -1.078E-3 & 4.666E-4 & 3.126E-4 & 0.037 \end{bmatrix}$$

$$[S]_{Compensation} = \begin{bmatrix} 31.365 & 4.611E-4 & 1.675E-3 & 3.388E-3 & 5.35E-3 \\ 0 & 31.365 & 6.222E-5 & 1.259E-4 & 1.987E-4 \\ 0 & -4.953E-4 & 31.363 & -3.639E-3 & -5.746E-3 \\ 0 & -3.723E-4 & -1.352E-3 & 31.362 & -4.319E-3 \\ 0 & 3.893E-4 & 1.414E-3 & 2.86E-3 & 31.37 \end{bmatrix}$$

Another advantage to the Compensation Matrix method is the ability to observe the distortion in the model-product specimen system by virtue of the perturbed matrix components. In this example the distortion in the system is calculated for the

Compensation Matrix method (see eqn. (6.14)) to be 3.09×10^{-8}, which is extremely small but still only qualitative without a baseline for comparison.

6.4.2 Beam Angle of Rotation

Using the same procedure the angle of rotation of the beam is evaluated as a function of the beam length. The predicted beam rotations using the two methods are shown in Fig. 6.14. The relative errors in each method are shown in Fig. 6.15. in comparison to the theoretical solution. As the figures clearly show, the prediction of the beam rotation using the both the Compensation Matrix and the Circulent Matrix approaches show extremely good correlation with the theoretical rotation of the beam.

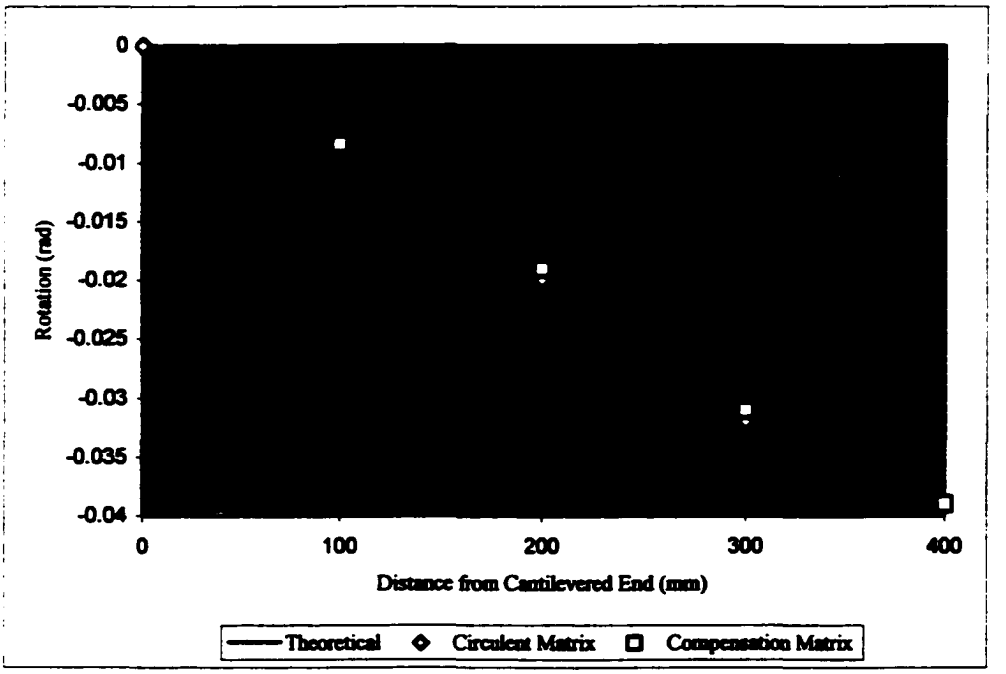

Fig. 6.14. Predicted Rotation using Circulent and Compensation Matrix Methods

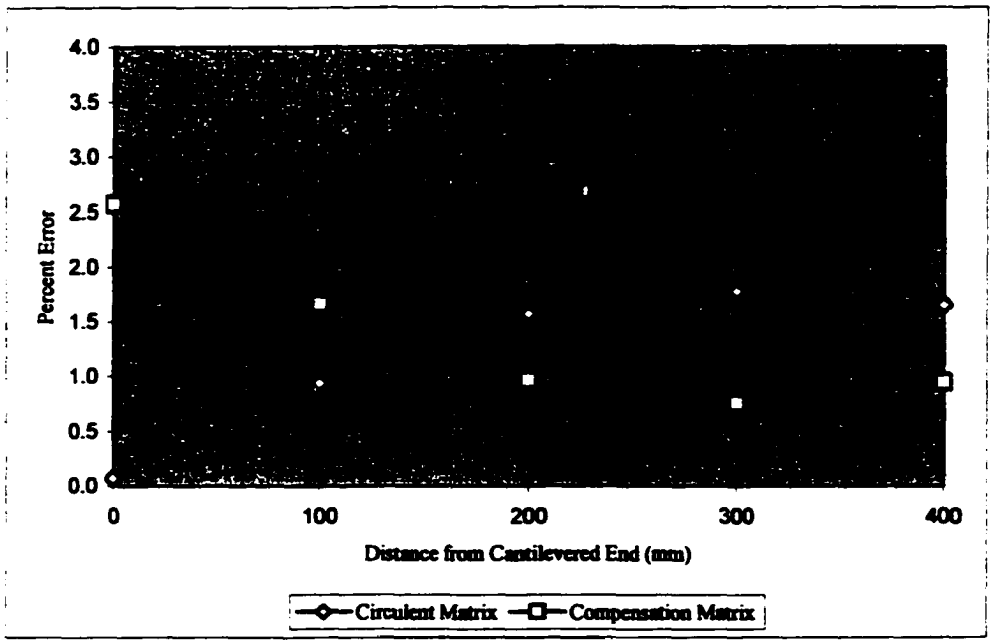

Fig. 6.15. Error in Predicted Beam Rotation

From the error graphs of Fig. 6.15. it can be seen that the error in the Compensation Matrix method is slightly less and thus, as with the prediction of the beam deflection, the overall prediction accuracy is improved over the Circulent Matrix method. Table 6.4. shows a summary of the error summation for each of the five points and a calculation of the diagonal norm for each of the methods. The table verifies that the Compensation Matrix method is superior for predicting the product beam deflection.

Table 6.4. Total Error and Diagonal Norm Comparisons for Beam Rotation

	Circulent	Compensation
Total Mean Error	5.94%	4.32%
Diagonal Norm	9.89×10^{-3}	1.23×10^{3}

The transformation matrices derived by each of the methods are again drastically different as is evident from the respective calculated diagonal norms. In this example the

distortion in the system is calculated for the Compensation Matrix method (see eqn. (6.12)) to be 1.69×10^{-7}, which is extremely small but still only qualitative without a baseline for comparison.

6.4.3 Beam Maximum Normal Stress

Using the same procedure the maximum normal planar stress in the beam as a function of the length is evaluated. The predicted maximum normal stress using the two methods is shown in Fig. 6.16. The relative errors in each method are shown in Fig 6.17. in comparison to the theoretical solution. As the figures clearly show, the prediction of the beam stress using the both the Compensation Matrix and the Circulent Matrix approaches show extremely good correlation with the theoretical stress of the beam.

From the error graphs of Fig. 6.17. it can be seen that the error in the Compensation Matrix method is slightly less and thus, as with the prediction of the beam deflection and rotation, the overall prediction accuracy is improved over the Circulent Matrix method. Table 6.5. shows a summary of the error summation for each of the five points and a calculation of the diagonal norm for each of the methods. The table verifies that the Compensation Matrix method is superior for predicting the product beam deflection.

Table 6.5. Total Error and Diagonal Norm Comparisons for Maximum Stress

	Circulent	Compensation
Total Mean Error	10.55%	10.27%
Diagonal Norm	0.095	4.146×10^{4}

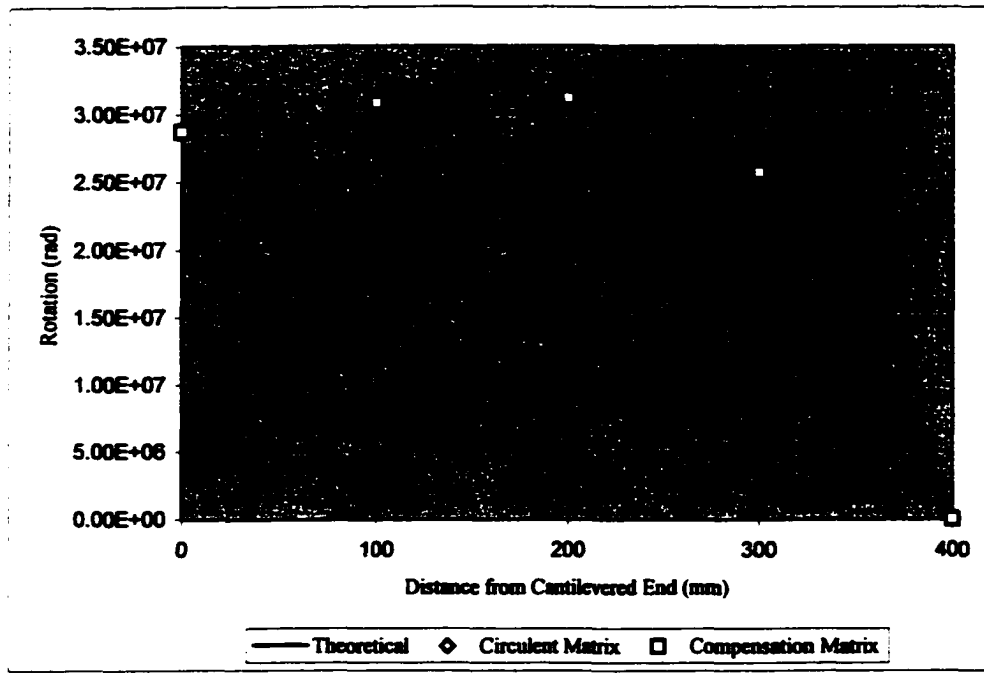

Fig. 6.16. Predicted Maximum Stress using Circulent and Compensation Matrix Methods

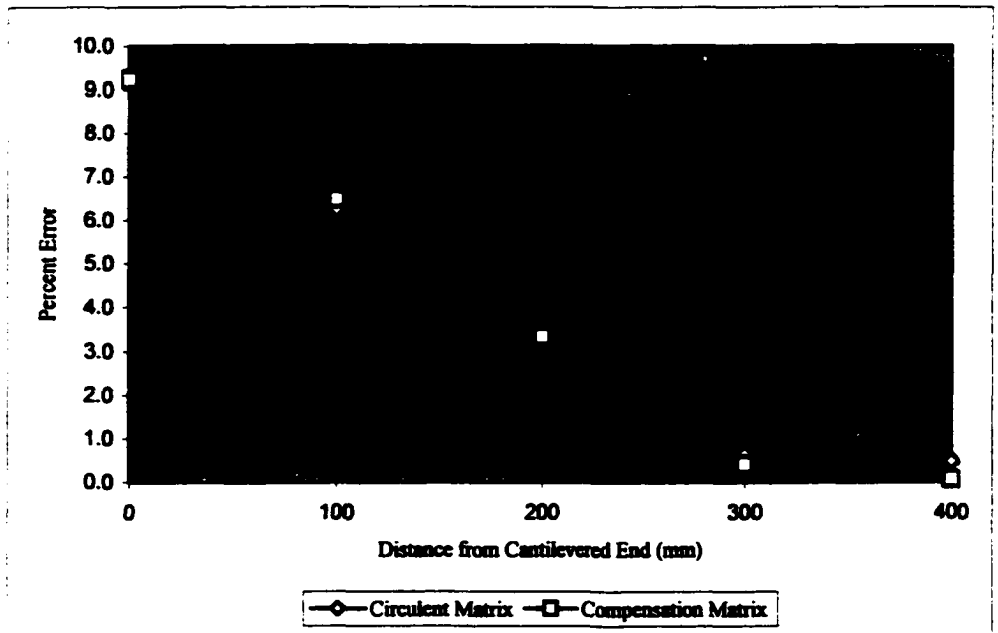

Fig. 6.17. Error in Predicted Beam Maximum Normal Stress

The transformation matrices derived by each of the methods are again drastically different as is evident from the respective calculated diagonal norms. In this example the distortion in the system is calculated for the Compensation Matrix method (see eqn. (6.12)) to be 4.16×10^{-6}, which is extremely small but still only qualitative without a baseline for comparison.

Research to date has shown significant inconsistencies in the degree of accuracy capable with the different ESM solution methods (Cho, 1999). The above example shows extremely precise correlation between the deflection, angle of rotation, and maximum normal stress of the product beam and the prediction using the Compensation Matrix approach. This method has proven to be the most accurate method developed yet to derive transformation matrices for the prediction of state vectors from specimen and model state vectors. Similar experimental studies have also shown drastic differences and levels of inaccuracy from the previous ESMs when applied to example problems where the actual solution has either been determined analytically or determined from empirical testing.

This Chapter has endeavored to present the latest in ongoing research directed toward enhancing the empirical predictive capabilities of a new generation of dimensional analysis based methods. The Compensation Matrix method presented herein has demonstrated a significant ability to manipulate scale and form transformation mapping to the prediction of product performance parameters using simple test specimens and a product representative scale model. The ease of manufacturing the specimens and model using rapid-prototyping technology further enhance the potential of the method.

Chapter 7

Further Applications of the Empirical Similarity Method

7.1 Introduction

The emphasis thus far, from an analysis standpoint, has been focused on development of a predictive methodology that can be used for the accurate modeling of the performance of a product or component(s) of a product. Due to the nature of how compliant members are often used in the design or redesign of products, the concentration has been on beam bending as a case study for the successful application of the empirical similarity analysis method. This approach satisfies the overall goal of developing a feasibility verification component for integration into the effort flow analysis methodology, which is the focus of this research.

The empirical similarity methods (ESMs) presented herein, and specifically the new Compensation Matrix method developed as part of this research, have shown the ability to accurately characterize the performance of a small, but representative, sample of mechanical transmission domain products or components of products. However, their range of applicability extends far beyond the limited examples presented here. Recall that the origin of the method was based on the fundamental principles of dimensional

analysis (Gukhman, 1965; Kline, 1986; Skoglund, 1967; Szirtes, 1998). Successful modeling is contingent upon the equality of corresponding dimensionless π groups or terms from the model and product composed of pertinent problem parameters (see Chapter 2). The requirement of equality of π terms is often too constraining to enable an efficient or even accurate solution.

7.1.1 Example Applications of the Empirical Similarity Method

In this the application domain of the ESM is extended through examples outside the realm of mechanical transmissions. The first example is a continuance of the steady state thermal conduction example introduced in Section 3.3.4.2 as proof of the potential of the method to conquer the limitations of the traditional method. In this example the new Compensation Matrix method is applied as further evidence of its superior performance over previously developed ESMs. The second example serves to demonstrate the ability of the method to predict the aerodynamic coefficients of airfoils based upon the wind tunnel measured states of a specimen airfoil set and a representative model.

Prior to proceeding with the analysis, a modification to the v_0 term of eqn. (6.10) and eqn. (6.13) is warranted.

$$\vec{X}_{ps} = [S_0 + \delta S]\vec{X}_{ms} + v_0\hat{e} \tag{6.10}$$

$$\vec{X}_{p} \cong [S_0 + \delta S]\vec{X}_{m} + v_0\hat{e} \tag{6.13}$$

Using the least squares method a value is determined for v_0 which results in a linear "best-fit" line between the $\vec{X}_{ms}$ and $\vec{X}_{ps}$ state vectors with a minimum error. In order to

use the transformation expression of eqn. (6.10) for the prediction of the $\bar{X}_p$ state vector from the $\bar{X}_m$ vector of eqn. (6.13), the v_0 term should be scaled to reflect the change in relative magnitude between the basis state vectors $\bar{X}_{ms}$ and $\bar{X}_m$. This scaling of the v_0 term would be best derived from a ratio of the relative magnitudes of the $\bar{X}_{ps}$ and $\bar{X}_p$ state vectors based upon the fundamental linear equations assumed relating $\bar{X}_{ms}$ to $\bar{X}_{ps}$ and $\bar{X}_m$ to $\bar{X}_p$. However, the state vector $\bar{X}_p$ is unknown and, therefore, cannot be used as a basis for determination of an appropriate v_0 term scaling. As a best approximation the scaling of the v_0 term is expressed as a ratio of the mean values of the elements of the $\bar{X}_m$ and $\bar{X}_{ms}$ state vectors respectively as shown in eqn. (7.1) below.

$$v_{0m} = v_0\left[\frac{mean(X_m)}{mean(X_{ms})}\right] \tag{7.1}$$

Equation (6.13) is now modified to include this scaled v_0 term as shown in eqn. (7.2) below.

$$\bar{X}_p \cong [S_0 + \delta S]\bar{X}_m + v_{0m}\hat{e} \tag{7.2}$$

7.1.2 Steady-State Thermal Conduction in a Manufacturing Mold

In this experimental example, conducted by Cho (Cho, 1999), the results of an empirical study of the prediction of the thermal conduction of a manufacturing mold are

presented. The study is based upon the measured temperatures of a model and specimen pair at corresponding points within the molds as graphically depicted in Fig. 7.1.

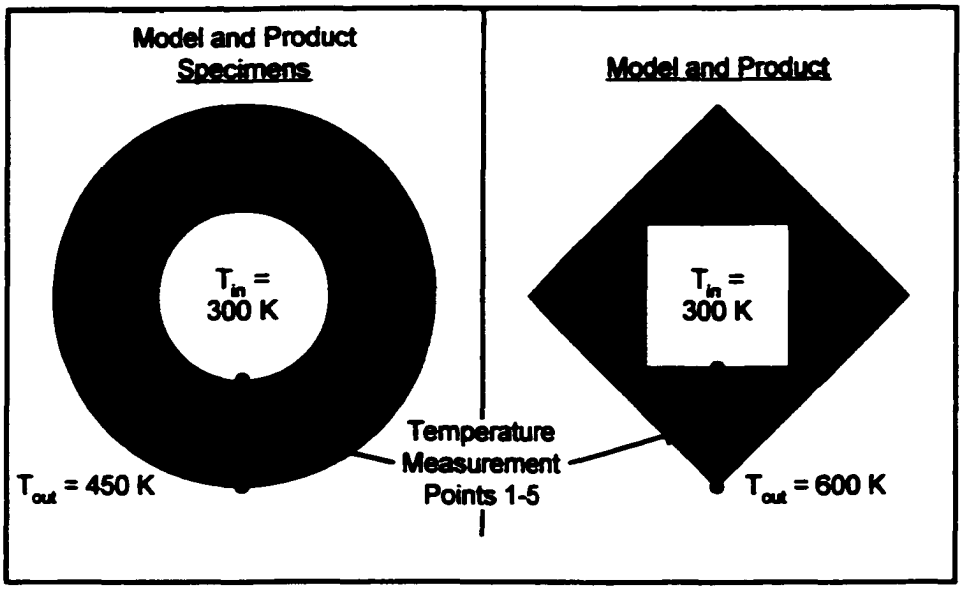

Fig. 7.1. Specimen Pair, Model and Product Test Parameters

The state vectors representing the measured temperatures of the four variants (model specimen, product specimen, model, product) are shown below.

$$[T_{ms}]=\begin{bmatrix}300\\330\\365\\400\\450\end{bmatrix} \quad [T_{ps}]=\begin{bmatrix}300\\360\\428\\500\\600\end{bmatrix} \quad [T_{m}]=\begin{bmatrix}300\\306\\333\\378\\450\end{bmatrix} \quad [T_{p}]=\begin{bmatrix}300\\312\\365\\460\\600\end{bmatrix}$$

Note the simplified geometry of the specimen molds, which are more easily manufactured than the more geometrically complex model and product counterparts. The model specimen and model were fabricated using a representative rapid-prototyped polymeric material and process, due to the greatly reduced time and expense as compared

to fabrication of full-scale material and process specific products. As such, the temperatures applied are significantly less due to the limitations of the material. The product specimen and product were fabricated using a material and process representative of the anticipated final design. The prediction results of the Circulent Matrix and Compensation Matrix methods are shown in Fig. 7.2.

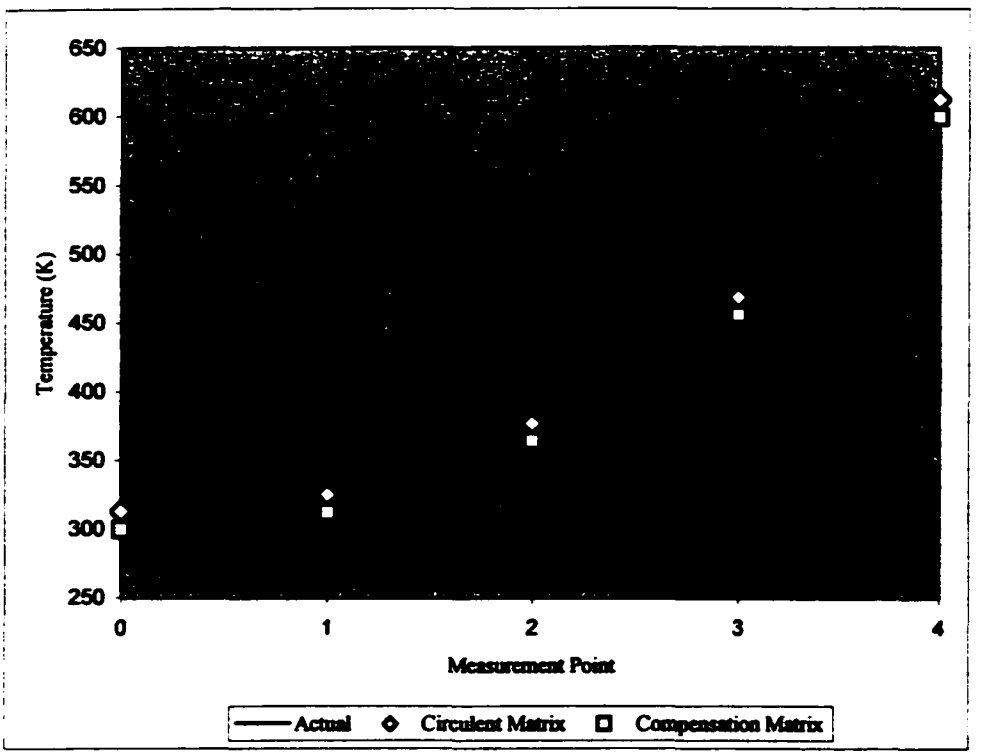

Fig. 7.2. Product Temperature Predictions

The relative errors in each method, using a mean square error measurement method (Dally and Riley, 1991), are shown in Fig. 7.3. in comparison to the measured temperatures of the product. As the figures clearly show, the prediction of the temperature gradient using both the Compensation Matrix and the Circulent Matrix approaches show extremely good correlation with the measured product temperatures.

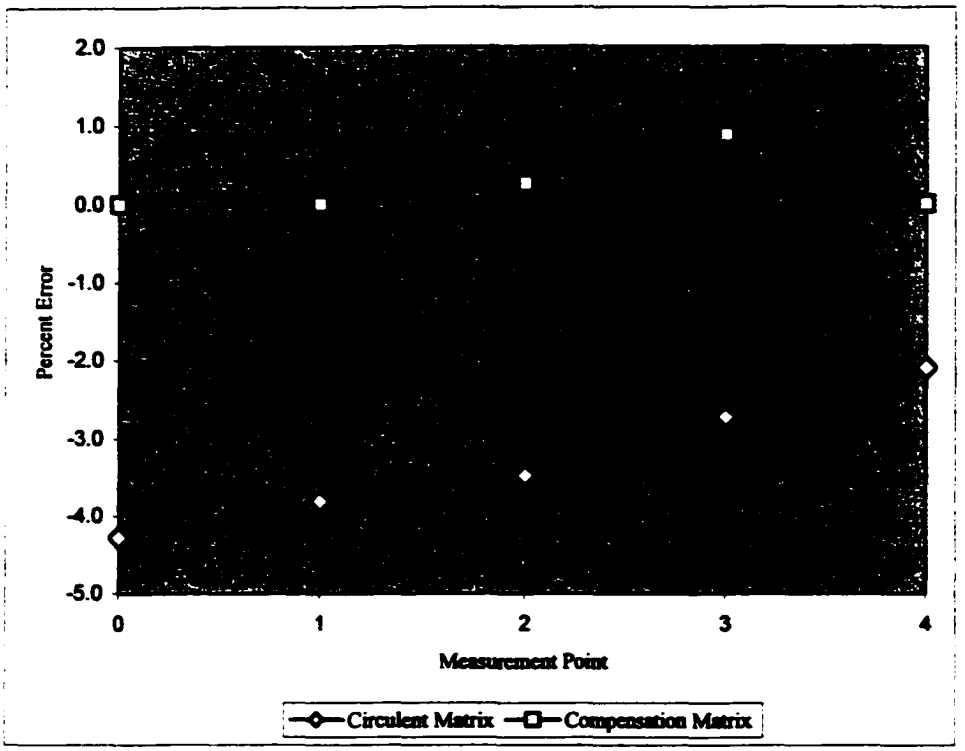

Fig. 7.3. Error in Prediction Methods

From the error graphs of Fig. 7.3. it can be seen that the error in the Compensation Matrix method is slightly less, and thus, the overall prediction accuracy improved, over the Circulent Matrix method.

Table 7.1. shows a summary of the error summation for each of the five points and a calculation of the diagonal norm for each of the methods. The table verifies that the Compensation Matrix method is superior for predicting the product temperature gradients. This example provides a direct comparison between the prediction capabilities of the Compensation Matrix and Circulent Matrix methods based upon measured test results.

Table 7.1. Total Error and Diagonal Norm Comparisons for Temp Predictions

	Circulent	Compensation
Total Mean Error	12.22%	0.276%
Diagonal Norm	16.88	20.01

The transformation matrices derived by each of the methods are not drastically different as is evident from the respective calculated diagonal norms. In this example the distortion in the system is calculated to be 2.3×10^{-7}, which is extremely small but still only qualitative without a baseline for comparison.

7.1.3 Airfoil Drag Coefficient

The force (F) on a body moving through a fluid is a function of the following parameters and variables:

1. Properties of the body – size, represented by length (L)
   shape
   orientation angle (α, B, Φ)
2. Properties of the fluid – density (ρ)
   viscosity (μ)
   elasticity, expressed in terms of speed of sound (a)
   density (ρ)
3. Relative velocity between the body and the fluid - velocity (V)

Through the dimensional analysis methods presented in Chapter 2 the following homogenous equation is derived, which represents the dimensionless π groups for the

problem of a body moving through a fluid in terms of the independent variables force (F), velocity (V), and length (L):

$$f\left(\frac{F}{\rho V^2 L^2}, \frac{\rho VL}{\mu}, \frac{V}{a}, \alpha, \beta, \phi\right) = 0 \tag{7.3}$$

It should be noted that the orientation angles are also considered independent variables but since they are not included in any other terms they are normally not included in the formulation of the Π groups. Equation (7.1) can be re-written in the following form:

$$\frac{F}{\rho V^2 L^2} = g\left(\frac{\rho VL}{\mu}, \frac{V}{a}\right) \tag{7.4}$$

where: $\frac{F}{\rho V^2 L^2}$ = Force coefficient (C_A, C_D, C_L, etc.)

$\frac{\rho VL}{\mu}$ = Reynolds number (Re)

$\frac{V}{a}$ = Mach number (M)

In order to have a dynamically similar system the following constraints must be satisfied:

$$\left[\frac{F}{\rho V^2 L^2}\right]_{\text{Model}} = \left[\frac{F}{\rho V^2 L^2}\right]_{\text{Prototype}}$$

$$\left[\frac{\rho VL}{\mu}\right]_{\text{Model}} = \left[\frac{\rho VL}{\mu}\right]_{\text{Prototype}}$$

$$\left[\frac{V}{a}\right]_{\text{Model}} = \left[\frac{V}{a}\right]_{\text{Product}}$$

Satisfying the above constraints is necessary for wind tunnel tests to be performed on a model to accurately characterize the product under study. This illustrates a common difficulty in wind tunnel testing, namely, the difficulty of correctly simulating both Mach number and Reynolds number simultaneously during the same test. Current practice in experimental aerodynamics does not attempt to simulate all the parameters simultaneously; rather, Mach number simulation is achieved in one test, and Reynolds number simulation in another test. The results from both tests are then analyzed and correlated to obtain reasonable values for the aerodynamic coefficients appropriate for free flight.

This example serves to illustrate the difficulty of full free flight simulation in a given wind tunnel and represents an opportunity for investigation into the potential application of empirical similarity applied in the fluid domain. It is hypothesized that empirical similarity could be used to alleviate some or all of the problems associated with meeting the above constraints.

The ESM process is shown graphically in Fig. 7.4. In the figure the *scale* transformation from the model specimen to the product specimen [*S*], is intended to capture the variation in body aerodynamic properties (represented by a state vector) brought about by a change in flow properties. This transformation assumes the geometry and other system parameters are not changed. This transformation is analogous to the scale transformation used in previous examples and in the development of the method.

Similarly the *form* transformation from the model specimen to the product specimen [*F*], is intended to capture the variation in geometric properties (represented by a state vector) between the model specimen and the model. This transformation assumes all parameters except the geometry remain constant. This transformation is analogous to the form transformation used in previous examples and in the development of the method. The mathematical manipulation of the model specimen, product specimen, and model state vectors through application of the Compensation Matrix method for prediction of the product state is identical to the previous approaches. Application of the Compensation Matrix method to the framework of this problem follows the structure shown in Fig. 7.4.

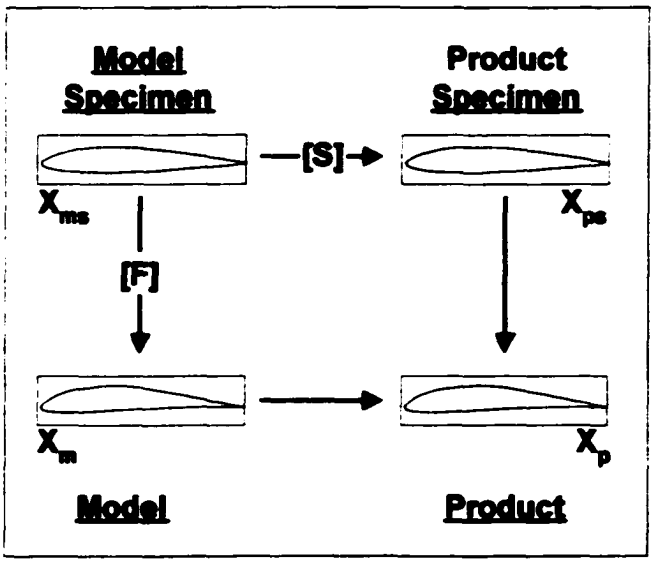

Fig. 7.4. Compensation Matrix Method for Aerodynamic Coefficient Modeling

The experimental data for this study is extracted from a Technical Report titled: *Summary of Low-Speed Airfoil Data* (Selig et al., 1995). This study is of particular interest to the empirical similarity research since it reports the results of experimental tests performed on two distinct airfoil shapes. Applying the ESM, the Gemini airfoil shape shown in Fig. 7.5 is used for the model and product specimen data. The E387 airfoil shown in Fig. 7.6 is used for the model and product data.

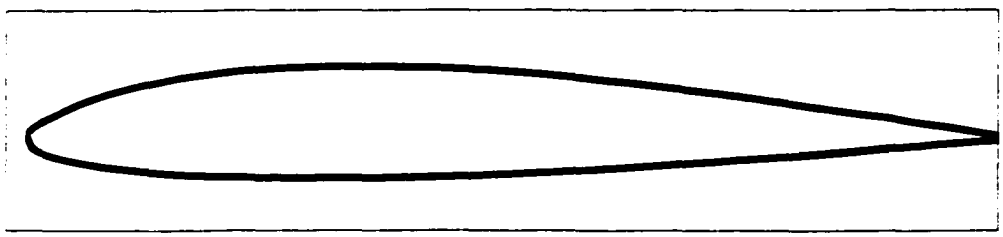

Fig. 7.5. Gemini Specimen Airfoil Shape

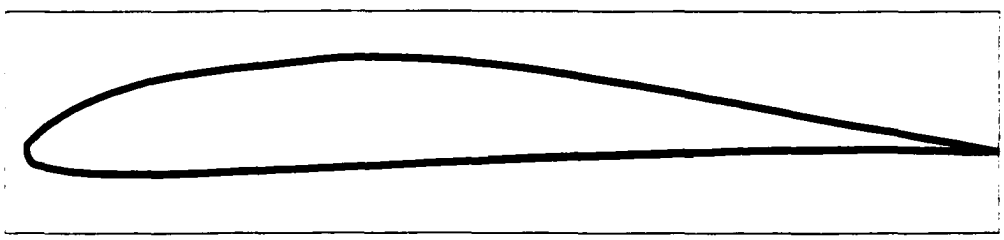

Fig. 7.6. E387 Model and Product Airfoil Shape

This example will predict the drag coefficients (C_D) for the E387 airfoil shape of Fig. 7.6. at angles-of-attack (α) ranging from –4 to 9 degrees and a Reynolds number of 204,100. The model family (model specimen and model) data represent the coefficient of drag at a Reynolds number between 101,800 and 102,300. The product family (product specimen and product) data represent the coefficient of drag at a Reynolds number

between 203,800 and 204,100. The vector states representing the drag coefficients of the four variants ($\bar{X}_{ms}, \bar{X}_{ps}, \bar{X}_{m}, \bar{X}_{p}$) from Fig. 7.4., along with appropriate experimental test parameters are included below.

7.1.3.1 Model Specimen ($\bar{X}_{ms}$):

Airfoil: Gemini
Reynolds No.: 102,300

$$\bar{X}_{ms} = \begin{bmatrix} 0.0176 \\ 0.016 \\ 0.0169 \\ 0.0172 \\ 0.0195 \\ 0.02 \\ 0.0186 \\ 0.0189 \\ 0.0204 \\ 0.0238 \\ 0.0255 \\ 0.027 \\ 0.0285 \\ 0.0296 \end{bmatrix}$$

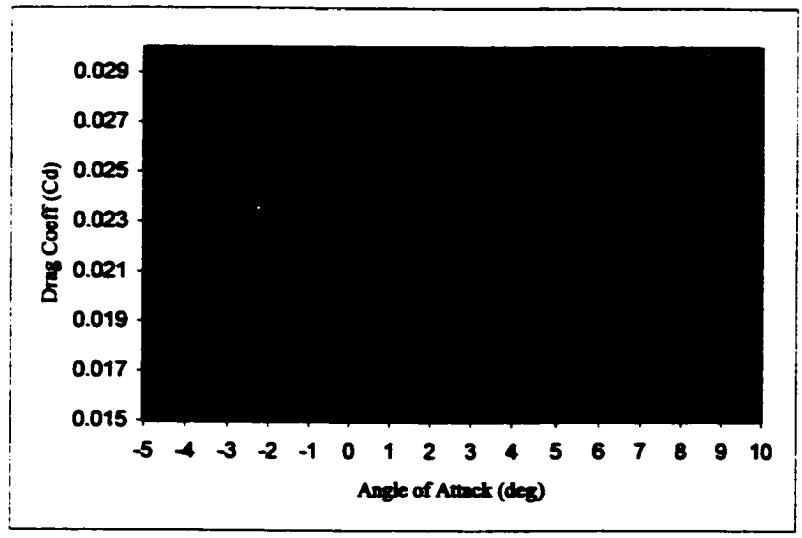

Fig. 7.7. Model Specimen Drag Coefficients

7.1.3.2 Product Specimen ($\bar{X}_{ps}$):

Airfoil: Gemini
Reynolds No.: 204,100

$$\bar{X}_{ps} = \begin{bmatrix} 0.012 \\ 0.01175 \\ 0.0119 \\ 0.012 \\ 0.01235 \\ 0.01235 \\ 0.0125 \\ 0.01315 \\ 0.01425 \\ 0.01575 \\ 0.0178 \\ 0.02 \\ 0.0215 \\ 0.0224 \end{bmatrix}$$

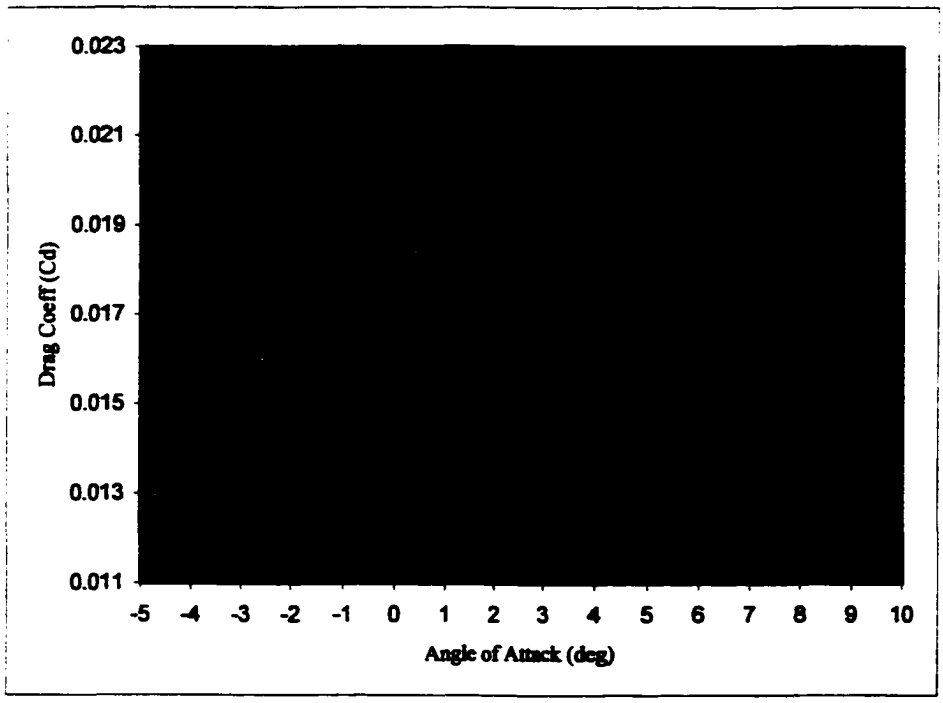

Fig. 7.8. Product Specimen Drag Coefficients

7.1.3.3 Model ($\bar{X}_m$):

Airfoil: E387
Reynolds No.: 101,800

$$\bar{X}_m = \begin{bmatrix} 0.0275 \\ 0.0195 \\ 0.0166 \\ 0.01665 \\ 0.0178 \\ 0.0198 \\ 0.0215 \\ 0.0226 \\ 0.02295 \\ 0.02298 \\ 0.02275 \\ 0.0227 \\ 0.0237 \\ 0.0278 \end{bmatrix}$$

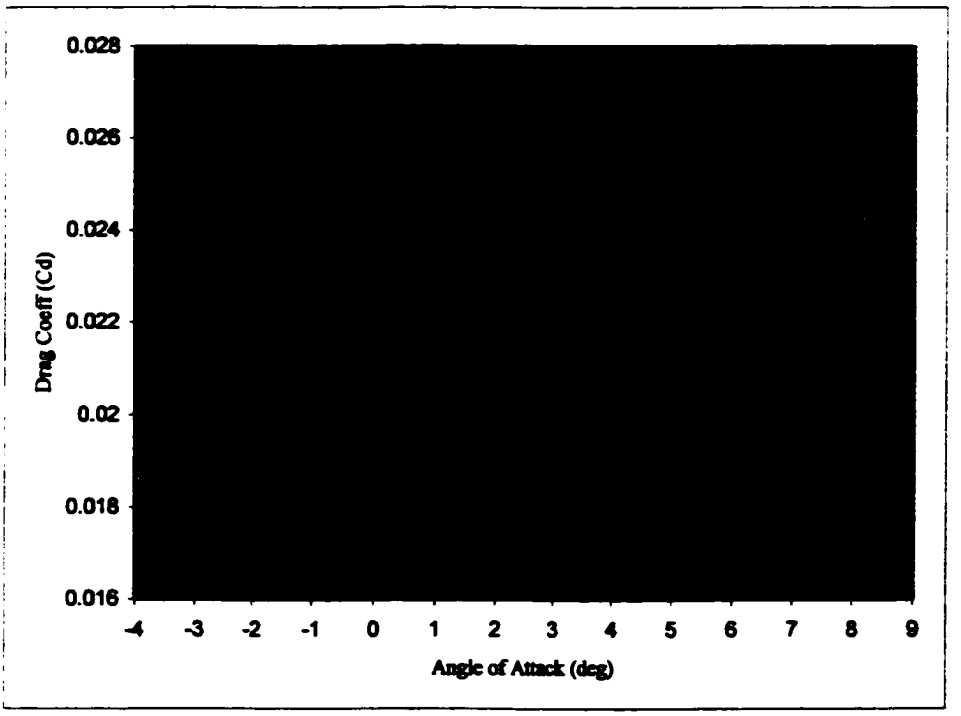

Fig. 7.9. Model Drag Coefficients

7.1.3.4 Product ($\bar{X}_p$):

Airfoil: E387
Reynolds No.: 203,800

$$\bar{X}_p = \begin{bmatrix} 0.0194 \\ 0.0144 \\ 0.01195 \\ 0.01065 \\ 0.0105 \\ 0.0113 \\ 0.0123 \\ 0.0133 \\ 0.01405 \\ 0.0146 \\ 0.0151 \\ 0.0158 \\ 0.0202 \\ 0.0276 \end{bmatrix}$$

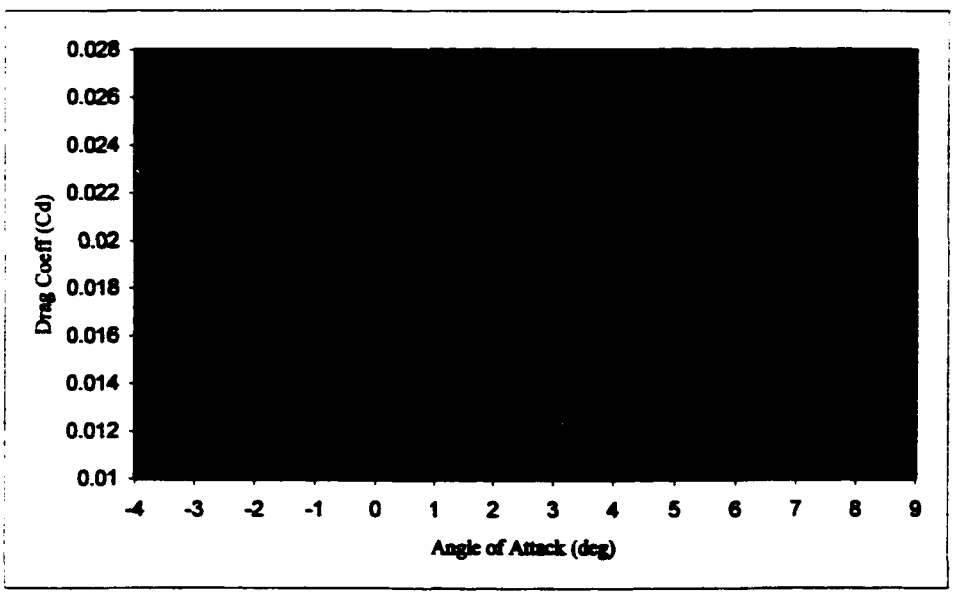

Fig. 7.10. Product Drag Coefficients

The drag coefficient prediction results from the Circulent Matrix and Compensation Matrix methods are shown in Fig. 7.11. together with the measured data from the product test.

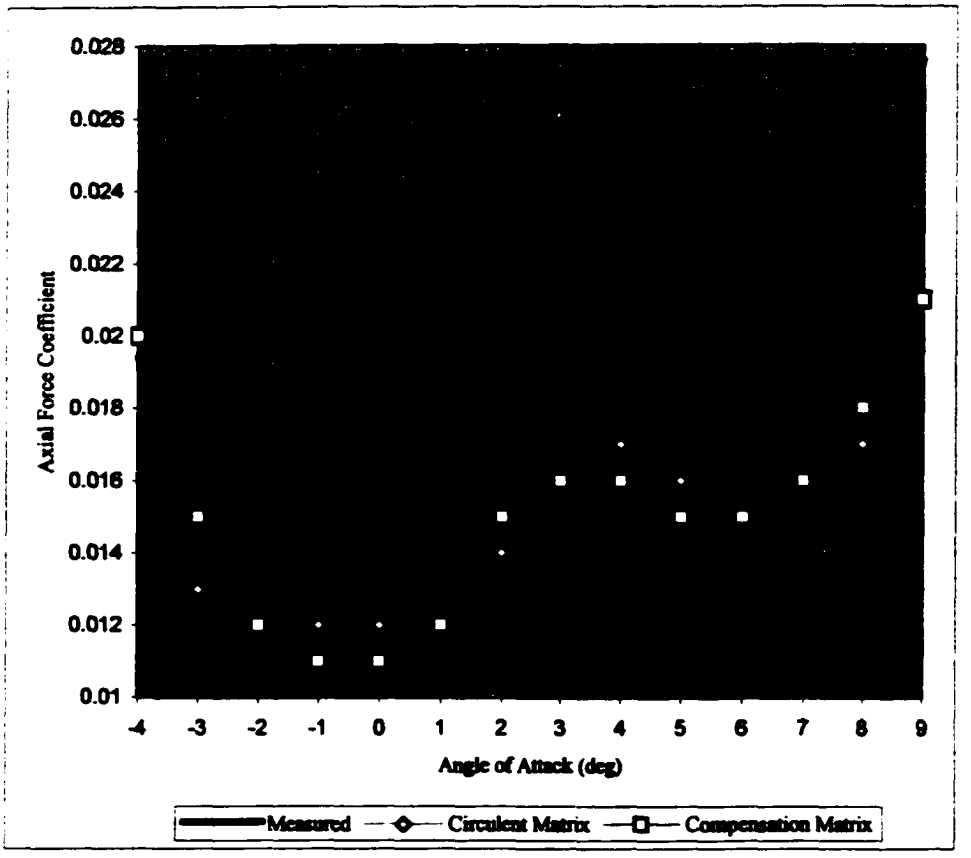

Fig. 7.11. Predicted Axial Force Coefficients

As the figure shows, the prediction of the coefficients using both the Compensation Matrix and Circulent Matrix approaches show a fair degree of correlation with the actual product measurements. From the figure it can also be concluded that the Compensation Matrix method provides a slightly more accurate prediction over the majority of the angle-of-attack range. In addition, the method also offers the potential for advanced analysis using the distortion characteristics available with the method. The error in the

predictions is likely due, in part, to the fact that the model and specimen were tested at slightly different Reynolds numbers and due to the inaccuracies inherent in model testing. This was unavoidable as the available test data was limited.

7.2 Results

The examples provided above suggest that the Compensation Matrix ESM, developed during the course of this research, is applicable to a wider range of problems than just the feasibility evaluation of compliant mechanisms design. The prediction of the performance of a product, whether it is a beam, an aerodynamic flow, a temperature gradient, or a host of others is achievable with this method.

Chapter 8

Conclusions and Future Work

8.1 Mission Accomplished

The contribution of this research will advance the field of relative motion based product design. Successful extension of the effort flow analysis (EFA) methodology coupled with an analytical tool to evaluate and iterate the design will provide a fully functional and proven process by which to attack product redesign. Development of the advanced similarity method and its successful integration with the EFA framework is only the beginning of the potential application areas of this research. Advancement of the current state of similarity to the point where it can be used as a viable analytical design tool providing both improved accuracy and increased range of applicability has been successfully achieved.

8.2 Contributions

The specific contributions are captured in the development of a methodology, complete with analytical evaluation capability, for the re-design of products whose motion based functionality affords the opportunity to take advantage of compliant materials and structures.

8.2.1 Effort Flow Analysis Methodology

A formal and systematic product evolution design and re-design methodology has been developed with a specific focus on the evolution of products through component combination afforded by the incorporation of compliant solutions. The elastic characteristics of non-rigid materials and structures are used to design and redesign components to take advantage of the relative motion properties afforded by the inclusion of flexible members. The method developed allows the redesign of products optimizing the number of components through the use of compliant materials and structures. A simple, unique, and yet comprehensive process has been developed for identifying and classifying component interfaces for subsequent design development based upon the relative motion they provide between the connected components.

The process is formalized through development of an enhanced EFA methodology that allows the designer to model the flow of energy through the components of a system by way of the component interfaces. The method provides an advanced degree of insight into the interrelationships between components for each of the product functions. The graphical nature of the EFA method provides a virtual and visual model of the system components and interfaces which allows the designer to clearly see the impacts of changes in the conceptual design of the system. A component link assignment scheme compliments the graphical structures contained in the effort flow diagram (EFD) and, together with the design guidelines developed herein, results in a formidable design tool. The method offers superior insight into the integrated nature of components we refer to as a system.

8.2.2 Empirical Product Study

In concert with the EFA methodology are the design guidelines developed to direct the EFD graph structure manipulations to affect the directed evolution of the product. The two components, EFDs and design guidelines, exhibit a circular cause and effect relationship. The design guidelines have been developed exclusively to direct the evolution of relative motion-based function products by a reduction in the number of system components, sharing of component functions, and incorporation of compliant materials and structures. Implementation of these guidelines results in the graphical manipulation of components and interfaces in the EFD in parallel with changes to the physical design of the system components. Changes in the graph structures making up the effort flow diagram offer the potential for further implementation of design guidelines and the iterative process continues until the complete design evolution of the product is achieved.

8.2.3 Advanced Similarity Methods

An analytical tool has been developed that will facilitate the evaluation of product modeling and performance predictions through the use of scaled functional tests performed on rapid-prototyped and other traditionally non-functional models. The approach has its origins in dimensional analysis theory established well over a century ago and still in use today. Recent developments in numerical methods and rapid-prototyping techniques have fueled the need to develop this method to correlate model tests with the predicted performance of products. The advanced similarity method developed in this study fill the void where traditional similarity methods often fail due to distortion in the model-product system. Dimensional and material property limitations of

rapid prototypes often prevent them from being used for functional testing without the use of similarity methods to correlate measured prototype behavior with predicted product behavior. The traditional similarity methods require the dimensionless parameters of the prototype and product systems be identical in order to correlate their states and accurately predict product performance. This requirement of identical dimensionless parameters is often impractical or even impossible to realize with the limited properties available from rapid prototyping technologies. The advanced similarity approach developed herein has demonstrated its ability in both prediction accuracy and domain of applicability by the infusion of empirical data, derived from material tests, into the equations that characterize the system parameters of interest.

8.3 Future Work

As with any effort of this magnitude and depth, each step reveals additional exploration paths and new ideas, a pattern which continues until the research possibilities seem endless. Below are a few key research areas where the envelope of current knowledge and understanding could be expanded in the hope that further developments would directly influence the application of the methods described herein.

8.3.1 Design Guideline Refinement

In Chapter 5 a summary of the guidelines derived during the course of the empirical product study were presented. This study was based upon the observation of some 24-product variants from 8 distinct product groups, where certain product groups contained more than just an original and an evolved variant. The trend in the study showed a

significant decrease in the development of new guidelines as the number of products observed increased. This was an expected outcome as a number of guidelines found application to almost every product studied. The exception was the special cases, which seemed to be dependent on the specific design of a particular product. Based upon this finding it is reasonable to hypothesize that the number of specialized guidelines would continue to increase with the number of products studied. Reason would suggest there must be a point where even the specialized guidelines find increased application as the sample size increases. Further study is therefore required to continue the development of a design guideline database and also continue development of a structured approach to application of the guidelines, which will optimize the evolutionary design process.

8.3.2 Distortion Quantification/Qualification

The Compensation Matrix method is comprised of both a scaled identity matrix component and a perturbed matrix component, the latter designed to capture the dissimilarity or distortion in the matrix transformation. The perturbed matrix component offers the potential for further analysis of the characteristics of the state transformation than conducted in this study. It has been demonstrated that for a non-distorted system the matrix perturbation component is equal to zero. A non-distorted system can be described mathematically as a linear relationship between the model specimen and the product specimen in the context of the empirical similarity method. As the relationship becomes increasingly non-linear the value of the perturbation component also increases. The detailed characteristics of this relationship are unknown at this point. A quantitative

relationship between the similar system contributions and the distorted contributions has been presented in the form of a distortion parameter defined in eqn. (6.14) as:

$$Distortion = \frac{\sum_{i=1}^{n}\sum_{j=1}^{n} \delta S_{ij}^{2}}{\sum_{i=1}^{n} S_{ii}^{2}}$$

However, this calculated parameter is of little significance without a known and understood reference point. Further study is required to characterize the value of this parameter as is relates to the prediction accuracy of the derived matrices.

8.3.3 Polynomial Compensation Method

The development of the Compensation Matrix method was largely constrained to linear or near linear relationships between the states of the model specimen and product specimen. A first order least squares approach was used to derive the scaled identity matrix component of the method. As was demonstrated, the method was capable of deriving an accurate transformation matrix even with a non-linear relationship due to the added flexibility afforded by the inclusion of the perturbed matrix component. It is hypothesized that as the degree of non-linearity increase, a point would be reached where the scaled identity matrix representing the similarity in the system would be better approximated by a 2^{nd} degree or higher order polynomial least squares approximation. There are two fundamental questions that need to be investigated:

1. What are the limits of applicability of the current Compensation Matrix method that is based upon a 1st order least squares approximation.

2. How to determine the appropriate order polynomial to use for a higher order least squares approximation.

The answer may be determined by the nature of the perturbed matrix component, which would require further study. The perturbed matrix is valuable from the standpoint that is ranges from zero for a non-distorted system to infinity for a highly distorted system. The majority of systems are, of course, somewhere in the middle and tend to be much less than one for the studies conducted thus far. The magnitude or other characteristic(s) of the matrix could be used to determine the action necessary or path required to choose the appropriate order polynomial. An iterative approach where the convergence of some characteristic(s) could be observed to provide an indication of the order required for the best approximation.

8.4 Conclusion

The progress made during the course of this work has resulted in a new approach for the conceptual design of products and/or components of products. The approach integrates the directed product evolution capabilities of EFA with the analytical evaluation capabilities of an empirically based Compensation Matrix similarity method. The two combine to form a new method for the conceptual development, optimization, and/or redesign of relative motion based products. The structural and material compliance characteristics of members have been captured in a formalized and systematic approach to afford a new dimension to evolutionary design.

Traditional dimensional analysis techniques for evaluating the performance of system components have been significantly advanced by the development of the Compensation

Matrix empirical similarity method. Improvements in both the degree of accuracy achievable and in the range of applicability have been demonstrated by the infusion of empirical specimen test data into the equations that characterize the system parameters of interest. Application of this technique provides an integral feasibility verification element to the EFA conceptual design process closing the loop on a complete method for the design and evaluation of compliant systems.

Bibliography

Altschuller, G. (1984). "Creativity as an Exact Science," New York, Gordon & Breach Publishers.

Ananthasuresh, G. K. and M. I. Frecker (2001). "Chapter 9 in Compliant Mechanisms," by L. L. Howell. New York, John Wiley & Sons.

Ananthasuresh, G. K. and S. Kota (1995). "Designing Compliant Mechanisms," Journal of Mechanical Engineering.

Ashley, S. (1995). "Cutting Costs and Time with DFMA," Journal of Mechanical Engineering.

Barr, D. (1984). "Consolidation of Basics of Dimensional Analysis," Journal of Engineering Mechanics, ASCE 10(9): 1357-1375.

Becker, H. A. (1976). "Dimensionless Parameters Theory and Practice," London, Applied Science Publishers LTD.

Berglund, M. D., et al. (2000). "Design Rules for Selecting and Designing Compliant Mechanisms for Rigid-Body Replacement Synthesis," *Proceedings of the ASME Design Engineering Technical Conference*, DETC00/DAC-14255, Baltimore, MY.

Birkhoff, G. (1960). "Hydrodynamics; a Study in Logic, Fact, and Similitude," Princeton, Princeton University Press.

Boothroyd, G., et al. (1994). "Product Design for Manufacturing," New York, Marcel Dekker.

Bridgman, P. W. (1922). "Dimensional Analysis," New Haven, Yale University Press.

Bridgman, P. W. (1931). "Dimensional Analysis," New Haven, Yale University Press.

Buckingham, E. W. (1914). "On Physically Similar Systems: "Illustrations of the use of Dimensional Equations," Phys. Rev. 4: 345-76.

Cho, U. (1999). "Novel Empirical Similarity Method for Rapid Product Testing and Development," Journal of Mechanical Engineering. Austin TX, University of Texas at Austin.

Cho, U., et al. (1998). "Novel Empirical Similitude Method for the Reliable Product Test with Rapid Prototypes," *Proceedings of the 1998 ASME DETC*, Atlanta, GA, ASME.

Chow, W. W. (1978). "Cost Reduction in Product Design," New York, Van Nostrand Reinhold Co.

Dally, J. W. and W. F. Riley (1991). "Experimental Stress Analysis," McGraw-Hill, Inc.

Defazio, T. L. and D. E. Whitney (1987). "Simplified Generation of Mechanical Assembly Sequences," IEEE Journal of Robotics and Automation RA-3(6): 640-656.

Dieter, G. E. (1991). "Engineering Design: A Materials and Processing Approach," New York, McGraw-Hill, Inc,.

Fourier, J. B. J. (1822). "Théorie analytique de la chaleur," Paris, Gauthier-Villars.

Gerald, C. F. and P. O. Wheatley (1989). "Applied Numerical Analysis," Reading, MA, Addison-Wesley.

Gukhman, A. A. (1965). "Introduction to the Theory of Similarity," New York, Academic Press.

Harary, F. (1969). "Graph Theory," Reading, MA, Addison-Wesley.

Hill, R. O. (1986). "Elementary Linear Algebra," Orlando, FL, Academic Press, Inc.

Howell, L. L. (2001). "Compliant Mechanisms," New York, John Wiley & Sons.

Huntley, H. E. (1951). "Dimensional Analysis," New York, Rinehart & Co.

Ishii, K., et al. (1995). "Design for Product Variety: Key to Product Line Structuring," *Proceedings of the ASME Design Engineering Technical Conference*, DETC95, Boston MA.

Jensen, D. D., et al. (2000). "Force Flow Analysis: Opportunities For Creative Component Combination," *Proceedings from the ASME International Mechanical Engineering Conference and Exposition*, Orlando, FL.

John, J. E. A. and W. L. Haberman (1980). "Introduction to Fluid Mechanics," Englewood Cliffs, Prentice-Hall Inc.

Juvenal, R. C. and K. M. Marshek (2000). "Fundamentals of Machine Component Design," Ney York, John Wiley & Sons, Inc.

Kline, S. J. (1986). "Similitude and Approximation Theory," New York, Springer-Verlag.

Langhaar, H. L. (1980). "Dimensional Analysis and Theory of Models," Huntington, R. E. Krieger Pub. Co.

Lee, S. and C. Ui (1994). "Force-Based Reasoning in Assembly Planning," ASME Flexible Assembly Systems DE-Vol. 73: 165-172.

Lefever, D. (1995). "Integrating Design for Assemblability Techniques and Reverse Engineering," Journal of Mechanical Engineering, Austin, University of Texas.

Lefever, D. and K. L. Wood (1996). "Design for Assembly Techniques in Reverse Engineering and Redesign," *Proceedings of the ASME Design Engineering Technical Conference*, DETC96/DTM, Irvine, CA.

McAdams, D. A., et al. (1998). "Understanding Product Similarity Using Customer Needs," *Proceedings of the ASME Design Engineering Technical Conference*, DETC98/DTM-5660.

Murphy, G. (1950). "Similitude in Engineering," New York, Ronald Press Co.

Nakos, G. and D. Joyner (1998). "Linear Algebra with Applications," Brooks/Cole Publishing.

Noble, B. and J. W. Daniel (1988). "Applied Linear Algebra," Englewood Cliffs, NJ, Prentice-Hall.

Nowack, M. L. (1997). "Design Guideline Support for Manufacturability," United Kingdom, Selwyn College, Cambridge University.

Otto, K. and K. L. Wood (2001). "Product Design: Techniques in Reverse Engineering and New Product Development," New York, Prentice Hall.

Palacios y Martínez, J. (1964). "Dimensional Analysis," New York, Macmillan; St. Martin's Press.

Paul, G. and W. Beitz (1996). "Engineering Design: A Systematic Approach," 2nd Edition. London, England, Springer-Verlag.

Pine, J. B., et al. (1993). "Making Mass Customization Work," Harvard Business Review. Sep-Oct: 108-119.

Poli, C., et al. (1986). "Rating Products for Ease of Assembly," Journal of Machine Design.

Pugh, S. (1991). "Total Design," New York, Addison-Wesley.

Rayleigh, L. (1915). "Investigations on Capillarity," Nature 95.

Salamon, B. A. and A. Midha (1998). "An Introduction to Mechanical Advantage in Compliant Mechanisms," Journal of Mechanical Design v120.

Schregenberger (1998). "The Further Development of Design Methodologies," Munich, Heidelberg, New York, Springer-Verlag.

Selig, M. S., et al. (1995). "Summary of Low-Speed Airfoil Data," Virginia Beach, Soartech Publications.

Skoglund, V. J. (1967). "Similitude: Theory and Applications," Scranton, Pa., International Textbook Co.

Steiner, M. W. (1999). "Evaluation of Mechanical Product Architecture Using Interaction Graphs to Model Part Connectivity and Joint Strength," *Proceedings of the ASME Design Engineering Technical Conference*, DETC99/DFM-9862, Las Vegas, NV.

Strang, G. (1988). "Linear Algebra and Its Applications," Harcourt Brace Jovanovich, Inc.

Szirtes, T. (1998). "Applied Dimensional Analysis and Modeling," New York, McGraw-Hill.

TSAI, L. (2000). "Mechanism Design: Enumeration of Kinematic Structures According to Function," Boca Raton, FL, CRC Press.

Ullman, D. G. (1997). "The Mechanical Design Process," New York, McGraw-Hill, Inc.

Ullrich, K. T. and S. D. Eppinger (1995). "Product Design and Development," New York, McGraw-Hill.

Van wie, M. J., et al. (2001). "Interfaces and Product Architecture," *Proceedings of the ASME Design Engineering Technical Conference*, DETC01/DTM-21689, Pittsburgh, PA.

Wall, M. B. e. a. (1991). "Making Sense of Prototyping Technologies for Product Design," ASME 3rd International Conference on Design Theory and Methodology, ASME.

Appendix A

Empirical Product Study - Wire Stripper

A.1 Product Description

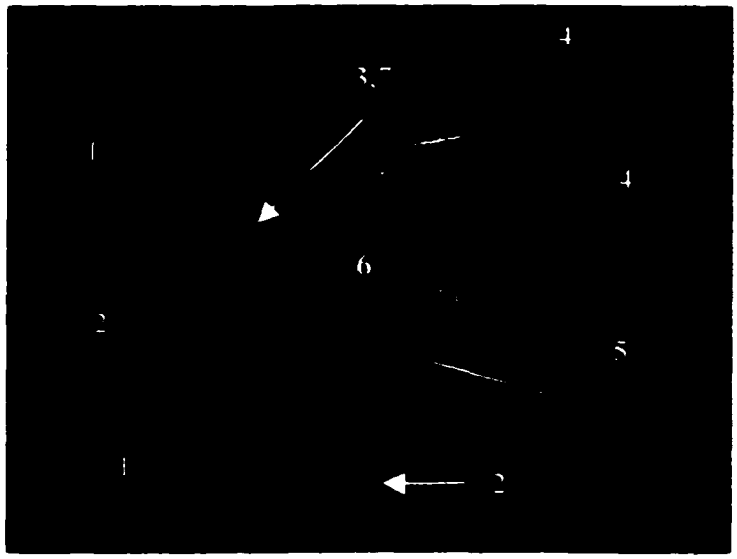

Fig. A.1: Original and Evolved Products

Table A.1: Product Components Identified/Labeled

Comp ID	Product Components	
	Original	Evolved
1.	Upper Jaw	Frame
2.	Lower Jaw	Cutter
3.	Pivot Bolt	
4.	Upper Grip	
5.	Lower Grip	
6.	Spring	
7.	Fastener	

Table A.2: Compliant Solution Contrasted

Traditional Solution	Type Compliant Solution
Revolute joint connecting jaws	Compliant handle incorporating joint through bending

A.2 Understand the Product

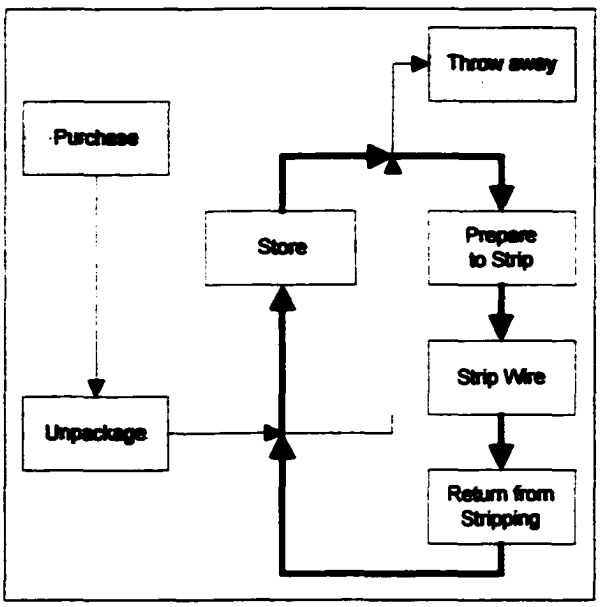

Fig. A.2: Activity Diagram

Rationale for inclusions/exclusions in Activity Diagram:

In this analysis only the user related functions are modeled. Functions related to the manufacturing and assembly are not included. This decision was based upon an attempt to isolate functions that are common between the original and the evolved products.

Design Life Class: Durable

A.3 Model Product Operation

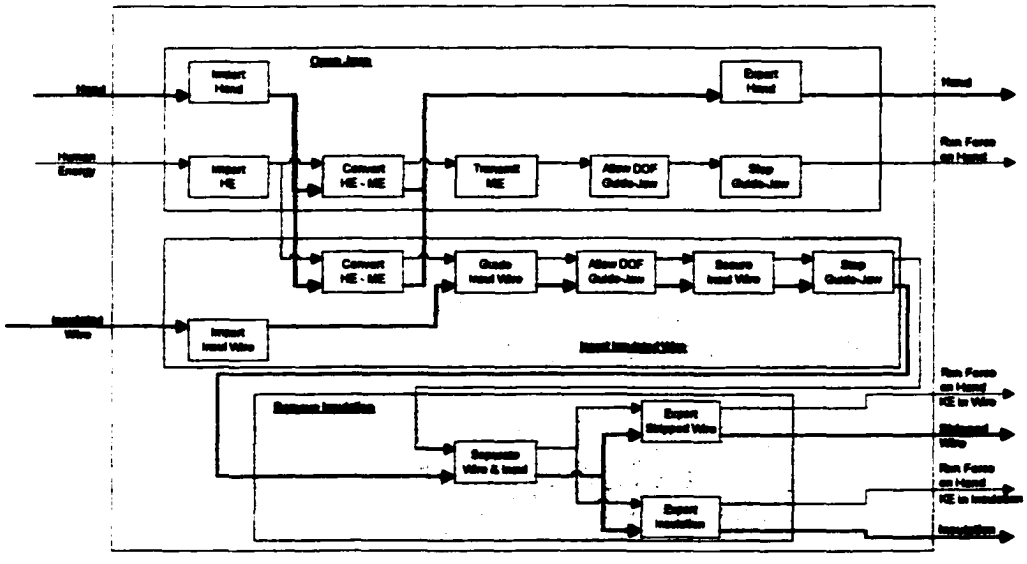

Fig. A.3: Function Structure

Table A.3: Relative Motion Functions and Components Involved

Basis Function	Operand	Associated Components	
		Original Design	Evolved Design
Actuate			
Allow DOF	Rotation	Pivot Bolt	Frame
Change			
Collect			
Condition			
Contain			
Convert	Human Energy to Mech Ener	Upper & Lower Grip, Insul Wire	Frame, Insul Wire
Couple			
Decrease			
Decrement			
Detect			
Display			
Distribute			
Divide			
Export	Hand	Upper & Lower Grip, Stripped Wire	Frame, Stripped Wire
	Wire	Hand	Hand
	Insulation	Upper & Lower Jaw	Frame, Cutter
	Mech Energy	Stripped Wire, Insulation	Stripped Wire, Insulation
Extract			
Guide	Translate	Insul Wire	Insul Wire
Import	Hand	Upper & Lower Grip, Insul Wire	Frame, Insul Wire
	Human Energy	Upper & Lower Grip, Insul Wire	Frame, Insul Wire
	Insul Wire	Upper & Lower Jaw	Frame, Cutter
Increase			
Increment			
Indicate			
Inhibit			
Join			
Link			
Measure			
Mix			
Position			
Prevent			

Basis Function	Operand	Associated Components	
		Original Design	Evolved Design
Prevent			
Process			
Regulate			
Remove			
Rotate			
Secure	Hold	Upper & Lower Jaw, Insul Wire	Frame, Insul Wire
Sense			
Separate	Insul Wire	Upper & Lower Jaw, Stripped Wire, Insulation	Frame, Stripped Wire, Insulation
Shape			
Stabilize			
Stop	Rotation	Upper & Lower Jaw	Frame
Store			
Supply			
Track			
Transfer			
Translate			
Transmit	Mech Energy	Upper & Lower Grip Upper & Lower Jaw	Frame
Transport			

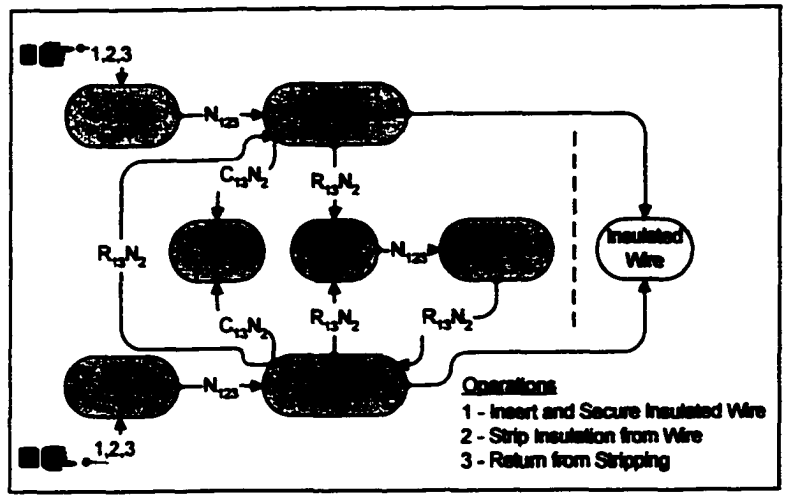

Fig. A.4: Effort Flow Diagram for Original Product

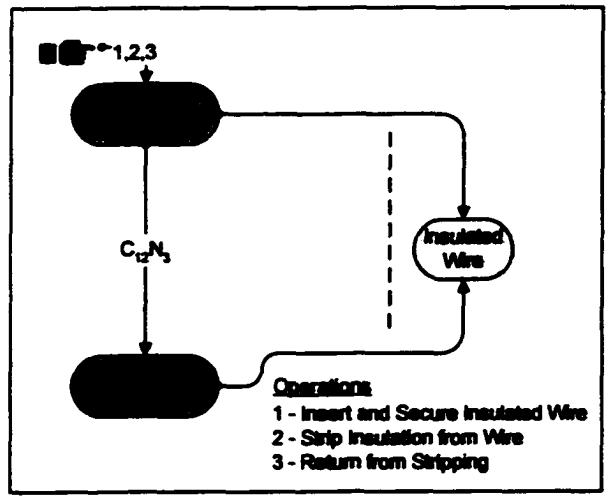

Fig. A.5: Effort Flow Diagram for Evolved Product

A.4 Analyze Product Model

A.4.1 N-Block Identification/Contraction

The product is analyzed using effort flow analysis. First the N-block component graph structures (Fig. A.6.) are identified for possible combination. Application of

design guidelines governing the contractions of N-Block graph structures are imposed resulting in the revised effort flow diagram of Fig. A.7.

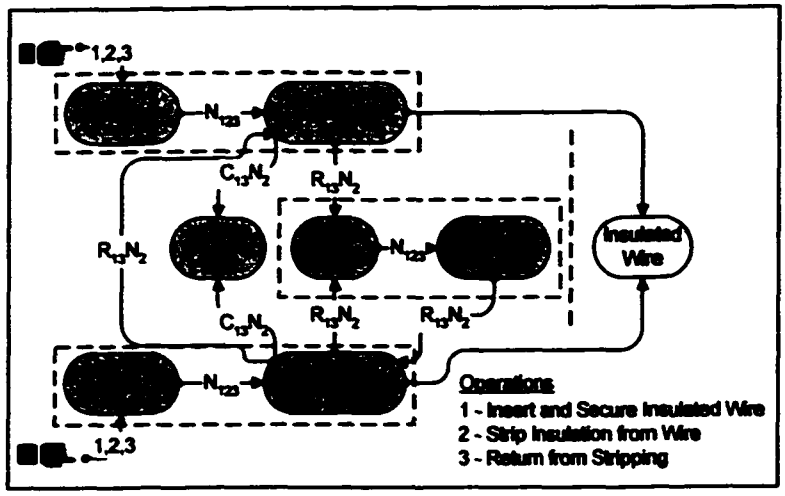

Fig. A.6: N-Block Graph Structures Identified for Original

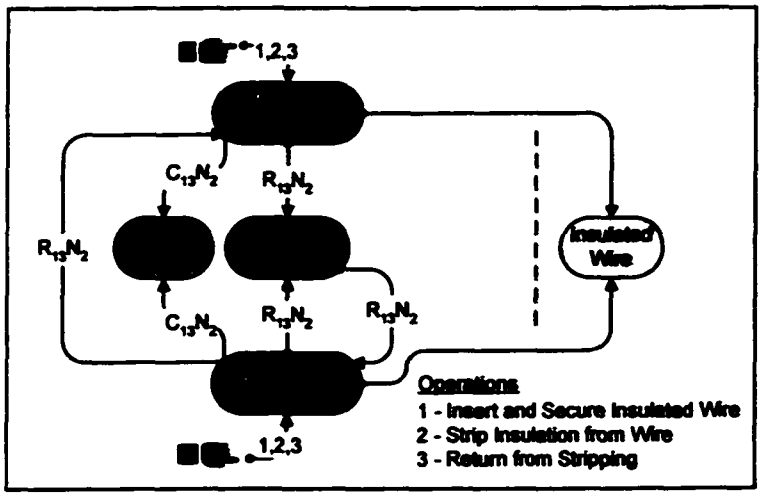

Fig. A.7: Evolution after N-Block Contraction

A.4.2 C-Block Identification/Contraction

The C-block component graph structures (Fig. A.8.) are identified for possible combination. Application of design guidelines governing the contractions of C-Block graph structures are imposed resulting in the revised effort flow diagram of Fig. A.9.

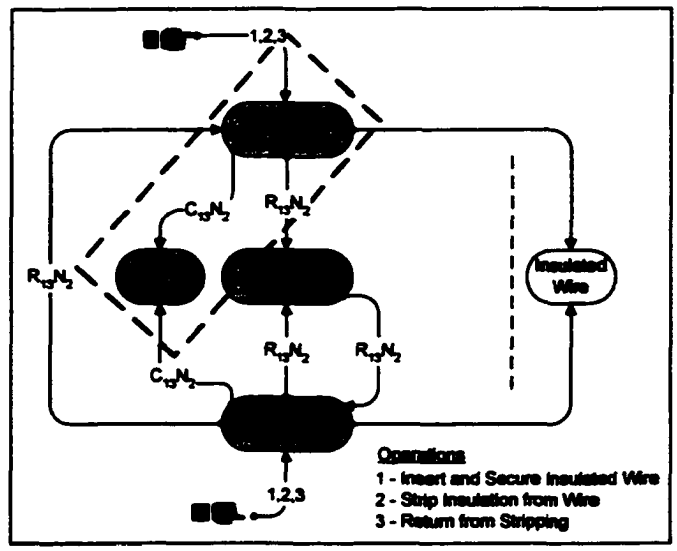

Fig. A.8: C-Block Graph Structures Identified for Original

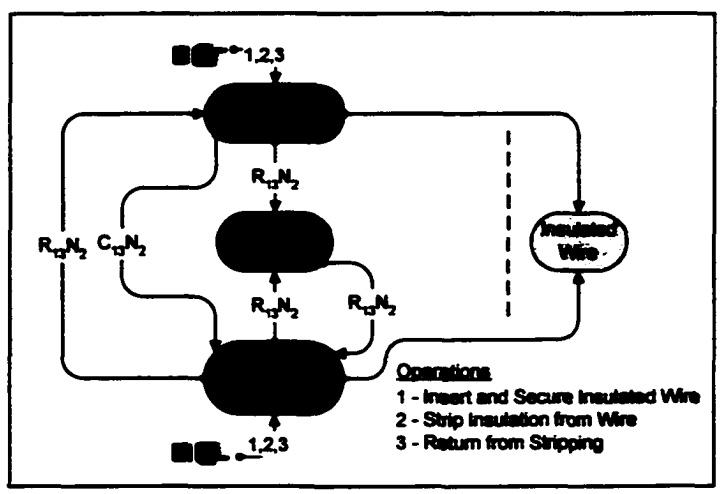

Fig. A.9: Evolution after C-Block Contraction

A.4.3 R-Block Identification/Contraction

The R-block component graph structures (Fig. A.10.) are identified for possible combination. Application of design guidelines governing the contractions of R-Block graph structures are imposed resulting in the revised effort flow diagram of Fig. A.11.

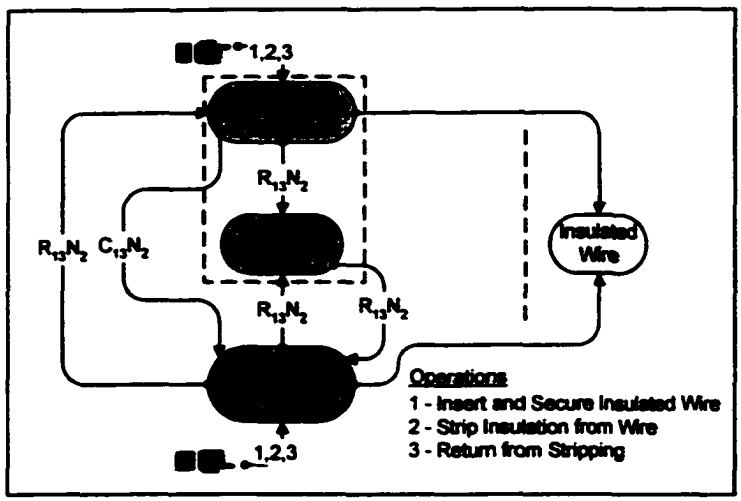

Fig. A.10: R-Block Graph Structures Identified for Original

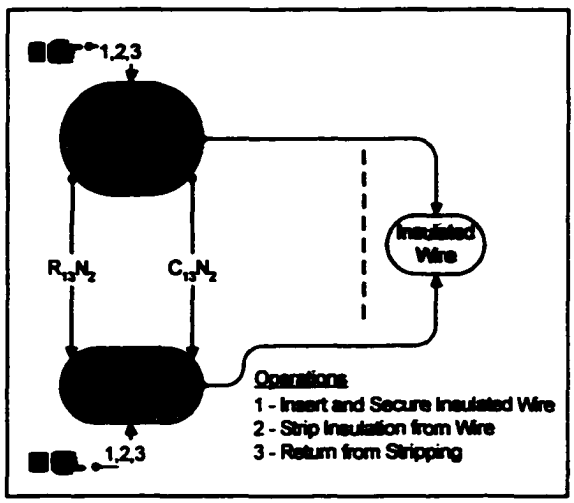

Fig. A.11: Evolution After R-Block Contraction

A.4.4 Higher Order Evolution

In order for further evolution to take place the next step involves separating the two remaining components into their functional equivalents. In this case the separation will be based upon the cutting function of the components, with the remaining functions remaining with the components. The modified effort flow diagram with functional components is shown in Fig. A.12.

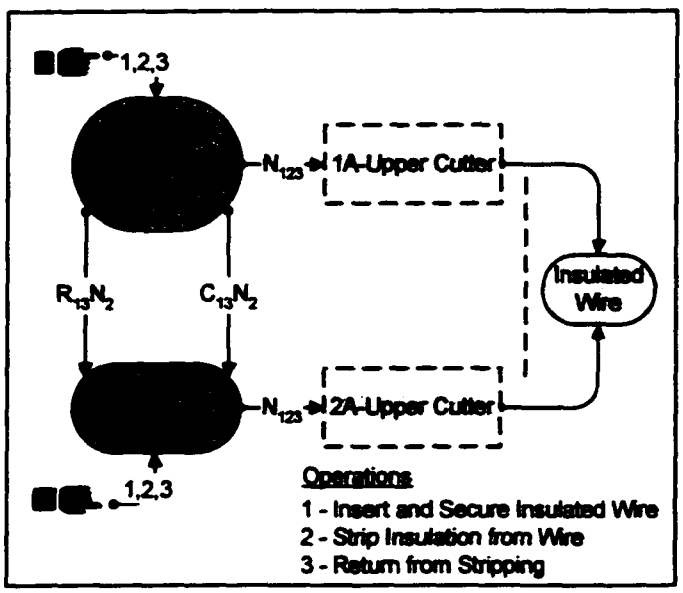

Fig. A.12: Separation into Functional Components

We again return to R-Block contraction guidelines resulting the effort flow diagram of Fig. A.13.

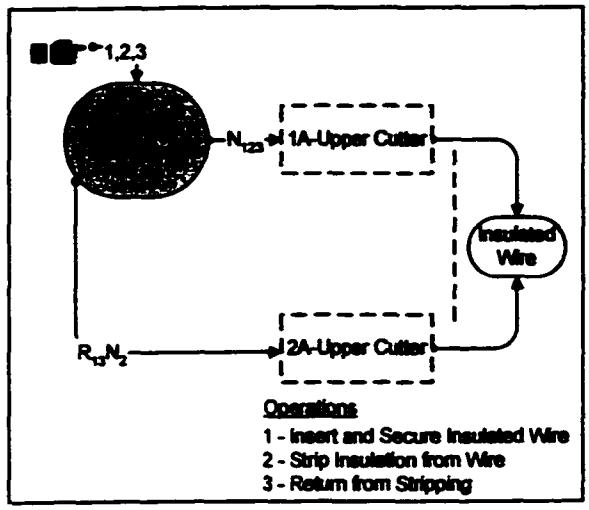

Fig. A.13: Separation into Functional Components

The final step in the evolution of this product is the contraction of the remaining N-Block graph structure as shown in Fig. 14.

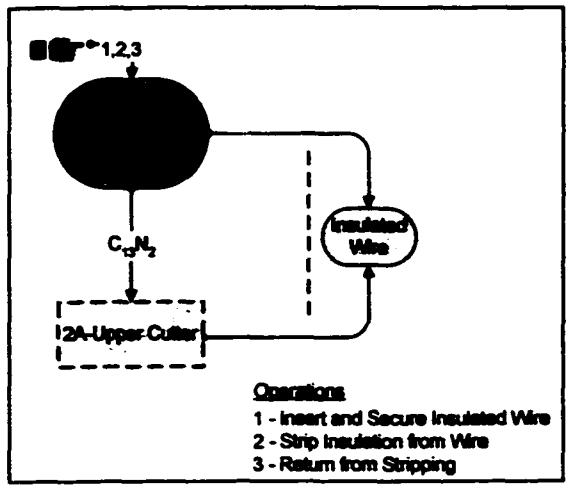

Fig. A.14: Fully Evolved Wire Stripper Design

Characteristics Promoting or Preventing Combination or Evolution of the Product:

The assumption of material compliance allows the combination of the spring into the lower jaw and then combination of the upper and lower jaws. However, a material with sufficient compliance to allow the degree of rotation required will not have enough strength to cut through the insulation of the wire. Therefore, combination of the upper and lower jaw results in the separation of the cutting surface from each jaw. The result is no reduction in the number of components. However, by combining the upper and lower jaws we are afforded the opportunity to also combine the pivot bolt and fastener into the jaw combination. The change of material required for the compliance discussed above also affords the opportunity to combine the upper and lower grips with no loss in function or customer need for a more comfortable grip.

The reduction from two cutting surfaces to one requires a change in function to remove the insulation from the wire from just squeezing the handles to squeezing the handles and rotating the wire to complete the cut.

A.5 Analysis Results

A.5.1 Metrics

Table A.4: Adjacency Matrix for Evolved Product

Component Name	Handle	Blade
Handle	E	1
Blade	1	E

Table A.5: Adjacency Matrix for Original Product

Component Name	Upper Jaw	Lower Jaw	Pivot Bolt	Upper Grip	Lower Grip	Spring	Fastener
Upper Jaw	E	1	1	1	0	1	0
Lower Jaw	1	E	1	0	1	1	1
Pivot Bolt	1	1	I	0	0	0	1
Upper Grip	1	0	0	E	0	0	0
Lower Grip	0	1	0	0	E	0	0
Spring	1	1	0	0	0	I	0
Fastener	0	1	1	0	0	0	I

Table A.6: Measured Indices

Metric	Original Design	Evolved Design	Difference
Number of Components	7	2	5
Number of Interfaces - I	8	1	7
Number of N-Links – N	0	0	0
Number of C-Links – C	4	1	3
Number of R-Links – R	4	0	4
Link Connectivity*	0.875	2	-1.125
Link to Interface Ratio N/I	0	0	0
Link to Interface Ratio C/I	0.5	1.0	-0.5
Link to Interface Ratio R/I	0.5	0	0.5
Degrees-Of-Freedom	1	1	0

*Link Connectivity = Number of Components/Number of Interfaces

A.5.2 Modeling Parameters for ESM Analysis

Table A.7: Modeling Parameters for Compliant Product

		Value	Relevant
Material	Type	Nylon	X
	Modulus (E, G)	E = 0.4 Msi	X
	Design: Strength or Stiffness	Stiffness	X
	Density (ρ)	.0412 lb/in3	
Geometry	Length (L)	1.25 in	X
	Cross Sectional Shape	Rect	
	Other (e.g. w, h, r_o, r_i, t)	w = .23 in	X
	Other (e.g. w, h, r_o, r_i, t)	h = .1 in	X
	Moment of Inertia (I, J)	I = 2e-5	X
	Deflection (δ or θ)	.1 in	X
Loading Type (bending, torsion, axial, comb)		Bending	X
Load		2 lb	X
Load Distribution (concentrated, distributed)		End/Point	X
Support Class (simply supported, cantilevered)		Cantilevered	X

A.5.3 Additional geometrical and/or loading characteristics affecting modeling:

None.

A.6 Observations

Using simple N, C, and R block contractions we were able to show a feasible product evolution from the original design to the evolved design with the exception of the 1 versus 2-cutter configuration discussed previously.

A.7 Hypothesized Guidelines

This product is unique in that in order to evolve the product to it's full potential we were forced to first separate the single-component jaws into two components according to their singular functional equivalents resulting in the addition of two components of different material.

1. Components that serve more than a single function can be separated into multiple, equivalent single-function components that can potentially afford combinations not previously feasible as a result of relaxation of material or other constraints for the single-function components.
2. Deflections (axial, lateral, rotational) are the primary measure of a successful compliant device. Force and material stress are secondary, although no less important but perhaps less constraining due to the designer's flexibility in effecting changes in these parameters. If we specify the required deflection in a compliant solution, we maintain the flexibility to change the geometry, the material, or the applied loading. See Ice Cream Scoop Empirical Study for discussion of deflection, geometry and the impact on material stress.

3. Components connected by R-Links, where the general relative motion is *small*, can be combined. Small might be determined by the endurance limit of the material at the point of maximum stress. Attempting to specify *smallness* as a function of a characteristic dimension or anything geometric would not capture the factors limiting the magnitude of the deflection.
4. When a C-Link enables a strain energy storage function, the components connected by the C-Link may be combined if the desired strain energy storage can be maintained using a compliant mechanism.

Appendix B

MathCAD File for Analysis of Tapered Cantilevered Beam Example

Comparison of TSM and ESM-Psuedo-Inverse, Circulent Matrix, and Compensation Matrix Approaches for a Tapered Cantilevered Beam Numerical Study

This model derives state vectors for the model specimen, product specimen, model, and product to determine the best method to use to predict the product.

Beam Parameters:

	Model Specimen (ms):	Product Specimen (ps):	Model (m):	Product (p):
Load (N):	$P_{ms} := .54$	$P_{ps} := 50$	$P_m := .54$	$P_p := 50$
Length (m):	$L_{ms} := .2$	$L_{ps} := .4$	$L_m := .2$	$L_p := .4$
Modulus (Pa):	$E_{ms} := 3.1 \cdot 10^9$	$E_{ps} := 72.3 \cdot 10^9$	$E_m := E_{ms}$	$E_p := E_{ps}$
Density (kg/m^3):	$\rho_{ms} := 1200$	$\rho_{ps} := 2783$	$\rho_m := \rho_{ms}$	$\rho_p := \rho_{ps}$
width_root (m):	$b_{ms\_r} := .025$	$b_{ps\_r} := .025$	$b_{m\_r} := .05$	$b_{p\_r} := .05$
width_tip (m):	$b_{ms\_t} := .025$	$b_{ps\_t} := .025$	$b_{m\_t} := .025$	$b_{p\_t} := .025$
height_root (m):	$h_{ms\_r} := .0032$	$h_{ps\_r} := .0032$	$h_{m\_r} := .0095$	$h_{p\_r} := .0095$
height_tip (m):	$h_{ms\_t} := .0032$	$h_{ps\_t} := .0032$	$h_{m\_t} := .005$	$h_{p\_t} := .005$

No. of Measurement Points: $n := 5$

Calculation Interval: $m := .1$

A. Theoretical Beam Deflection

Moment of Inertia Variation:

$$b_{ms}(x) := \left[\frac{(b_{ms\_t} - b_{ms\_r})}{L_{ms}}\right]\cdot x + b_{ms\_r} \qquad h_{ms}(x) := \left[\frac{(h_{ms\_t} - h_{ms\_r})}{L_{ms}}\right]\cdot x + h_{ms\_r} \qquad I_{ms}(x) := b_{ms}(x)\cdot\frac{h_{ms}(x)^3}{12}$$

$$b_{ps}(x) := \left[\frac{(b_{ps\_t} - b_{ps\_r})}{L_{ps}}\right]\cdot x + b_{ps\_r} \qquad h_{ps}(x) := \left[\frac{(h_{ps\_t} - h_{ps\_r})}{L_{ps}}\right]\cdot x + h_{ps\_r} \qquad I_{ps}(x) := b_{ps}(x)\cdot\frac{h_{ps}(x)^3}{12}$$

$$b_m(x) := \left[\frac{(b_{m\_t} - b_{m\_r})}{L_m}\right]\cdot x + b_{m\_r} \qquad h_m(x) := \left[\frac{(h_{m\_t} - h_{m\_r})}{L_m}\right]\cdot x + h_{m\_r} \qquad I_m(x) := b_m(x)\cdot\frac{h_m(x)^3}{12}$$

$$b_p(x) := \left[\frac{(b_{p\_t} - b_{p\_r})}{L_p}\right]\cdot x + b_{p\_r} \qquad h_p(x) := \left[\frac{(h_{p\_t} - h_{p\_r})}{L_p}\right]\cdot x + h_{p\_r} \qquad I_p(x) := b_p(x)\cdot\frac{h_p(x)^3}{12}$$

A1. Deflection due to Applied Load:

Moment Equation:

$$M1_{ms}(x) := P_{ms}\cdot(L_{ms} - x) \qquad M1_{ps}(x) := P_{ps}\cdot(L_{ps} - x) \qquad M1_m(x) := P_m\cdot(L_m - x) \qquad M1_p(x) := P_p\cdot(L_p - x)$$

Deflection:

$$\delta l_{ms}(x) := \int_0^x\int_0^x \frac{-M1_{ms}(x)}{E_{ms}\cdot I_{ms}(x)}\,dx\,dx \qquad \delta l_{ps}(x) := \int_0^x\int_0^x \frac{-M1_{ps}(x)}{E_{ps}\cdot I_{ps}(x)}\,dx\,dx$$

$$\delta l_m(x) := \int_0^x\int_0^x \frac{-M1_m(x)}{E_m\cdot I_m(x)}\,dx\,dx \qquad \delta l_p(x) := \int_0^x\int_0^x \frac{-M1_p(x)}{E_p\cdot I_p(x)}\,dx\,dx$$

A2. Deflection due to Beam Weight:

Distributed Weight:

$$w_{ms}(x) := -\rho_{ms}\cdot b_{ms}(x)\cdot h_{ms}(x) \qquad w_m(x) := -\rho_m\cdot b_m(x)\cdot h_m(x)$$

$$w_{ps}(x) := -\rho_{ps}\cdot b_{ps}(x)\cdot h_{ps}(x) \qquad w_p(x) := -\rho_p\cdot b_p(x)\cdot h_p(x)$$

Constants of Integration:

$$Cl_{ms}(x) := \int w_{ms}(x)\,dx \;\Big|\; \begin{matrix}\text{simplify}\\ \text{float},3\end{matrix} \rightarrow -\left(9.60\cdot10^{-2}\right)\cdot x_* \qquad Cl_{ms} := Cl_{ms}(L_{ms})$$

$$C2_{ms}(x) := \int\int w_{ms}(x)\,dx\,dx - Cl_{ms}\cdot x \;\Big|\; \begin{matrix}\text{simplify}\\ \text{float},3\end{matrix} \rightarrow -\left(4.80\cdot10^{-2}\right)\cdot x^2 + 1.92\cdot10^{-2}\cdot x_* \qquad C2_{ms} := C2_{ms}(L_{ms})$$

$$C1_{ps}(x) := \int w_{ps}(x)\,dx \;\text{simplify, float,3}\rightarrow -.223\cdot x_{\bullet} \qquad C1_{ps} := C1_{ps}(L_{ps})$$

$$C2_{ps}(x) := \int\int w_{ps}(x)\,dx\,dx - C1_{ps}\cdot x \;\text{simplify, float,3}\rightarrow -.111\cdot x^2 + 8.92\cdot 10^{-2}\cdot x_{\bullet} \qquad C2_{ps} := C2_{ps}(L_{ps})$$

$$C1_{m}(x) := \int w_{m}(x)\,dx \;\text{simplify, float,3}\rightarrow -1.13\cdot x^3 + 1.39\cdot x^2 - .570\cdot x_{\bullet} \qquad C1_{m} := C1_{m}(L_{m})$$

$$C2_{m}(x) := \int\int w_{m}(x)\,dx\,dx - C1_{m}\cdot x \;\text{simplify, float,3}\rightarrow -.281\cdot x^4 + .463\cdot x^3 - .285\cdot x^2 + 6.74\cdot 10^{-2}\cdot x_{\bullet} \qquad C2_{m} := C2_{m}(L_{m})$$

$$C1_{p}(x) := \int w_{p}(x)\,dx \;\text{simplify, float,3}\rightarrow -.652\cdot x^3 + 1.61\cdot x^2 - 1.32\cdot x_{\bullet} \qquad C1_{p} := C1_{p}(L_{p})$$

$$C2_{p}(x) := \int\int w_{p}(x)\,dx\,dx - C1_{p}\cdot x \;\text{simplify, float,3}\rightarrow -.163\cdot x^4 + .536\cdot x^3 - .661\cdot x^2 + .312\cdot x_{\bullet} \qquad C2_{p} := C2_{p}(L_{p})$$

Moment Equation:

$$M2_{ms}(x) := \int\int -w_{ms}(x)\,dx\,dx + C1_{ms}\cdot x + C2_{ms} \;\text{simplify, float,3}\rightarrow 4.80\cdot 10^{-2}\cdot x^2 - 1.92\cdot 10^{-2}\cdot x + 1.92\cdot 10^{-3}_{\bullet}$$

$$M2_{ps}(x) := \int\int -w_{ps}(x)\,dx\,dx + C1_{ps}\cdot x + C2_{ps} \;\text{simplify, float,3}\rightarrow .111\cdot x^2 - 8.92\cdot 10^{-2}\cdot x + 1.79\cdot 10^{-2}_{\bullet}$$

$$M2_{m}(x) := \int\int -w_{m}(x)\,dx\,dx + C1_{m}\cdot x + C2_{m} \;\text{simplify, float,3}\rightarrow .281\cdot x^4 - .463\cdot x^3 + .285\cdot x^2 - 6.74\cdot 10^{-2}\cdot x + 5.33\cdot 10^{-3}_{\bullet}$$

$$M2_{p}(x) := \int\int -w_{p}(x)\,dx\,dx + C1_{p}\cdot x + C2_{p} \;\text{simplify, float,3}\rightarrow .163\cdot x^4 - .536\cdot x^3 + .661\cdot x^2 - .312\cdot x + 4.92\cdot 10^{-2}_{\bullet}$$

Deflection:

$$\delta 2_{ms}(x) := \int_0^x\int_0^x \frac{-M2_{ms}(x)}{E_{ms}\cdot I_{ms}(x)}\,dx\,dx \qquad \delta 2_{m}(x) := \int_0^x\int_0^x \frac{-M2_{m}(x)}{E_{m}\cdot I_{m}(x)}\,dx\,dx$$

$$\delta 2_{ps}(x) := \int_0^x\int_0^x \frac{-M2_{ps}(x)}{E_{ps}\cdot I_{ps}(x)}\,dx\,dx \qquad \delta 2_{p}(x) := \int_0^x\int_0^x \frac{-M2_{p}(x)}{E_{p}\cdot I_{p}(x)}\,dx\,dx$$

A3. Combined Load and Beam Weight:

Deflection:

$x_{ms} := 0, m .. L_{ms}$ $\quad \delta 3_{ms}(x_{ms}) := \delta 1_{ms}(x_{ms}) + \delta 2_{ms}(x_{ms})$

$x_{ps} := 0, m .. L_{ps}$ $\quad \delta 3_{ps}(x_{ps}) := \delta 1_{ps}(x_{ps}) + \delta 2_{ps}(x_{ps})$

$x_m := 0, m .. L_m$ $\quad \delta 3_m(x_m) := \delta 1_m(x_m) + \delta 2_m(x_m)$

$x_p := 0, m .. L_p$ $\quad \delta 3_p(x_p) := \delta 1_p(x_p) + \delta 2_p(x_p)$

A4. Deflection Array Converted to (nx1) Vector:

Vector size: $q := 0 .. n - 1$

Deflection Vectors:

$$\delta_{ms_q} := \delta 3_{ms}\left(q \cdot \frac{L_{ms}}{n-1}\right) \qquad \delta_{m_q} := \delta 3_m\left(q \cdot \frac{L_m}{n-1}\right)$$

$$\delta_{ps_q} := \delta 3_{ps}\left(q \cdot \frac{L_{ps}}{n-1}\right) \qquad \delta_{p_q} := \delta 3_p\left(q \cdot \frac{L_p}{n-1}\right) \qquad \delta_{Theor} := \delta 3_p$$

B. Traditional Similarity Method (TSM) based upon Theoretical Data:

$P_1 = (EL^2/P)$
$P_2 = (rL^3/P)$

All otherP numbers are unity due to the assumption that characteristic lengths are identical for both beams

P_1 satisfied:

$$\Pi_1 := \frac{E_p \cdot L_p^{\,2}}{P_p} \qquad P_{mt\_\Pi 1} := \frac{E_m \cdot L_m^{\,2}}{\Pi_1}$$

P_2 satisfied:

$$\Pi_2 := \frac{\rho_p \cdot L_p^{\,3}}{P_p} \qquad P_{mt\_\Pi 2} := \frac{\rho_m \cdot L_m^{\,3}}{\Pi_2}$$

Deflection, Rotation, and Normal Stress due to Applied Load: $P_{mt} := P_{mt\_\Pi 1}$

Moment Equation: $M1_{mt}(x) := P_{mt} \cdot (L_m - x)$

Deflection:

$$\delta 1_{mt}(x) := \int_0^x \int_0^x \frac{-M1_{mt}(x)}{E_m \cdot I_m(x)} dx\,dx$$

Rotation:

$$\theta 1_{mt}(x) := \int_0^x \frac{-M1_{mt}(x)}{E_m \cdot I_m(x)} dx$$

Stress:

$$\sigma 1_{mt}(x) := M1_{mt}(x) \cdot \frac{\left(\frac{h_m(x)}{2}\right)}{I_m(x)}$$

Deflection due to Combined Load and Beam Weight:

$\delta 3_{mt}(x_m) := \delta 1_{mt}(x_m) + \delta 2_m(x_m)$

TSM Predicted Product Beam Deflection: $s := .0, .04 .. 1$

Normalized beam length: $\delta_{nor\_mt}(s) := \delta_{mt}(s \cdot L_m)$

P_3 = d/L $\Pi_3(s) := \dfrac{\delta_{nor\_mt}(s)}{L_m}$

Normalized Predicted Model Beam Deflection: $\delta_{nor\_TSM}(s) := \Pi_3(s) \cdot L_p$

Predicted Model Beam Deflection: $\delta_{TSM}(x) := \delta_{nor\_TSM}\left(\dfrac{x}{L_p}\right)$

Discretized TSM Model Beam Deflection: $X_{p\_TSM_q} := \delta_{TSM}\left(q \cdot \dfrac{L_p}{n-1}\right)$

C. Empirical Similitude Methods (ESMs) based upon Theoretical Data:

Deflection State Vectors Defined: $X_{ms} := \delta_{ms}$ $X_{ps} := \delta_{ps}$ $X_m := \delta_m$ $X_p := \delta_p$

C1. Psuedo Inverse Method:

Deflection:

Psuedo Inverse: $X_{ms\_plus} := \left(X_{ms}^{T} \cdot X_{ms}\right)^{-1} \cdot X_{ms}^{T}$

Geometry [G] Transformation: $G\delta_{psdo} := X_m \cdot X_{ms\_plus}$

Material [M] Transformation: $M\delta_{psdo} := X_{ps} \cdot X_{ms\_plus}$

Product Prediction: **X_{ps}*[G] matrix:** $X_{p\_psdo\_G\delta} := G\delta_{psdo} \cdot X_{ps}$

X_m*[M] matrix: $X_{p\_psdo\_M\delta} := M\delta_{psdo} \cdot X_m$

C2. Circulant Matrix Method:

Deflection:

$cir_{ms} :=$
$c \leftarrow 0$
for $i \in 0,1..n-1$
  $r \leftarrow c$
  for $j \in c,c+1..n-1$
    $cir_{ms_{r,c}} \leftarrow X_{ms_{r-c}}$
    $r \leftarrow r+1$
  $c \leftarrow c+1$
$cir_{ms_{n-1,n-1}} \leftarrow X_{ms_0}$
$c \leftarrow 1$
for $i \in 0,1..n-2$
  $r \leftarrow 0$
  for $j \in 0,1..c-1$
    $cir_{ms_{r,c}} \leftarrow X_{ms_{n-c+r}}$
    $r \leftarrow r+1$
  $c \leftarrow c+1$
cir_{ms}

$cir_m :=$
$c \leftarrow 0$
for $i \in 0,1..n-1$
  $r \leftarrow c$
  for $j \in c,c+1..n-1$
    $cir_{m_{r,c}} \leftarrow X_{m_{r-c}}$
    $r \leftarrow r+1$
  $c \leftarrow c+1$
$cir_{m_{n-1,n-1}} \leftarrow X_{m_0}$
$c \leftarrow 1$
for $i \in 0,1..n-2$
  $r \leftarrow 0$
  for $j \in 0,1..c-1$
    $cir_{m_{r,c}} \leftarrow X_{m_{n-c+r}}$
    $r \leftarrow r+1$
  $c \leftarrow c+1$
cir_m

Geometry [G] Transformation: $G\delta_{circ} := cir_m \cdot cir_{ms}^{-1}$

Product Prediction: X_{ps}***[**G_{circ}**] matrix:** $X_{p\_circ} := G\delta_{circ} \cdot X_{ps}$

C3. Compensation Matrix Method:

Number of Test Points: $n := rows(X_{ms})$

Deflection:

Identity Matrix Defined: $I := identity(n)$

Least Squares Solution:

Defines Least Squares solution vector for order 1

$LS\_c :=$
$c \leftarrow 0$
for $j \in 0..1$
  $r \leftarrow 0$
  for $i \in 0..n-1$
    $V_{r,c} \leftarrow (X_{ms_r})^c$
    $r \leftarrow r+1$
  $w \leftarrow (V^T \cdot V)^{-1} \cdot V^T \cdot X_{ps}$
  $c \leftarrow c+1$
w

State transformation matrix assuming the two specimen systems are well-scaled: $M_c := LS\_c_1 \cdot I$

Compensation Matrix for Distorted Systems: $\delta M_c := \left(X_{ps} - LS\_c_0 - M_c \cdot X_{ms}\right) \cdot X_{ms\_plus}$

Product Prediction: $X_{p\_comp} := \left(M_c + \delta M_c\right) \cdot X_m + LS\_c_0$

C4. Verification of Accuracy of Compensation Matrix:

Xps Predicted from Transformation Matrix: $X_{ps\_comp} := \left(M_c + \delta M_c\right) \cdot X_{ms} + LS\_c_0$

Estimated Error in [M] Transformation Matrix:

Chi-Squared Error at each Measurement Point: $E_c(z) := 100 \cdot \left[\frac{\left(X_{ps_z} - X_{ps\_comp_z}\right)^2}{\left(X_{ps_z}\right)^2} \right]^{.5}$

Summation of Measurement Point Errors: $\Sigma E_c := \sum_{z=1}^{n-1} E_c(z)$

R-Squared %Fit Measurement: $R_c := \left(\frac{\sum \left(X_{ps\_comp} - mean\left(X_{ps}\right)\right)^2}{\sum \left(X_{ps} - mean\left(X_{ps}\right)\right)^2} \right)^{0.5} \cdot 100$

Absolute Error Calculated: $absE_c(z) := \left| X_{ps_z} - X_{ps\_comp_z} \right|$

Summation of Absolute Error: $\Sigma absE_c := \sum_{z=0}^{n-1} absE_c(z)$

D. Error Estimate:

Estimated Error in Prediction of Xp:

$z := 0..n-1$ **(Required to prevent division by zero in error calculations)**

Relative Error Calculation:

Solution Method:	Chi-Squared Error at each Measurement Point	Summation of Measurement Point Errors
TSM	$Error_{TSM}(z) := 100\left[\frac{\left(X_{p_z} - X_{p\_TSM_z}\right)^2}{\left(X_{p_z}\right)^2}\right]^{.5}$	$\Sigma Error_{TSM} := \sum_{z=1}^{n-1} Error_{TSM}(z)$
Psuedo_Inverse-G	$Error_{psdo\_G}(z) := 100\left[\frac{\left(X_{p_z} - X_{p\_psdo\_G\,\delta_z}\right)^2}{\left(X_{p_z}\right)^2}\right]^{.5}$	$\Sigma Error_{psdo\_G} := \sum_{z=1}^{n-1} Error_{psdo\_G}(z)$
Psuedo_Inverse-M	$Error_{psdo\_M}(z) := 100\left[\frac{\left(X_{p_z} - X_{p\_psdo\_M\,\delta_z}\right)^2}{\left(X_{p_z}\right)^2}\right]^{.5}$	$\Sigma Error_{psdo\_M} := \sum_{z=1}^{n-1} Error_{psdo\_M}(z)$
Circulent	$Error_{circ}(z) := 100\left[\frac{\left(X_{p_z} - X_{p\_circ_z}\right)^2}{\left(X_{p_z}\right)^2}\right]^{.5}$	$\Sigma Error_{circ} := \sum_{z=1}^{n-1} Error_{circ}(z)$
Compensation	$Error_{comp}(z) := 100\left[\frac{\left(X_{p_z} - X_{p\_comp_z}\right)^2}{\left(X_{p_z}\right)^2}\right]^{.5}$	$\Sigma Error_{comp} := \sum_{z=1}^{n-1} Error_{comp}(z)$

Absolute Error Calculation:

Solution Method:	Absolute Error at each Measurement Point	Summation of Measurement Point Errors
TSM	$absError_{TSM}(z) := \left\lvert X_{p_z} - X_{p\_TSM_z}\right\rvert$	$\Sigma absError_{TSM} := \sum_{z=0}^{n-1} absError_{TSM}(z)$
Psuedo_Inverse-G	$absError_{psdo\_G}(z) := \left\lvert X_{p_z} - X_{p\_psdo\_G\,\delta_z}\right\rvert$	$\Sigma absError_{psdo\_G} := \sum_{z=0}^{n-1} absError_{psdo\_G}(z)$

Psuedo_Inverse-M

$$absError_{psdo\_M}(z) := \left| X_{p_z} - X_{p\_psdo\_M\ \delta_z} \right| \qquad \Sigma absError_{psdo\_M} := \sum_{z=0}^{n-1} absError_{psdo\_M}(z)$$

Circulent

$$absError_{circ}(z) := \left| X_{p_z} - X_{p\_circ_z} \right| \qquad \Sigma absError_{circ} := \sum_{z=0}^{n-1} absError_{circ}(z)$$

Compensation

$$absError_{comp}(z) := \left| X_{p_z} - X_{p\_comp_z} \right| \qquad \Sigma absError_{comp} := \sum_{z=0}^{n-1} absError_{comp}(z)$$

R-Squared %Fit Measurement:

Solution Method:

TSM

$$R_{TSM} := \left(\frac{\sum \overrightarrow{(X_{p\_TSM} - mean(X_p))^2}}{\sum \overrightarrow{(X_p - mean(X_p))^2}} \right)^{0.5} \cdot 100$$

Psuedo_Inverse-G

$$R_{psdo\_G} := \left(\frac{\sum \overrightarrow{(X_{p\_psdo\_G\ \delta} - mean(X_p))^2}}{\sum \overrightarrow{(X_p - mean(X_p))^2}} \right)^{0.5} \cdot 100$$

Psuedo_Inverse-M

$$R_{psdo\_M} := \left(\frac{\sum \overrightarrow{(X_{p\_psdo\_M\ \delta} - mean(X_p))^2}}{\sum \overrightarrow{(X_p - mean(X_p))^2}} \right)^{0.5} \cdot 100$$

Circulent

$$R_{circ} := \left(\frac{\sum \overrightarrow{(X_{p\_circ} - mean(X_p))^2}}{\sum \overrightarrow{(X_p - mean(X_p))^2}} \right)^{0.5} \cdot 100$$

Compensation

$$R_{comp} := \left(\frac{\sum \overrightarrow{(X_{p\_comp} - mean(X_p))^2}}{\sum \overrightarrow{(X_p - mean(X_p))^2}} \right)^{0.5} \cdot 100$$

E. Comparison of Theoretical and Theoretical based TSM and ESMs:

Graph Parameter Initialization: $x_q := q \cdot \frac{L_p}{n-1}$ x_p indicates a continuous curve (e.g. 50 points) while x indicates a discrete curve (e.g. 5 points)

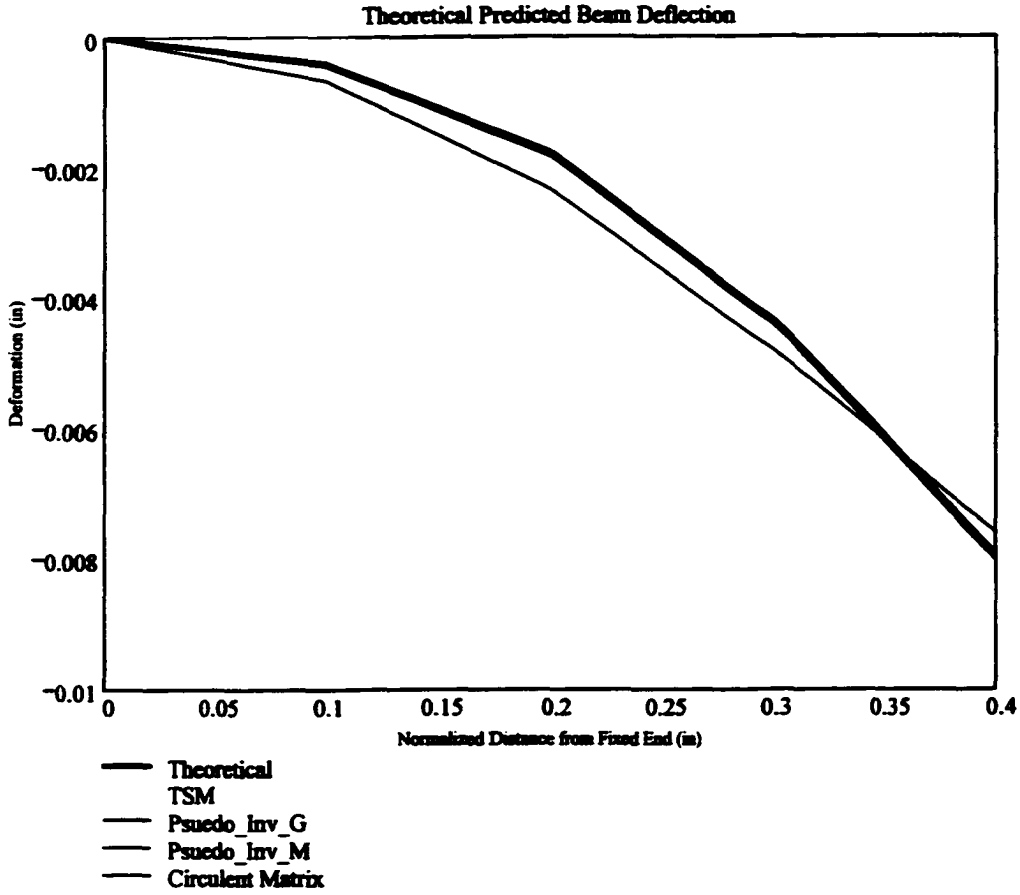

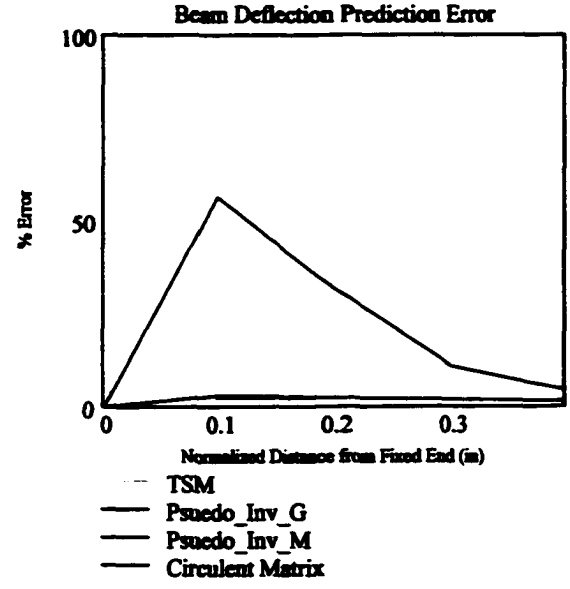

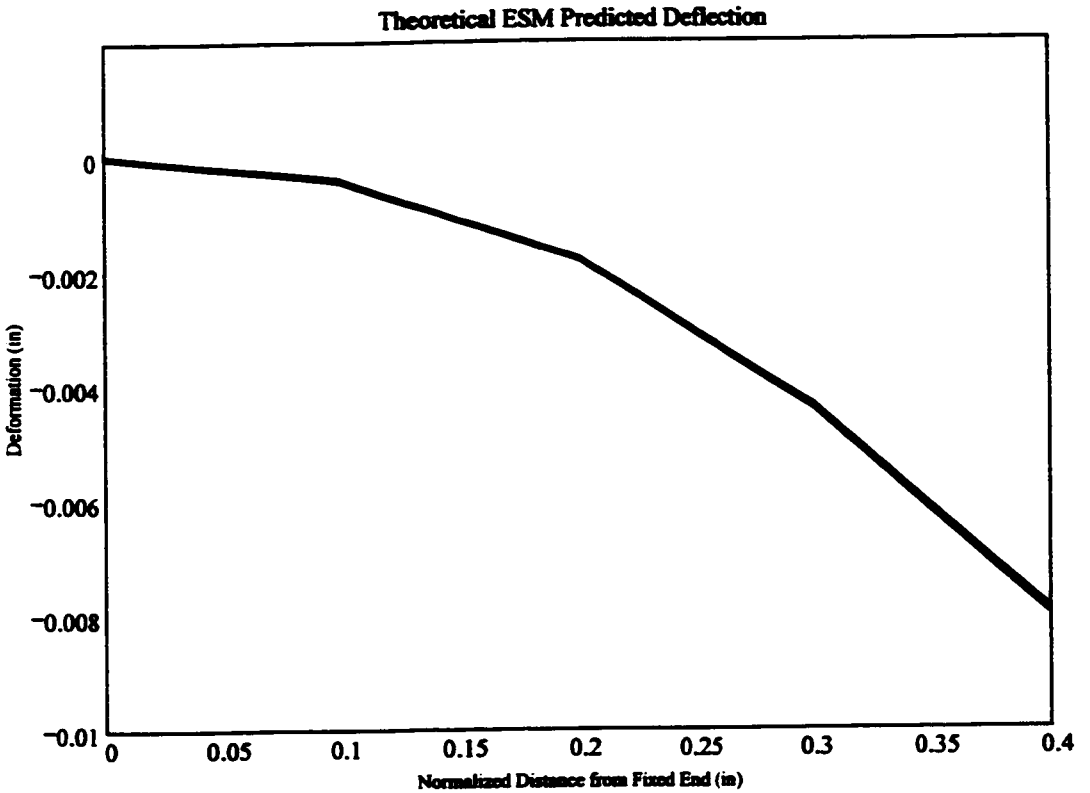

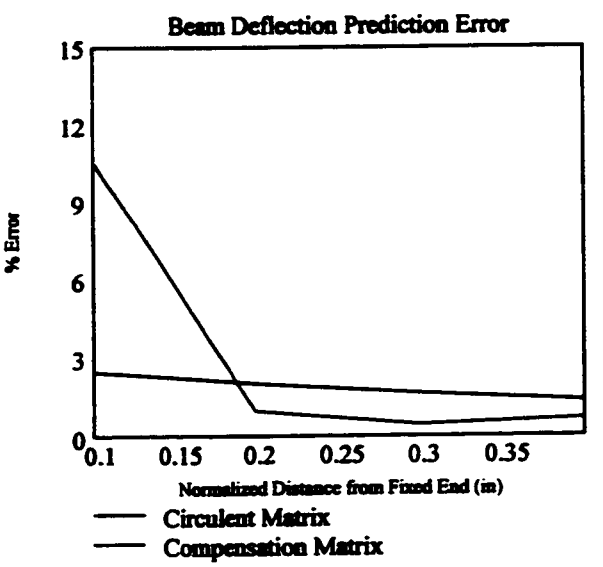

F. Error Summary:

	Relative Error Summation:	Absolute Error Summation:	R^2 Error:
TSM	$\Sigma Error_{TSM} = 374.167$	$\Sigma absError_{TSM} = 0.014$	$R_{TSM} = 92.506$
Psuedo_Inverse-G	$\Sigma Error_{psdo\_G} = 7.935$	$\Sigma absError_{psdo\_G} = 2.27 \times 10^{-4}$	$R_{psdo\_G} = 101.276$
Psuedo_Inverse-M	$\Sigma Error_{psdo\_M} = 103.007$	$\Sigma absError_{psdo\_M} = 1.621 \times 10^{-3}$	$R_{psdo\_M} = 95.582$
Circulent	$\Sigma Error_{circ} = 7.405$	$\Sigma absError_{circ} = 2.227 \times 10^{-4}$	$R_{circ} = 101.311$
Compensation	$\Sigma Error_{comp} = 12.443$	$\Sigma absError_{comp} = 1.834 \times 10^{-4}$	$R_{comp} = 101.305$

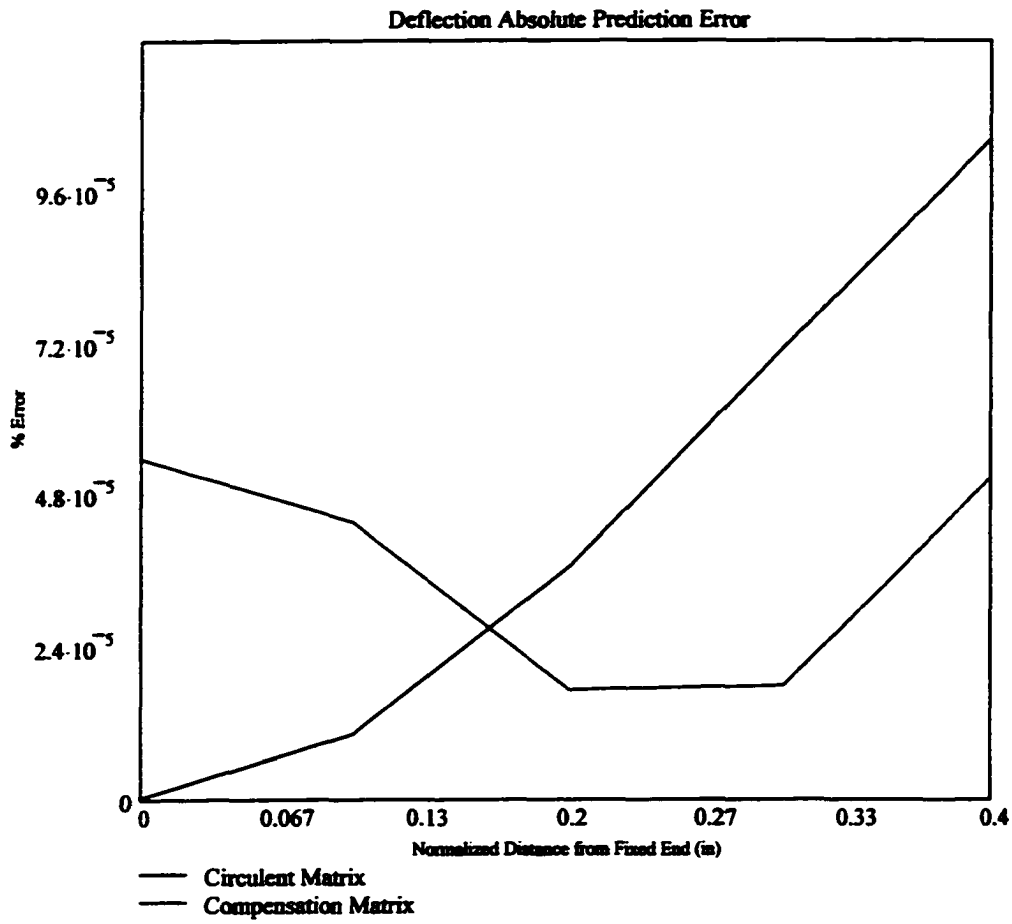

G. Mean Error Calculations:

$$Mean\_Error_{circ}(z) := 100 \cdot \left[\frac{\left(X_{p_z} - X_{p\_circ_z}\right)^2}{mean\left(X_p\right)^2} \right]^{.5} \qquad \Sigma MeanError_{circ} := \sum_{z=1}^{n-1} Mean\_Error_{circ}(z)$$

$$Mean\_Error_{comp}(z) := 100 \cdot \left[\frac{\left(X_{p_z} - X_{p\_comp_z}\right)^2}{mean\left(X_p\right)^2} \right]^{.5} \qquad \Sigma MeanError_{comp} := \sum_{z=1}^{n-1} Mean\_Error_{comp}(z)$$

$Mean\_Error_{circ}(z) =$

$8.349 \cdot 10^{-3}$
0.351
1.257
2.452
3.585

$Mean\_Error_{comp}(z) =$

1.844
1.506
0.591
0.615
1.752

$\Sigma MeanError_{circ} = 7.655$

$\Sigma MeanError_{comp} = 4.464$

H. Diagonal Norm Calculations:

$$Circ_{norm} := \sum_{j=0}^{n-1} \left(G\delta circ_{j,j}\right)^2 \qquad Circ_{norm} = 6.856 \times 10^{-3}$$

$$Comp_{norm} := \sum_{j=0}^{n-1} \left(M_{c_{j,j}} + \delta M_{c_{j,j}}\right)^2 \qquad Comp_{norm} = 4.919 \times 10^{3}$$

H. Distortion Calculations:

$$Mag\_\delta M := \sum_{i=0}^{n-1} \sum_{j=0}^{n-1} \left(\delta M_{c_{i,j}}\right)^2 \qquad Mag\_M_0 := \sum_{i=0}^{n-1} \sum_{j=0}^{n-1} \left(M_{c_{i,j}}\right)^2$$

$$Distort := \frac{Mag\_\delta M}{Mag\_M_0} \Longrightarrow \qquad Distort = 3.085 \times 10^{-8}$$